Effect of Suction and Cooling on the Stability of Subsonic and Supersonic Boundary Layers

by

Ayman Adnan Al-Maaitah

Dissertation submitted to the Faculty of the

Virginia Polytechnic Institute and State University

in partial fulfillment of the requirements for the degree of

Doctor Of Philosophy

in

Engineering Mechanics

APPROVED:

Ali H. Nayfeh, Chairman

Saad A. Ragab

Dean T. Mook

Scott L. Hendricks

John A. Burns

March, 1989

Blacksburg, Virginia

Effect of Suction and Cooling on the Stability of Subsonic and Supersonic Boundary Layers

by

Ayman Adnan Al-Maaitah

Ali H. Nayfeh, Chairman

Engineering Mechanics

(ABSTRACT)

An investigation is conducted into the effect of cooling and suction on the stability of subsonic flows over two-dimensional roughness elements and supersonic flows over flat plates. First, the effect of wall cooling on the two-dimensional linear stability of subsonic flows over two-dimensional surface imperfections is investigated. Results are presented for flows over smooth humps and backward-facing steps with Mach numbers up to 0.8. The results show that, whereas cooling decreases the viscous instability, it increases the shear-layer instability and hence it increases the growth rates in the separation region. The coexistence of more than one instability mechanism makes a certain degree of wall cooling most effective. For the Mach numbers 0.5 and 0.8, the optimum wall temperatures are about 80% and 60% of the adiabatic wall temperature, respectively. Increasing the Mach number decreases the effectiveness of cooling slightly and reduces the optimum wall temperature.

Second, the effect of suction on the stability of compressible flows over backward-facing steps is investigated. Mach numbers up to 0.8 are

considered. As expected, suction considerably reduces the separation region. The results show that continuous suction stabilizes the flow outside the separation bubble, as expected, but it destabilizes the flow inside it. Nevertheless, the overall N factor decreases as the suction level increases. This is due to the considerable reduction in the separation bubble. For the same suction flow rate, properly distributed suction strips are more effective in stabilizing the flow than continuous-suction distributions. Furthermore, the size of the separation bubble, and hence its effect on the instability, can be considerably reduced by placing strips with high suction velocities in the separation region.

Third, the effect of suction on the stability of supersonic and hypersonic boundary layers is investigated. Calculations are performed for non-similar and self-similar boundary layers. The variation of the maximum growth rate with Mach number at low levels of suction is different from that at high levels of suction. This is due to the coexistence of viscous and inviscid instability mechanisms in supersonic and hypersonic boundary layers. Suction is more effective in stabilizing the viscous instability, and hence it is more effective at low Mach numbers. Although suction decreases the maximum growth rate of second-mode waves, small levels of suction increase the growth rates of disturbances having certain frequencies. On the other hand, first-mode waves are stabilized by suction at all frequencies. Constant-suction distributions considerably move the critical Reynolds numbers of second-mode waves to higher values while the critical Reynolds numbers of first-mode waves are not sensitive to suction.

To my wife and my son

Acknowledgements

I am deeply indebted to Dr. Ali H. Nayfeh, the Chairman of my committee, for his guidance, help, and encouragement throughout the years. His invaluable knowledge and support were indispensable for this work. Dr. Nayfeh's inspiring patience and devotion to science were a prime driver of my work. In addition I would like to express my sincere gratitude to Dr. Saad A. Ragab who participated greatly in the work of Chapters 2 and 3 of this dissertation. His guidance and interest were vital for this work. I would also like to thank Dr. Dean T. Mook, Dr. Scott L. Hendricks, and Dr. John A. Burns for their serving on my committee.

Thanks are also extended to Mu'tah University, Jordan for sponsoring my studies. This work was also supported by the NASA Langley Research Center under Grant No. NAG-1-714 and the United States Office of Naval Research under Contract No. N00014-85-K-0011, NR 4325201. Moreover, I would like to thank for being of great help in typing this manuscript.

Finally, a profound debt of gratitude is expressed to my family at home and my wife for their support and patience during this work. Without their encouragement and sacrifice this dissertation would not have come to existence.

Table of Contents

Chapter 1

Introduction

The subject of boundary-layer control was pursued since the beginning of this century. In fact some of Prandtl's early papers described several experiments in which the boundary layer was controlled[1]. Out of the same stream a subject termed laminar flow control (LFC) emerged in the sixties[2,3]. While boundary-layer control aims to affect the whole flow in a desired direction by influencing the structure of the boundary layer, LFC is concerned with maintaining laminar flow over a body or surface for the longest distance possible by delaying the transition to turbulence. A flight demonstration program, the X-21 program[4] which was terminated in the sixties, provided preliminary information about LFC. Later in the seventies and due to the energy crisis more emphasis was placed on LFC, especially since the turbulent skin friction is the order of 50% of the total cruise drag[5] of some aircraft. The portion of the turbulent friction drag gets higher for other

hydrodynamic applications. For example, for a vehicle having a moderate Reynolds number, application of laminar flow control provides a lucrative increase in fuel efficiency[4]. As the time passed by, the prospect of making LFC practical have increased because of many factors that include production of advanced high strength materials, modern fabrication and manufacturing techniques, and super-critical airfoils[6] . For attached flows, laminar flow control can be obtained by one or a combination of the following methods: suction, heating in water, cooling in air, favorable pressure gradients in two-dimensional or axisymmetric flows, and convex curvature. Good reviews of these techniques and their applications can be found in Refs. 7 and 8. These techniques are also used in the area of boundary-layer control.

To efficiently apply LFC one needs to understand how transition occurs. Experiments performed on flat plates identified one possible route for transition from laminar flow into a fully developed turbulent flow[1]. First, two-dimensional Tollmien-Schlichting (T-S) waves grow downstream. Second, three-dimensional unstable waves and vortices develop in the flow. Third, secondary instabilities take place, resulting in either spikes or low-frequency modulations. Finally, turbulent spots form. These spots then get closer to each other, forming a fully developed turbulent boundary layer. Although many characteristics of the second stage can be explained by the secondary instability theory[9,10], the first stage is the only one that is fully understood. The linear stability theory can accurately predict the shape and the growth rate of instability waves. More importantly the linear theory, and especially the non-parallel theory[11] , can accurately predict the critical locations where these

waves first become unstable. The development of the linear theory promoted theoretical investigations into LFC methods.

The linear theory gained a big boost when augmented by the e^N method[12-14]. Although this method does not take into consideration the initial amplitude of the disturbance, comparing linear calculations with experimental measurements made in low disturbance wind tunnels showed that transition locations can be correlated with the locations where the logarithmic amplification of T-S waves reaches a certain value N; therefore it is called the e^N method. For different instability mechanisms, the N factor is found to be in the range between 7.0 and 11.0[12-16].

Most of the theoretical LFC investigations studied flows with single instability mechanism, mainly the viscous instability of T-S waves. However, most of flows with practical interest have more than one mechanism of instability. Even if the linear theory is used, these mechanisms might interact in a nonlinear fashion through the mean flow. Thus the effect of their coexistence is not merely an algebraic sum of their separate effects. Here, we investigate LFC techniques for flows with more than one mechanism of instability.

A problem that is rich with instability mechanisms is the flow over surface imperfections[15,16]. The mechanisms by which two-dimensional (2-D) roughness elements cause transition include amplification of T-S waves, Kelvin-Hemholtz instability (for separated flows), amplification of cross-flow vorticity, Goertler instability, and enhancement of the receptivity of freestream turbulence and acoustic disturbances[17]. Nayfeh and Al-Maaitah[18] studied the

subharmonic interaction between the Goertler vortices and the T-S waves and found it to have a small effect on the T-S wave. Malik[19], however, found that higher-order interactions can considerably modify the growth rates of T-S waves. Nayfeh et al [15] investigated the stability of flows over 2-D bulges. They accounted for T-S and shear-layer instabilities. They found that experimentally determined transition locations can be correlated with an N factor in the range 7.4-10.0.

The unavoidable existence of these imperfections demands investigations into the control of flows around them. In Chapters 2 and 3 we use the e^N method To gage the effectiveness of wall cooling and suction in controlling flows around 2-D humps and backward-facing steps. We demonstrate in Chapter 2 how the inviscid instability turns cooling into a destabilizing mechanism for the detached flow. Moreover, we show that cooling beyond an optimum level results in increasing the overall N factor.

In Chapter 3 we investigate the effect of suction on the stability of subsonic flows over backward-facing steps. We find that properly distributed suction strips stabilize the flow more than continuous-suction distributions with the same total flow rate. Moreover, we show that unlike cooling, increasing suction monotonically decreases the maximum N factor. This is due to the significant reduction in the separation bubble with suction.

In Chapter 4, we consider the effect of suction on the compressible stability of supersonic and hypersonic boundary layers. While the inviscid instability in the separation region is due to the reversed flow, the inviscid instability of the supersonic boundary layer is due to the existence of a

generalized inflection point. The results show that suction loses its effectiveness at high Mach numbers. Moreover, we show that high and low levels of suction have different effects on the maximum growth rate of first-mode waves. Two suction distributions are investigated: a spatially varying distribution that results in a self-similar boundary layer and a uniform-suction distribution that results in a non-similar boundary layer. The mean flow is calculated using self-similar and non-similar compressible boundary-layer equations.

Chapter 5 contains a summary of the results and recommendations for future research.

Chapter 2

Effect of Wall Cooling on the Stability of Compressible Subsonic Flows Over Smooth Humps and Backward-Facing Steps

2.1. *Introduction*

Due to the proven achievability of Natural Laminar Flow[20] (NLF), there is an increasing interest in its use for the design of high performance aircraft. The substantial drag reduction with NLF has promoted more analyses of ways to achieve and maintain NLF on airfoils and other aerodynamic geometries. The maintenance of NLF is critically sensitive to the location of transition, which is strongly affected by surface imperfections. Since many of these

imperfections cannot be avoided by modern manufacturing techniques[21,22], a guide is needed for their allowable sizes and methods that should be used to control their effect on NLF.

There are some empirically based criteria in the literature[23,24] for prediction of the transition of flows around imperfections. But these criteria are for special cases and geometries, and they do not explain the instability mechanisms enhanced by the imperfections or the physics of ways to control them. Bestek et al[25] solved the unsteady Navier-Stokes equations using finite-differences; they concluded that the unsteadiness of the separated flow can be regarded as a phenomenon governed by the hydrodynamic instability. Their calculations show that Tollmien-Schlichting waves considerably amplify once the separation is enhanced in agreement with the results of Nayfeh et al[15] . Burnel et al[26] and Gougat and Martin[27] experimentally investigated the flow over 2-D imperfections. Their measurements of the amplified disturbances show that they damp down in the region of favorable pressure gradients. A similar trend is seen in the calculations of Nayfeh et al[15].

Recently, the effect of compressibility on the achievability of NLF has received more attention for non-lifting surfaces. High subsonic and supersonic Mach-number flows develop density gradients across the boundary layer, which provide additional damping to 2-D and axisymmetric T-S waves. For certain geometries this advantage can be offset by the increase in the adverse pressure gradients. Vijgen et al[28] showed that increasing the freestream Mach number has a stabilizing effect on subsonic laminar boundary layers over

fuselages. Their Mach number varied from low subsonic to 0.8. Hastings et al[29] reported that NLF extended as far as 37% on a NLF fairing installed on a turbo-fan nozzle.

In spite of the previous investigations more understanding of the physics of the instability of such flows and ways to control them are still needed, especially for compressible flows. The two most common ways for laminar flow control are wall cooling in air (or heating in water) and wall suction. Wall cooling stabilizes incompressible flows over flat plates in air and destabilizes them in water[30-33] . Mack[34] and Malik[35] found that for compressible flows, wall cooling stabilizes first-mode waves but destabilizes second-mode waves. The question arises on how does wall cooling affect flows around surface imperfections, and whether these flows can be stabilized by this technique, especially, since more than one instability mechanism coexist. The purpose of this work is to study the effect of wall cooling on the subsonic two-dimensional stability of boundary layers around two-dimensional smooth backward-facing steps and humps.

2.2. *Mean Flow*

The sizes of the two-dimensional imperfections under consideration are such that strong viscous-inviscid interactions and small separation bubbles are unavoidable. The conventional laminar boundary-layer formulation cannot

predict such flows. An alternative is to solve the full Navier-Stokes equations, but in such a case the grid should be fine enough so that important flow characteristics are not smeared by the truncation error and artificial dissipation. However, due to the large number of cases that need to be investigated, solving the full Navier-Stokes equations is a very expensive task. A more economical alternative is to solve the interacting boundary-layer (IBL) equations[36] or the nonlinear triple-deck equations.

We calculated the two-dimensional compressible laminar boundary layers over flat plates with 2-D surface imperfections using the interacting boundary-layer equations (IBL). The flowfield is assumed to be governed by the steady compressible boundary-layer equations as follows:

x-momentum equation

$$\rho u \frac{\partial u}{\partial x} + \rho v \frac{\partial u}{\partial y} = - \frac{dp}{dx} + \frac{1}{Re} \frac{\partial}{\partial y} \left(\mu \frac{\partial u}{\partial y} \right) \tag{2.1}$$

continuity equation

$$\frac{\partial (\rho u)}{\partial x} + \frac{\partial (\rho v)}{\partial y} = 0 \tag{2.2}$$

energy equation

$$\begin{aligned} \rho u \frac{\partial T}{\partial x} + \rho v \frac{\partial T}{\partial y} &= (\gamma - 1) M_\infty^2 u \frac{dp}{dx} \\ &+ \frac{1}{RePr} \frac{\partial}{\partial y} \left(\kappa \frac{\partial T}{\partial y} \right) + \frac{(\gamma - 1)}{Re} M_\infty^2 \mu \left(\frac{\partial u}{\partial y} \right)^2 \end{aligned} \tag{2.3}$$

and equation of state for a perfect gas

$$\rho T = \rho_e T_e \tag{2.4}$$

where velocities are normalized with respect to the freestream velocity U^*_∞, lengths are normalized with respect to L*, which is the distance from the leading edge to the center of the imperfection, and the temperature and the viscosity and thermal-conductivity coefficients are normalized with respect to their freestream values T^*_∞, μ^*_∞ , and κ^*_∞, respectively. Here,

$$Re = \frac{U^*_\infty L^* \rho^*_\infty}{\mu^*_\infty}, \quad Pr = \frac{\mu^*_\infty C^*_p}{\kappa^*_\infty}, \quad \text{and } \gamma = \frac{C^*_p}{C^*_v} \tag{2.5}$$

where C^*_p and C^*_v are the gas specific-heat coefficients at constant pressure and volume, respectively.

The boundary conditions at the wall are

$$u = v = 0 \text{ and } T = T_w \quad at \quad y = f[\zeta(x)] \tag{2.6}$$

where $f(\zeta)$ is the shape of the wall with the imperfections. For the step

$$f(\zeta) = \frac{1}{2} h[1 + \text{erf}(\zeta)], \zeta = Re^{-3/8} \lambda^{5/4} (x - 1) \tag{2.7}$$

and for the hump

$$f(\zeta) = \begin{cases} h(1 - 12\zeta^2 + 16\zeta^3), \text{ if } \zeta \leq 0.5 \\ 0.0, \text{ if } \zeta > 0.5 \end{cases}$$

$$\zeta = | \frac{(x-1)}{x_w} |$$

where x_w is the width of the hump, erf is the error function, h is the height of the step or the hump, and $\lambda = 0.332057$. Away from the wall

$$u \to U_e \text{ and } T \to T_e \text{ as } y \to \infty \tag{2.8}$$

where the subscript e stands for edge variables.

Using the Prandtl transposition theorem,

$$z = y - f[\zeta(x)], \; w = v - u\frac{df}{dx} \tag{2.9}$$

we rewrite Eqs. (2.1)-(2.3), (2.6), and (2.8) as

$$\rho u \frac{\partial u}{\partial x} + \rho w \frac{\partial u}{\partial z} = -\frac{dp}{dx} + \frac{1}{Re}\frac{\partial}{\partial z}\left(\mu \frac{\partial u}{\partial z}\right) \tag{2.10}$$

$$\frac{\partial(\rho w)}{\partial x} + \frac{\partial(\rho w)}{\partial z} = 0 \tag{2.11}$$

$$\begin{aligned} \rho u \frac{\partial T}{\partial x} + \rho w \frac{\partial T}{\partial z} &= (\gamma - 1) M_\infty^2 u \frac{dp}{dx} + \frac{1}{RePr}\frac{\partial}{\partial z}\left(\kappa \frac{\partial T}{\partial z}\right) \\ &+ \frac{(\gamma - 1)}{Re} M_\infty^2 \mu \left(\frac{\partial u}{\partial z}\right)^2 \end{aligned} \tag{2.12}$$

$$u = w = 0, \; T = T_w \text{ at } z = 0 \tag{2.13}$$

$$U \to U_e \text{ and } T \to T_e \text{ as } z \to \infty \tag{2.14}$$

Next we use the Levy-Lees variables

$$\xi(x) = \int_0^x \rho_e \mu_e U_e dx \quad \text{and} \quad \eta(x, z) = \frac{\sqrt{Re}\, U_e}{\sqrt{2\xi}} \int_0^z \rho dz \tag{2.15}$$

and transform Eqs. (2.10)-(2.12) into

$$2\xi F F_\xi + V F_\eta - \frac{\partial}{\partial \eta}\left(\theta \frac{\partial F}{\partial \eta}\right) + \beta_0 (F^2 - Q) = 0 \tag{2.16}$$

$$2\xi F_\xi + V_\eta + F = 0 \tag{2.17}$$

$$2\xi F Q_\xi + V Q_\eta - \frac{\partial}{\partial \eta}\left(\frac{\theta}{Pr} \frac{\partial Q}{\partial \eta}\right) - (\gamma - 1) M_\infty^2 \frac{U_e^2}{T_e} \theta F_\eta^2 = 0 \tag{2.18}$$

where

$$F = \frac{u}{U_e}, \quad Q = \frac{T}{T_e} \tag{2.19a}$$

$$V = \frac{\sqrt{2\xi}}{\rho_e U_e \mu_e}\left[\sqrt{Re}\, \rho w + \eta_x \sqrt{2\xi}\, F\right] \tag{2.19b}$$

$$\theta = \frac{\rho \mu}{\rho_e \mu_e} \text{ and } \beta_0 = \frac{2\xi}{U_e} \frac{dU_e}{d\xi} \tag{2.19c}$$

The boundary conditions become

$$F = V = 0 \text{ and } Q = Q_w \quad at \quad \eta = 0 \tag{2.20a}$$

$$F \to 1 \text{ and } Q \to 1 \quad \text{as} \quad \eta \to \infty \tag{2.20b}$$

$$F = F(\xi_0, \eta) \text{ and } Q = Q(\xi_0, \eta) \quad \text{at} \quad \xi = \xi_0 \tag{2.20c}$$

To account for viscous-inviscid interactions, we need to calculate the inviscid flow over the displaced surface. This is done through the interaction law, which relates the edge velocity to the displacement thickness. Using thin airfoil theory, we obtain

$$U_e = \overline{U}_e + \frac{1}{\beta\pi}\int_{LE}^{\infty} U_e\delta \frac{d(\ln\rho_e)/dt}{x-t}\,dt + \frac{1}{\beta\pi}\int_{LE}^{\infty} \frac{d(U_e\delta)/dt}{x-t}\,dt \tag{2.21}$$

where $\beta = \sqrt{1 - M_\infty^2}$, the displacement thickness δ is given by

$$\delta = \frac{1}{\sqrt{Re}} \frac{\sqrt{2\xi}}{\rho_e u_e} \int_0^{\infty} (Q - F)d\eta \tag{2.22}$$

and $\overline{U}_e$ is the inviscid surface velocity in the absence of the boundary layer, which, in the case of small imperfections, can be expressed as

$$\overline{U}_e = 1 + \frac{1}{\beta\pi}\int_{LE}^{\infty} \frac{df/dt}{x-t}\,dt \tag{2.23}$$

Defining $\chi = f + U_e\delta$, we rewrite Eq. (2.21) as

$$U_e = 1 + \frac{1}{\beta\pi}\int_{LE}^{\infty} U_e\delta\,\frac{d(\ln\rho_e)/dt}{x-t}\,dt + \frac{1}{\beta\pi}\int_{LE}^{\infty}\frac{d\chi/dt}{x-t}\,dt \qquad (2.24)$$

The principal values of the integrals in Eqs. (2.23) and (2.24) are assumed.

Following Davis and Werle[37] and Nayfeh et al[15], we integrate the interaction law by parts to eliminate the derivative of χ. We assume χ to vary linearly over a differencing interval to obtain a second-order quadratic expression for the edge velocity. Furthermore, we calculate the second term in Eq. (2.24) explicitly from the previous iteration. By assuming the flow far away from the imperfection to be a Blasius flow, we can write the interaction law as

$$V_N + \phi\beta_{oi} = \psi \qquad (2.25)$$

For a definition of ϕ and ψ and a detailed derivation of Eq. (2.25), we refer the reader to Ref. 15.

Equations (2.16)-(2.18) and (2.20) are solved simultaneously with Eq. (2.25) using central differences in the transverse direction and three-point backward differencing in the streamwise direction.

Ragab, Nayfeh, and Krishna[38] compared the IBL calculations with solutions of the thin-layer compressible Navier-Stokes equations obtained using the computer code "ARC2D" developed at NASA Ames (Version 1.5 GAMMA). The results obtained using the IBL agree very well with those obtained using the Navier-Stokes solver; this is true for both the mean flow[39] and the stability[38] characteristics. In Ref. 38 insulated wall conditions were used. In the present

work, we investigate the influence of continuous- and strip-cooling distributions.

2.3. Stability Calculations

In this work, we consider the linear two-dimensional quasi-parallel stability of the mean flow calculated using the interacting boundary-layer formulation. The quasi-parallel assumption was justified a posteriori by Nayfeh et al[15]. They found that the wavelengths of the disturbances are the order of the boundary-layer thickness. The calculations are performed for constant specific heats and Prandtl number. Since we are limiting our calculations to subsonic flows, this assumption has a small effect on the accuracy of the stability results. Moreover, the viscosity and thermal-conductivity coefficients μ and κ are assumed to be functions of temperature only. Since Pr and C_p^* are constant we take $\kappa = \mu$.

To derive the stability equations, we superimpose 2-D disturbances on the mean flow calculated using the interacting boundary-layer formulation to obtain the total-flow quantities

$$\overline{\rho} = \rho_m(y) + \rho(x,y,t) \tag{2.26a}$$

$$\overline{u} = u_m(y) + u(x,y,t) \tag{2.26b}$$

$$\bar{v} = v(x,y,t) \tag{2.26c}$$

$$\bar{p} = p_m(y) + p(x,y,t) \tag{2.26d}$$

$$\bar{\mu} = \mu_m(y) + \mu(x,y,t) \tag{2.26e}$$

$$\bar{\lambda} = \lambda_m(y) + \lambda(x,y,t) \tag{2.26f}$$

$$\bar{T} = T_m(y) + T(x,y,t) \tag{2.26g}$$

where λ and μ appear in the definition of the bulk-viscosity coefficient k as

$$k = \lambda + \frac{2}{3}\mu$$

The subscript m refers to mean-flow quantities and the overbar refers to total flow quantities. Since $\bar{\mu}$ and $\bar{\lambda}$ are functions of temperature only, we have

$$\lambda = \frac{d\lambda_m}{dT_m} T = \lambda'_m(T_m)T \quad \text{and} \quad \mu = \frac{d\mu_m}{dT_m} T = \mu'_m(T_m)T \tag{2.27}$$

Substituting Eqs. (2.26) and (2.27) into the 2-D compressible Navier-Stokes equations, subtracting the mean-flow quantities, and linearizing the resulting equations, we obtain

$$\frac{\partial \rho}{\partial t} + u_m \frac{\partial \rho}{\partial x} + \frac{d\rho_m}{dy} v + \rho_m \left(\frac{\partial u}{\partial x} + \frac{\partial v}{\partial y} \right) = 0 \tag{2.28}$$

$$\rho_m\left(\frac{\partial u}{\partial t}+u_m\frac{\partial u}{\partial x}+\frac{du_m}{dy}v\right)+\frac{\partial p}{\partial x}$$
$$-\frac{1}{R}\frac{\partial}{\partial x}\left[r\mu_m\frac{\partial u}{\partial x}+m\mu_m\frac{\partial v}{\partial y}\right] \tag{2.29}$$
$$-\frac{1}{R}\frac{\partial}{\partial y}\left[\mu_m\left(\frac{\partial u}{\partial y}+\frac{\partial v}{\partial x}\right)+\mu\frac{du_m}{dy}\right]$$

$$\rho_m\left(\frac{\partial v}{\partial t}+u_m\frac{\partial v}{\partial x}\right)+\frac{\partial p}{\partial y}-\frac{1}{R}\frac{\partial}{\partial y}\left[r\mu_m\frac{\partial v}{\partial y}+m\mu_m\frac{\partial u}{\partial x}\right]$$
$$-\frac{1}{R}\frac{\partial}{\partial x}\left[\mu_m\left(\frac{\partial v}{\partial x}+\frac{\partial u}{\partial y}\right)+\mu\frac{du_m}{dy}\right]=0 \tag{2.30}$$

$$\rho_m\left(\frac{\partial T}{\partial t}+u_m\frac{\partial T}{\partial x}+\frac{dT_m}{dy}v\right)-(\gamma-1)M_\infty^2\left(\frac{\partial p}{\partial t}+u_m\frac{\partial p}{\partial x}\right)$$
$$=\frac{\mu_m}{RPr}\left(\frac{\partial^2 T}{\partial x^2}+\frac{\partial^2 T}{\partial y^2}\right)+\frac{1}{RPr}\frac{\partial\mu}{\partial y}\frac{dT_m}{dy} \tag{2.31}$$
$$+\frac{1}{RPr}\frac{d\mu_m}{dy}\frac{dT}{dy}+\frac{(\gamma-1)M_\infty^2\phi}{R}+\frac{\mu}{RPr}\frac{d^2T_m}{dy^2}$$

where

$$\phi=2\mu_m\left[\left(\frac{\partial u}{\partial y}+\frac{\partial v}{\partial x}\right)\frac{du_m}{dy}\right]+\mu\left(\frac{du_m}{dy}\right)^2 \tag{2.32}$$

$$m=\frac{\lambda_m}{\mu_m},\ r=2+m, \tag{2.33}$$

$$R=\frac{U_\infty^*\delta_0^*}{\nu_\infty^*},\quad \delta_0^*=\sqrt{\frac{\nu_\infty^* x^*}{U_\infty^*}} \tag{2.34}$$

The linearized equation of state for a perfect gas is

$$\gamma M_\infty^2 p = \rho_m T + \rho T_m$$

or

$$\rho = (\gamma M_\infty^2 p - \rho_m T)/T_m \tag{2.35}$$

The boundary conditions are

$$u = v = 0, T = 0 \quad \text{at} \quad y = 0 \tag{2.36}$$

$$u, v, p, T \to 0 \quad \text{as} \quad y \to \infty \tag{2.37}$$

Since the coefficients in Eqs. (2.28)-(2.31), (2.36), and (2.37) are functions of y only, we seek normal-mode solutions of the form

$$q = \hat{q}(y) \exp\{i \int \alpha dx - i\omega t\} + \text{complex conjugate} \tag{2.38}$$

where q stands for (u, v, p, T), α is the wavenumber, and ω is the frequency. For spatial stability analysis α is complex and ω is real, whereas for temporal-stability analysis ω is complex and α is real. In this work, we analyze the spatial stability case and determine ω from the non-dimensional frequency F as $\omega = F/R$.

Dropping the hat from $\hat{q}$ for convenience and defining

$$\Omega = \omega - \alpha u_m \tag{2.40}$$

we find that α is governed by the eigenvalue problem

$$Dv = -i\alpha u + \frac{DT_m}{T_m} v + \frac{i\Omega p}{p_m} - \frac{i\Omega T}{T_m} \tag{2.41}$$

$$\begin{aligned} D^2u = &\left(\frac{-i\rho_m \Omega R}{\mu_m} + r\alpha^2 \right) u - \left(\frac{\mu'_m DT_m}{\mu_m} Du \right) \\ &+ \left[\frac{\rho_m R Du_m}{\mu_m} - i\alpha \frac{\mu'_m DT_m}{\mu_m} \right] v - i(1+m)\alpha Dv \\ &+ \frac{iR\alpha}{\mu_m} p - \left[\frac{Du_m}{\mu_m} D(\mu'_m) + \frac{D^2u_m}{\mu_m} \mu'_m \right] T - \frac{\mu'_m}{\mu_m} Du_m DT \end{aligned} \tag{2.42}$$

$$\begin{aligned} \chi_0 Dp = &-i\alpha \left(r \frac{DT_m}{T_m} + \frac{2\mu'_m DT_m}{\mu_m} \right) u - i\alpha Du \\ &+ \left(\frac{iR\Omega}{\mu_m T_m} - \alpha^2 + r \frac{D^2T_m}{T_m} + \frac{r\mu'_m (DT_m)^2}{\mu_m T_m} \right) v \\ &+ i \frac{r}{p_m} \left[\Omega \left(\frac{DT_m}{T_m} + \frac{\mu'_m}{\mu_m} DT_m \right) - \alpha Du_m \right] p \\ &+ \left[i(\alpha Du_m) \left(\frac{\mu'_m}{\mu_m} + \frac{r}{T_m} \right) - \frac{ir\Omega\mu_m}{\mu_m T_m} DT_m \right] T - \frac{ir\Omega}{T_m} DT \end{aligned} \tag{2.43}$$

$$\begin{aligned} D^2T = &-2(\gamma-1)M_\infty^2 Pr Du_m Du + \left[RPr \frac{\rho_m DT_m}{\mu_m} - 2i(\gamma-1)M_\infty^2 Pr\alpha Du_m \right] v \\ &+ i(\gamma-1)M_\infty^2 PrR \frac{\Omega}{\mu_m} p + \left[-iRPr\Omega \frac{\rho_m}{\mu_m} + \alpha^2 - \frac{(DT_m)^2 \mu''_m}{\mu_m} \right. \\ &\left. - \mu'_m \frac{D^2T_m}{\mu_m} - (\gamma-1)\ M_\infty^2 Pr \frac{\mu'_m}{\mu_m} (Du_m)^2 \right] T - 2 \frac{\mu'_m DT_m}{\mu_m} DT \end{aligned} \tag{2.44}$$

$$u = v = T = 0 \quad \text{at} \quad y = 0 \tag{2.45}$$

$$u, v, p, T, \rightarrow 0 \quad \text{as} \quad y \rightarrow \infty \tag{2.46}$$

where

$$D = \frac{d}{dy}, \chi_0 = \frac{R}{\mu_m} - ir\frac{\Omega}{p_m}, \text{ and } p_m = \frac{1}{\gamma M_\infty^2} \tag{2.47}$$

2.4. Numerical Results

Following the procedure described in Section 2.2, we calculated the mean flow over a backward-facing step for different wall temperatures. Figure 2.1 shows the influence of cooling on the skin-friction coefficient

$$C_f = \frac{2U_e^2\mu(T_w)}{T_w\sqrt{2Re\xi}}\frac{\partial F}{\partial \eta}\Big|_{\eta=0} \tag{2.48}$$

In the case of cooling, the separation point is almost fixed but the reattachment point moves slightly upstream, resulting in a slightly smaller separation bubble. Moreover, cooling causes a larger negative shear prior to reattachment. The pressure coefficient $C_p = 2(\rho_e T_e - 1)/(\gamma M_\infty^2)$ is plotted in Figure 2.2. Although cooling does not have much effect on C_p far away from the imperfection, it causes steeper adverse and favorable pressure gradients around the separation bubble. In Figure 2.3, we compare the mean profiles of the flows over adiabatic and cooled walls at several locations. In general,

cooling results in fuller velocity profiles compared to the adiabatic case. In the separation region, although the mean-velocity profiles are still fuller away from the wall for the cooled wall case, they develop inflection points close to the wall, and more negative flows develop near reattachment. The corresponding temperature profiles are shown in Figure 2.4. The combined effect of cooling on the velocity and temperature profiles is a movement of the generalized inflection point closer to the wall in the separation region, as shown in Figure 2.5.

For a given mean flow, ω, and R, we solved for the eigenvalue α and the eigenfunctions, and then determined the amplification factor from

$$N = -\int_{R_0}^{R} 2\alpha_i dR \tag{2.49}$$

where R_0 corresponds to Branch I of the neutral stability curve and α_i is the imaginary part of α . The eigenvalue problem was solved using the second-order finite-difference subroutine DBVPFD[40], which is much faster than SUPORT[41]; the results of DBVPFD are in full agreement with those of SUPORT. In all cases, the results are for the most dangerous frequency, defined to be the one that results in an N factor of 9.0 in the shortest distance[15,38,42]. For an adiabatic wall, it is 50 x 10^{-6} and the maximum N factor is 9. Figure 2.6 shows the N factors for various frequencies when $T_\omega = 0.55T_{ad}$. Thus, in the case of cooling, it appears that $F = 50x10^{-6}$ produces the largest N factor in the shortest distance. Hence, all the calculations are made for an $F = 50x10^{-6}$.

We analyzed the stability of the mean profiles calculated using the IBL code for flows over a backward-facing step. The present analysis accounts for both viscous and shear-layer instabilities in the separation region. The effect of wall cooling on the stability of such flows is different from its effect on the stability of flows over flat plates. Figure 2.7 shows the growth rates for the cases of adiabatic and cooled walls. The temperature of the cooled wall is 55% of the adiabatic wall temperature T_{ad}. We note that the instability is due to the viscous mechanism in the attached region and due to a combination of the viscous and shear-layer mechanisms in the separation region. Figure 2.7 shows that cooling decreases the growth rates and hence it is stabilizing in the attached flow regions because cooling produces fuller velocity profiles. On the other hand, in the separation region cooling increases the growth rates due to the increase in the negative shear flow in the separation bubble and the movement of the generalized inflection points closer to the cooled wall. However, the growth-rate curve corresponding to the cooled case is narrower around the peak value than that corresponding to the adiabatic case because the cooled flow reattaches ahead of the adiabatic flow. Figure 2.8 shows the variation of the growth rate with streamwise distance for different wall temperatures. Decreasing the wall temperature destabilizes the flow in the separation bubble and stabilizes it in the attached flow region. Moreover the growth-rate curve gets narrower as the wall temperature decreases. Consequently, the overall effect of cooling as measured by the N factor depends on the wall temperature, as shown in Figure 2.9. When $T_w = 0.95T_{ad}$,

the boundary layer is completely stable ahead of separation and the overall N factor is less than that of the adiabatic wall. As T_w decreases below 0.8 T_{ad} the increase in the growth rates in the separation region overcomes the reduction in the growth rates elsewhere, and the net result is an increase in the maximum N factor.

For a Mach number of 0.8, Figure 2.10 shows the growth rates for various wall temperatures. The increase in the growth rates in the separation region when $M_\infty = 0.8$ is less than that when $M_\infty = 0.5$. Moreover, the peak growth rate when $M_\infty = 0.8$ is wider than that when $M_\infty = 0.5$. This makes the optimum wall temperature to be $T_w = 0.6T_{ad}$ as it is clear from the resulting N factors shown in Figure 2.11. Figure 2.11 also shows that at $M_\infty = 0.8$ cooling has a slightly smaller effect than at $M_\infty = 0.5$.

The previous results seem to be general and apply to other imperfections. For example, Figure 2.12 shows the growth rates for a flow at $M_\infty = 0.8$ around a cubic hump. The hump width is 0.2 L* and height is 0.003 L*. The behavior of the growth rates with cooling is similar to that of the step case. The resulting N factors are plotted in Figure 2.13. This figure shows that the optimum wall temperature is about $T_w = 0.8T_{ad}$.

In an attempt to lower the growth rates in the separation region, we performed calculations for a wall that is cooled everywhere except in the separation bubble. The results indicate that this distribution has a very small effect on the N factor as shown in Figure 2.14. The growth rates are slightly changed as shown in Figure 2.15. The reason for this small effect is that the

mean profiles in the separated region are influenced by cooling ahead of the separation bubble due to the non-similarity of the boundary layer.

Next we show the influence of the step position on the N factors for a constant frequency. The results shown in Figure 2.16 are for $M_\infty = 0.5$ and adiabatic wall conditions. Unlike the incompressible case the most dangerous step location is not the one corresponding to Branch I of the neutral stability curve, but it is the one corresponding to a distance half-way between Branches I and II. Figure 2.17 shows that a similar trend is true for the cubic hump.

From the previous results it is clear that the coexistence of viscous and shear-layer instability mechanisms complicates the effect of cooling on the stability of such flows. Since cooling decreases the viscous instability and increases the shear-layer instability, there exists an optimum wall temperature that reduces the amplification factor.

Chapter 3

Effect of Wall Suction on the Stability of Compressible Subsonic Flows Over Smooth Two-Dimensional Backward-Facing Steps

3.1. Introduction

The increasing interest in high performance aircraft has promoted more research in the area of laminar flow control (LFC). Boundary-layer transition does not only affect the lift and drag characteristics of lifting surfaces, it also affects airplane stability and control[43]. Surface imperfections have a significant effect on the transition process. Unfortunately, the sizes of some unavoidable imperfections cannot be always reduced to significantly diminish their effect.

This demands the investigation of methods for controlling the flows around such imperfections. Such investigations must take into consideration the coexistence of different instability mechanisms in such flows[15,17,21,24]. In this chapter we study the effectiveness of wall suction on the stabilization of flows around two-dimensional (2-D) backward-facing steps.

Carmichael, Whites, and Pfenninger[44] and Carmichael and Pfenninger[45] performed flight experiments on the wing glove of an F-94A airplane. The modified 652-213 airfoil had 69 suction slots distributed between 41 and 95% chord. They investigated single and multiple sinusoidal waves located at 15%, 28%, and 64% chord. Their results show that the allowable sizes of the waves increase when embedded in the suction region. They found that to maintain laminar flow across the airfoil requires an 8% increase in the suction level over the clear airfoil case. Carmichael[46] established empirical criteria relating the height to width ratio of the waves to the Reynolds number. However, these criteria are valid only for the configurations and the conditions investigated in the experiments. Moreover, they do not indicate the minimum suction levels needed to reduce the effect of the waviness. Spence and Randall[47] investigated the effect of uniform suction on the stability of boundary layers over plates with sinusoidal surface waves. They derived a closed-form expression for the asymptotic mean profile. By using the parallel stability theory of Lin[48], they calculated the suction velocity needed to make the critical Reynolds number larger than the flow Reynolds number. Separation was not

taken into consideration. Their results show that as the wavelength increases smaller suction velocities are needed.

More recently, Nayfeh and Reed[49] and Reed and Nayfeh[50] proposed a numerical-perturbation scheme to study the effect of porous suction strips on the stability of boundary layers over axisymmetric bodies and flat plates. To optimize the effect of the porous strip configuration, they suggested the concentration of suction near Branch I of the neutral stability curve. Their calculations show good agreement with the experiments of Reynolds and Saric[51]and Saric and Reed[52]. Hahn and Pfenninger[53] experimentally investigated the effect of suction on the transition over a backward-facing step. They placed closely spaced suction slots downstream of the step. Suction levels were found for the prevention of premature transition downstream. Their measurements show that suction considerably moves the reattachment point upstream. They found that suction is more effective when the strips are placed slightly upstream of the reattachment region. However, they stopped short of performing stability measurements.

Although existing investigations indicate that wall suction can be used to stabilize flows around surface imperfections, none of them gives a detailed physical understanding of how this can be done. Questions still need to be answered about the most effective suction levels and distributions. Furthermore, an understanding of how does the coexistence of different instability mechanisms alter the effectiveness of suction is still lacking.

In this chapter we investigate the effect of uniform suction as well as suction strips on the stability of flows over 2-D backward-facing steps. The mean profiles are calculated using the interacting boundary-layer equations[36] (IBL) modified for the case of wall suction. These equations account for the upstream influence resulting from the separation bubble and the suction strips. The stability of the mean profiles is calculated using a quasi-parallel linear stability theory for 2-D compressible flows. The theory accounts for both viscous and shear-layer instabilities coexisting in the separation region. The effectiveness of suction is then measured by the reduction in the resulting N factor[54,55].

3.2. Mean Flow

The flowfield is assumed to be governed by the interacting boundary-layer equations. The governing equations are given in Section 2.2. For convenience, we list them below modified for the case of suction. After applying the Prandtl transposition theorem and using the Levy-Lees variables, one can write the boundary-layer equations as

$$2\xi F F_{\xi} + VF_{\eta} - \frac{\partial}{\partial \eta}\left(\theta \frac{\partial F}{\partial \eta}\right) + \beta_0(F^2 - Q) = 0 \tag{3.1}$$

$$2\xi F_{\xi} + V_{\eta} + F = 0 \tag{3.2}$$

$$2\xi FQ_{\xi} + VQ_{\eta} - \frac{\partial}{\partial \eta}\left(\frac{\theta}{Pr}\frac{\partial Q}{\partial \eta}\right) - (\gamma - 1)M_{\infty}^{2}\frac{U_e^2}{T_e}\theta F_{\eta}^{2} = 0 \tag{3.3}$$

where

$$F = \frac{u}{U_e}, \quad Q = \frac{T}{T_e} \tag{3.4a}$$

$$V = \frac{\sqrt{2\xi}}{\rho_e U_e \mu_e}\left[\sqrt{Re}\,\rho w + \eta_x \sqrt{2\xi}\,F\right] \tag{3.4b}$$

$$\theta = \frac{\rho\mu}{\rho_e \mu_e} \text{ and } \beta_0 = \frac{2\xi}{U_e}\frac{dU_e}{d\xi} \tag{3.4c}$$

The Levy-Lees coordinates ξ and η are given by

$$\xi(x) = \int_0^x \rho_e \mu_e U_e dx \quad \text{and} \quad \eta(x, z) = \frac{\sqrt{Re}\,U_e}{\sqrt{2\xi}}\int_0^z \rho dz \tag{3.5}$$

and the Prandtl transposed z and w variables are defined as

$$z = y - f[\zeta(x)],\ w = v - u\frac{df}{dx} \tag{3.6}$$

where $f(\zeta)$ is the shape of the wall defined as

$$f(\zeta) = \frac{1}{2}h[1 + erf(\zeta)],\ \zeta = Re^{-3/8}\lambda^{5/4}(x - 1) \tag{3.7}$$

In equations (3.1)-(3.6) the velocities u and v are normalized with respect to the freestream velocity U_∞^*, lengths are normalized with respect to L*, which is the distance from the leading edge to the center of the step, and the temperature and viscosity and thermal-conductivity coefficients are normalized with respect to their freestream values T_∞^*, μ_∞^*, and κ_∞^*. Here

$$Re = \frac{U_\infty^* L^* \rho_\infty^*}{\mu_\infty^*}, Pr = \frac{\mu_\infty^* C_p^*}{\kappa_\infty^*}, \text{ and } \gamma = \frac{C_p^*}{C_v^*} \tag{3.8}$$

where C_p^* and C_v^* are the gas specific heat coefficients at constant pressure and volume, respectively. The Prandtl transposed boundary conditions at the wall are

$$F = 0, \frac{\partial Q}{\partial \eta} = 0 \text{ and } V = V_w \text{ at } \eta = 0 \tag{3.9a}$$

where

$$V_w = \frac{\sqrt{2\xi Re}}{Q_w U_e \mu_e} v_w \tag{3.9b}$$

$$Q_w = T_w / T_e \tag{3.9c}$$

T_w is the adiabatic wall temperature and the physical suction velocity v_w is normalized with respect to U_∞^*. Away from the wall

$$F \to 1 \text{ and } Q \to 1 \text{ as } \eta \to \infty \tag{3.10a}$$

To complete the problem formulation, we need to impose initial conditions upstream of the step; that is,

$$F = F(\xi_0, \eta) \text{ and } Q = Q(\xi_0, \eta) \quad \text{at} \quad \xi = \xi_0 \tag{3.10b}$$

and F and Q are taken to correspond to the Blasius flow.

The edge velocity is calculated from the interaction law which relates it to the displacement thickness. Using thin airfoil theory, we obtain

$$U_e = 1 + \frac{1}{\beta\pi}\int_{LE}^{\infty} U_e\delta \frac{d(\ln\rho_e)/dt}{x-t}\,dt + \frac{1}{\beta\pi}\int_{LE}^{\infty} \frac{d\chi/dt}{x-t}\,dt \tag{3.11}$$

where

$$\beta = \sqrt{1 - M_\infty^2}\,, \chi = f + U_e\delta \tag{3.12a}$$

and the displacement thickness δ is given by

$$\delta = \frac{1}{\sqrt{Re}} \frac{\sqrt{2\xi}}{\rho_e\mu_e} \int_0^{\infty} (Q - F)d\eta \tag{3.12b}$$

Integrating equation (3.2) we obtain

$$V_N + K(\eta_N) + V_w = \sqrt{2\xi}\,\frac{d}{d\xi}(U_e\xi_e\delta) \tag{3.13}$$

where

$$K(\eta_N) = \int_0^{\eta_N} (Q + 2\xi \frac{\partial Q}{\partial \xi}) d\eta \tag{3.14}$$

V_N is the vertical velocity at the edge of the boundary layer, and η_N is the corresponding value of η. Following Davis and Werle[37], Nayfeh et al[15],and Ragab et al[38], we integrate equation (3.11) by parts to eliminate the derivative of χ. We assume χ to vary linearly over a differencing interval to obtain a second-order quadratic expression for the edge velocity. By combining the resulting expression with the interaction law, we obtain

$$V_N + \phi \beta_{oi} = \psi - V_w \tag{3.15}$$

For a definition of ϕ and ψ and a detailed derivation of equation (3.15), we refer the reader to Refs. 15 and 16.

Equations (3.1)-(3.3) are solved simultaneously with equation (3.15) using central differencing in the transverse direction and three-point backward differencing in the streamwise direction. The suction velocity appears in the interaction law and the boundary conditions at the wall. This demands extra care in inverting the resulting matrix. For the flow prescribed, the skin-friction coefficient C_f and the pressure coefficient C_p are defined as

$$C_f = \frac{2U_e^2 \mu(T_w)}{T_w \sqrt{2Re\xi}} \frac{\partial F}{\partial \eta} \Big|_{\eta=0} \text{ and } C_p = 2 \frac{\rho_e T_e - 1}{\gamma M_\infty^2}$$

3.3. Stability Calculations

We consider the linear two-dimensional quasi-parallel stability of the mean flow described in Section 3.2. The disturbance equations have the same form as equations (2.28)-(2.32). When most of the suction flow is directed normal to the surface and for small suction velocities, Lekoudis[56] showed that the boundary conditions for these equations can be reasonably expressed as

$$u = v = 0 \text{ at } y = 0 \tag{3.16}$$

Furthermore, for high frequency disturbances, we have

$$T = 0 \text{ at } y = 0 \tag{3.17}$$

Since disturbances decay away from the wall,

$$u, v, p, T \to 0 \text{ as } y \to \infty \tag{3.18}$$

Seeking a normal mode solution of equations (2.28)-(2.32) and (3.16)-(3.18), we obtain the eigenvalue problem defined by equations (2.41)-(2.46) listed in Chapter 2. For known basic-state profiles, the eigenvalue α and corresponding eigenfunctions ζ_i are calculated using the finite-difference subroutine DBVPFD[40]. Specifying R and ω to be real, we find the eigenvalue

$$\alpha = \alpha_r + i\alpha_i \tag{3.19}$$

where α_r and α_i are the real and imaginary parts of α, respectively. Then $-\alpha_i$ is the spatial growth rate of the disturbance. The amplification factor is then calculated using equation (2.49).

3.4. Results and Discussion

First, we investigate the influence of suction on the mean-flow characteristics. Figure 3.1 shows the effect of continuous suction on the skin-friction coefficient of flows over a backward-facing step located at x = 1.0. As expected, suction reduces the size of the separation bubble. Hahn and Pfenninger[53] reported a reduction of 20% in the separation region. When $v_w = 5x10^{-4}$ the size of the separation bubble reduces to 67% of that when no suction is applied. Moreover, suction increases the positive shear in the attached flow region and decreases the negative shear in the separated flow region. Figure 3.2 shows the effect of continuous suction on the pressure coefficient C_p. Although continuous suction does not have much effect on C_p far away from the step, it results in steeper pressure gradients around it. At different locations on the plate, Figure 3.3 shows a comparison between the mean profiles when $v_w = 0.0$ and $v_w = 5x10^{-4}$. Away from separation, suction results in fuller velocity profiles. This is also true in the separation region, however the generalized inflection point moves closer to the wall. For the same conditions, Figure 3.4 shows that suction slightly alters the temperature

profiles. Outside the separation bubble, Figure 3.5 shows that suction reduces the vorticity throughout the boundary-layer except near the wall. However, in the separation region, suction widens the region of increase in the vorticity, as shown in Figure 3.6.

Figure 3.7 shows that the size of the separation bubble is reduced significantly when a concentrated suction strip is placed around the step. The strip starts at x = 0.9 and ends at x = 1.3, $v_w = 1x10^{-3}$, $M_\infty = 0.8$, and the height of the step is 0.003 L*. The resulting separation bubble extends over a distance of 0.04 L*, which is 22% of the size of that when no suction is applied. For the same conditions but with the step height = 0.002 L*, Figure 3.8 shows that the separation bubble extends over a distance of 0.017 L*, which is 25% of that when no suction is applied. Figures 3.7 and 3.8 show a large increase in the positive shear around the suction strips.

Next we analyze the stability characteristics of the mean profiles calculated using the IBL. Figure 3.9 shows the growth rates for the cases when $v_w = 5x10^{-4}$ and $v_w = 0.0$. Outside the separation region suction stabilizes the boundary layer due to the resulting fuller velocity profiles. In the separation bubble suction has a destabilizing influence on the boundary layer due to the movement of the inflection point towards the wall and the increase in the vorticity near the wall. Figure 3.10 shows the growth rates for different suction levels. As v_w increases the flow is stabilized in the attached flow region and destabilized in the separation region. A similar trend was noted in the case of wall cooling. Whereas the variation of the N factor with wall temperature

has a relative minimum, Figure 3.11 shows that the N factor monotonically decreases with suction. Thus, increasing the suction level results in a greater reduction in the overall N factor and hence in stabilizing the boundary layer. This is due to the significant reduction in the separation bubble.

To optimize the distribution of suction strips, Reed and Nayfeh[50] suggested that the strips be located around the smallest growth rate location. In the flow over backward-facing steps, these regions are near Branch I of the neutral-stability curve of the Blasius flow, slightly ahead of the step, and around the end of separation. To study the effect of suction-strip distributions, we locate three suction strips of width 0.2 L^* at x = 0.360, 0.723, and 1.103, each has a $v_w = 2.33 \times 10^{-4}$. The total flow rate equals to that when a continuous suction is applied with $v_w = 1.0 \times 10^{-4}$ from the leading edge to a distance of 1.4 L^*. In Figure 3.12 we compare the growth rates obtained using the suction strips with those obtained using a continuous-suction distribution with $v_w = 1.0 \times 10^{-4}$ and the case of no suction. In the case of suction strips, the growth rates are lower than those corresponding to $v_w = 0.0$ except in the separation bubble. However, they are lower than those corresponding to the continuous suction case only around the strip locations, with the exception of the separation region. The strips gradually decrease the growth rate near the beginning of the strips. Their effect, however, continues downstream of the strips. A similar trend was noted by Reed and Nayfeh[50] and Hahn and Pfenninger[53]. The resulting N factors shown in Figure 3.13 demonstrate that the same amount of flow rate can stabilize the flow more when properly

distributed in strips. Although in Ref. 53 suction was placed only downstream of the step, suction was found to be most effective when placed near the reattachment region. This corresponds to the place where the third strip is located in the present work.

As discussed previously in Figures 3.7 and 3.8, the separation bubble can be reduced significantly when a concentrated suction strip is placed across it. Figures 3.14 and 3.15 show the resulting N factors for the same flow conditions of Figures 3.7 and 3.8, respectively. The maximum N factor in Figure 14 was reduced from 9.0 to 4.0. In Figure 3.15 the effect of separation was nearly eliminated.

The stability characteristics are calculated for the most dangerous frequency[15,38,43]. Suction does not have much effect on this frequency. Figure 3.16 shows the N factors for different frequencies when continuous suction is applied. A similar trend turns out to be true in the case of suction strips.

In conclusion, we note that suction reduces the viscous instability and increases the shear-layer instability. While cooling loses its efficiency as the wall temperature decreases below a critical value, increasing the suction results in a monotonic stabilization of the boundary layer owing to the significant reduction in the separation bubble by suction. Properly distributing suction in strips results in more stabilization of the boundary-layer. Moreover, concentrating the suction in the separation region can eliminate the effect of the separation bubble.

Chapter 4

Effect of Suction on the Stability of Supersonic and Hypersonic Boundary-Layers

4.1. Introduction

The compressible stability theory of laminar boundary layers differs in many ways from the incompressible theory. The most important feature of the stability of supersonic laminar boundary layers is that there can be more than one mode of instability contributing to the growth of the disturbance. For a comprehensive review of the stability of compressible boundary layers, we refer the reader to the articles of Mack[34,57] and Nayfeh[59]. Using extensive numerical calculations, Mack[59] found that there are multiple values of wavenumbers for a single disturbance phase velocity whenever there is a

region of supersonic mean flow relative to the disturbance phase velocity. The first mode is similar to the Tollmien-Schlichting instability mode of incompressible flows, while the second and higher unstable modes are unique to compressible flows. For the inviscid case, Mack[34,57] found that the lowest Mach number at which the higher modes exist in the boundary layer on an insulated flat plate is 2.2. The lowest of these modes is called the second mode and it is the most amplified of the higher modes.

It is an interesting facet of compressible 2D boundary layers that the most unstable first-mode wave need not be parallel to the freestream as the Mach number approaches unity[34,59]. In contrast with incompressible stability theory, at supersonic speeds, 3D first modes are more unstable than their corresponding 2D waves. However, 3D second-mode waves are more stable than their corresponding 2D waves. As the Mach number increases to the hypersonic regime, second-mode waves display growth rates that are higher than those of 3D first-mode waves. However, the maximum growth rate is less than that of the first mode at zero Mach number. Mack showed that below $M_\infty = 2.2$, the boundary layer on an insulated flat plate is virtually stable to inviscid 2D waves and that above $M_\infty = 2.2$ the second mode is the most unstable mode. Moreover, the maximum amplification rate increases sharply as M_∞ increases beyond 2.2, and above $M_\infty = 5$ the first mode is not even the second most unstable mode.

Again, using extensive numerical calculations, Mack[34] investigated the influence of Mach number on the viscous instability of supersonic flows past flat plates. He found that viscosity is stabilizing for both 2D and 3D first-mode

waves when $M_\infty \geq 3.8$ and for second-mode waves at all Mach numbers; that is, the maximum amplification rate (over all frequencies, and wave angles in case of 3D waves, at constant Reynolds number) decreases with decreasing Reynolds number. At $M_\infty = 1.6$, Mack found that compressibility drastically reduces the viscous instability. As the Mach number increases beyond 1.6, the viscous instability continues to weaken although the effect of the increase in the inviscid instability continues to extend to lower and lower Reynolds numbers. When M_∞ reaches 3.8, the viscous instability disappears and viscosity acts only to damp out the inviscid instability. This result was disputed by Wazzan, Taghavi, and Keltner[60] who did not find a transition from viscous to inviscid instability with increasing Mach number but found that the viscous instability persists to $M_\infty = 6.0$. Mack[61] reconfirmed his calculations for the case of temporal stability and obtained spatial stability results that agree with his earlier conclusions on the influence of viscosity on compressible stability. Moreover, the spatial stability calculations of El-Hady and Nayfeh[62] and the present results agree with those of Mack for at least three significant figures.

As in the inviscid case, the numerical results of Mack[34,57] suggest that 2D second- and higher-mode waves are more unstable than their corresponding 3D waves. Moreover, the maximum growth rate of second-mode waves drops sharply as the wave angle increases from zero.

The lowest Mach number at which Mack[57] was able to calculate 2D second-mode waves is $M_\infty = 3.0$ at which the minimum critical Reynolds number is 13,900. Moreover, the inviscid instability increases rapidly with

increasing Mach number and hence one would expect the minimum critical Reynolds number to decrease rapidly to lower values as the Mach number increases. In fact, Mack found that the minimum critical Reynolds number drops to 235 as the Mach number increases to 4.5. Moreover, at higher Mach numbers second-mode waves have much higher growth rates than oblique first-mode waves.

Whereas cooling can stabilize 2D and 3D first-mode waves, Mack[34] found that cooling destabilizes inviscid second-mode waves. Including the effects of viscosity, Malik[35] studied the influence of cooling on oblique first-mode waves at $\psi = 60°$ for $M_\infty = 2$ and 4.5 and second-mode waves for $M_\infty = 4.5$; in these calculations R = 1500 and the stagnation temperature is $560° R$. His results show that oblique first-mode waves at $M_\infty = 2$ are completely stabilized when $T_w/T_{ad} = 0.7$ whereas those at $M_\infty = 4.5$ are stabilized only when $T_w/T_{ad} = 0.48$. On the other hand, his results show that second-mode waves are destabilized by cooling. In fact, the maximum growth rate increases rapidly with cooling. Malik found that the frequency of the most amplified first-mode wave decreases with cooling whereas that of the most amplified second-mode wave increases with cooling.

Malik[35] also investigated the influence of favorable pressure gradients and self-similar suction distributions on the stabilization of second-mode waves at $M_\infty = 4.5$ and $R = 1500$. He found that each of them shifts the band of unstable frequencies to higher values and reduces the peak amplification. Consequently, it appears that, whereas cooling cannot be used to stabilize second-mode waves, they can be stabilized using either suction or wall

shaping to produce a favorable pressure gradient. However, his calculations, are for a single Reynolds number and a single Mach number. In this work we present a detailed study of the effect of self-similar as well as uniform suction distributions on the compressible stability of supersonic and hypersonic boundary layers. Both first- and second-mode waves of instability are investigated. Our results show that, suction is not as effective at $M_\infty = 6$ and 7 as at $M_\infty = 4.5$.

4.2. Mean Flow

We consider 2D compressible flows over adiabatic flat plates of an ideal calorically perfect gas. The basic flowfield is governed by the non-dimensional 2D boundary-layer equations

x-momentum equation

$$\rho u \frac{\partial u}{\partial x} + \rho v \frac{\partial u}{\partial y} = - \frac{dp}{dx} + \frac{1}{Re} \frac{\partial}{\partial y} \left(\mu \frac{\partial u}{\partial y} \right) \tag{4.1}$$

continuity equation

$$\frac{\partial (\rho u)}{\partial x} + \frac{\partial (\rho v)}{\partial y} = 0 \tag{4.2}$$

energy equation

$$\rho u \frac{\partial T}{\partial x} + \rho v \frac{\partial T}{\partial y} = (\gamma - 1) M_\infty^2 u \frac{dp}{dx} + \frac{1}{RePr} \frac{\partial}{\partial y}\left(\kappa \frac{\partial T}{\partial y}\right) + \frac{(\gamma - 1)}{Re} M_\infty^2 \mu \left(\frac{\partial u}{\partial y}\right)^2 \tag{4.3}$$

where velocities are normalized with respect to the freestream velocity U_∞^*, lengths are normalized with respect to a reference length L^*, and the temperature, viscosity, and thermal conductivity coefficients are normalized with respect to their freestream values T_∞^*, μ_∞^*, and κ_∞^*, respectively. Here,

$$Re = \frac{U_\infty^* L^* \rho_\infty^*}{\mu_\infty^*}, \quad Pr = \frac{\mu_\infty^* C_p^*}{\kappa_\infty^*}, \quad \text{and } \gamma = \frac{C_p^*}{C_v^*} \tag{4.4}$$

where C_p^* and C_v^* are the gas specific heat coefficients at constant pressure and volume, respectively. For a perfect gas the non-dimensional equation of state has the form

$$\rho T = 1 \tag{4.5}$$

Away from the wall, the boundary conditions are

$$u \to 1 \text{ and } T \to 1 \text{ as } y \to \infty$$

Moreover, the temperature gradient at the wall should vanish for adiabatic wall conditions; that is,

$$\frac{\partial T}{\partial y} = 0 \text{ at } y = 0 \tag{6a}$$

Here we consider the case of continuous wall suction. Assuming that the suction velocity is directed normal to the plate, we have

$$u = 0 \text{ at } y = 0 \tag{6b}$$

$$v = -v_w \text{ at } y = 0 \tag{6c}$$

where v_w can vary with x in general. However, there are two restrictions on the suction velocity. First, v_w should not be too large so that the boundary-layer assumption continues to be valid. Second, v_w should not vary abruptly, as in the case of suction strips. In the latter case the conventional boundary-layer equations cannot predict the upstream influence of the abrupt changes. Instead one should use a triple-deck formulation or the interactive boundary-layer equations.

It is convenient to reformulate the problem using the Levy-Lees variables

$$\xi(x) = \int_0^x \rho_e \mu_e U_e dx \text{ and } \eta(x,y) = \frac{\sqrt{Re}\, U_e}{\sqrt{2\xi}} \int_0^y \rho dy \tag{4.7}$$

and transform Eqs. (4.1)-(4.6) into

$$2\xi F F_\xi + V F_\eta - \frac{\partial}{\partial \eta}\left(\theta \frac{\partial F}{\partial \eta}\right) + \beta_0 (F^2 - Q) = 0 \tag{4.8}$$

$$2\xi F_\xi + V_\eta + F = 0 \tag{4.9}$$

$$2\xi FQ_{\xi} + VQ_{\eta} - \frac{\partial}{\partial\eta}\left(\frac{\theta}{Pr}\frac{\partial Q}{\partial\eta}\right) - (\gamma-1)M_{\infty}^{2}\frac{U_e^2}{T_e}\theta F_{\eta}^{2} = 0 \qquad (4.10)$$

where

$$F = \frac{u}{U_e}, Q = \frac{T}{T_e} \qquad (4.11a)$$

$$V = \frac{\sqrt{2\xi}}{\rho_e U_e \mu_e}\left[\sqrt{Re}\,\rho v + \eta_x\sqrt{2\xi}\,F\right] \qquad (4.4.11b)$$

$$\theta = \frac{\rho\mu}{\rho_e\mu_e} \text{ and } \beta_0 = \frac{2\xi}{U_e}\frac{dU_e}{d\xi} \qquad (4.11c)$$

and the subscript e refers to conditions at the edge of the boundary layer. The boundary conditions become

$$F \to 1 \text{ and } Q \to 1 \text{ as } \eta \to \infty \qquad (4.12a)$$

$$F = 0 \text{ and } \frac{\partial Q}{\partial\eta} = 0 \text{ at } \eta = 0 \qquad (4.12b)$$

$$V = \frac{\sqrt{2\xi Re}}{\rho_e U_e \mu_e}\rho(0)v_w \text{ at } \eta = 0 \qquad (4.12c)$$

Equations (4.7)-(4.12) represent the non-similar boundary-layer equations. Under certain conditions these equations admit self-similar solutions. These conditions include flows over an adiabatic flat plate with no suction or blowing. In the case of uniform suction distributions V_w varies along the plate and hence self-similar solutions do not exist. However, when V_w is constant, and hence

the physical suction velocity v_w is proportional to $\xi^{-1/2}$, Eqs. (4.7)-(4.12) admit self-similar solutions for flows over adiabatic flat plates. In the latter case, $u_e = T_e = \mu_e = 1.0$ and $F_\xi = 0$ and $Q_\xi = 0$. Letting $V = -f(\eta)$ and solving Eq. (4.9), we have $F = f'$. Then, using Eq. (4.5), we rewrite Eqs. (4.8) and (4.10) as

$$\left(\frac{\mu}{T} f'\right)' + ff'' = 0 \tag{4.13}$$

$$\left(\frac{\mu}{TPr} T'\right)' + fT' + (\gamma - 1)M_\infty^2 \left(\frac{\mu}{T}\right)(f'')^2 = 0 \tag{4.14}$$

where the prime denotes the derivative with respect to η. The boundary conditions (4.12) become

$$f' \to 1 \text{ and } T \to 1 \text{ as } \eta \to \infty \tag{4.15}$$

$$f' = T' = 0 \text{ and } f = \sqrt{2}\, V_w \text{ at } \eta = 0 \tag{4.16}$$

where

$$V_w = \frac{\sqrt{\xi Re}}{T(0)} v_w = \text{ constant} \tag{4.17}$$

Thus, the physical wall velocity must be proportional to $\frac{T(0)}{\sqrt{\xi}}$. In the self-similar calculations, we specify V_w instead of v_w.

Equations (4.7)-(4.12) are solved using central differences in the transverse direction and three-point backward differencing in the streamwise direction, whereas Eqs. (4.13)-(4.17) are solved using the finite-difference code DBVPFD[40]. The calculated displacement thickness for different M_∞ are in

agreement with the fourth-order calculations of Malik[63] for zero suction velocity.

4.3. Stability Analysis

We consider the linear quasi-parallel 3D compressible stability of the calculated 2D mean flowfield. We superimpose on it a small disturbance and obtain the total-flow quantities in the form

$$\hat{q}(x,y,z,t) = q_b(y) + q(x,y,z,t) \tag{4.18}$$

where q stands for u, v, w, ρ, p, μ, and T; the hat stands for the total-flow quantities; and the subscript b stands for the basic-flow quantities. Substituting Eq. (4.18) into the compressible Navier-Stokes equations, recalling that the basic flow satisfies the Navier-Stokes equations, and linearizing with respect to q, we obtain the disturbance equations

$$\frac{\partial \rho}{\partial t} + \rho_b \frac{\partial u}{\partial x} + u_b \frac{\partial \rho}{\partial x} + \frac{\partial}{\partial y}(\rho_b v) + \rho_b \frac{\partial w}{\partial z} = 0 \tag{4.19}$$

$$\rho_b\left(\frac{\partial u}{\partial t} + u_b \frac{\partial u}{\partial x} + v \frac{du_b}{dy} \right) = -\frac{\partial p}{\partial x} + \frac{1}{R}\left\{ \mu_b \frac{\partial}{\partial x}\left(r \frac{\partial u}{\partial x} + m \frac{\partial v}{\partial y} + m \frac{\partial w}{\partial z} \right) + \frac{\partial}{\partial y}\left[\mu_b\left(\frac{\partial u}{\partial y} + \frac{\partial v}{\partial x} \right) + \mu \frac{du_b}{dy} \right] + \mu_b \frac{\partial}{\partial z}\left(\frac{\partial w}{\partial x} + \frac{\partial u}{\partial z} \right) \right\} \tag{4.20}$$

$$\rho_b\left(\frac{\partial v}{\partial t}+u_b\frac{\partial v}{\partial x}\right)=-\frac{\partial p}{\partial y}+\frac{1}{R}\left\{\frac{\partial}{\partial x}\left[\mu_b\left(\frac{\partial u}{\partial y}+\frac{\partial v}{\partial x}\right)+\mu\frac{du_b}{dy}\right]\right.$$
$$\left.+\frac{\partial}{\partial y}\left[\mu_b\left(m\frac{\partial u}{\partial x}+r\frac{\partial v}{\partial y}+m\frac{\partial w}{\partial z}\right)\right]+\mu_b\frac{\partial}{\partial z}\left(\frac{\partial v}{\partial z}+\frac{\partial w}{\partial y}\right)\right\} \tag{4.21}$$

$$\rho_b\left(\frac{\partial w}{\partial t}+u_b\frac{\partial w}{\partial x}\right)=-\frac{\partial p}{\partial z}+\frac{1}{R}\left\{\mu_b\frac{\partial}{\partial x}\left(\frac{\partial w}{\partial x}+\frac{\partial u}{\partial z}\right)\right.$$
$$\left.+\frac{\partial}{\partial y}\left[\mu_b\left(\frac{\partial v}{\partial z}+\frac{\partial w}{\partial y}\right)\right]+\mu_b\frac{\partial}{\partial z}\left(m\frac{\partial u}{\partial x}+m\frac{\partial v}{\partial y}+r\frac{\partial w}{\partial z}\right)\right\} \tag{4.22}$$

$$\rho_b\left(\frac{\partial T}{\partial t}+u_b\frac{\partial T}{\partial x}+v\frac{dT_b}{dy}\right)=(\gamma-1)M_\infty^2\left[\frac{\partial p}{\partial t}+u_b\frac{\partial p}{\partial x}+\frac{1}{R}\phi\right]$$
$$+\frac{1}{RPr}\left\{\mu_b\frac{\partial^2 T}{\partial x^2}+\frac{\partial}{\partial y}\left(\mu_b\frac{\partial T}{\partial y}+\mu\frac{dT_b}{dy}\right)+\mu_b\frac{\partial^2 T}{\partial z^2}\right\} \tag{4.23}$$

$$\phi=2\mu_b\left(\frac{\partial u}{\partial y}+\frac{\partial v}{\partial x}\right)\frac{du_b}{dy}+\mu\left(\frac{du_b}{dy}\right)^2 \tag{4.24}$$

where

$$r=\frac{2}{3}(e+2)\text{ and }m=\frac{2}{3}(e-1) \tag{4.25}$$

and e = 0 corresponds to the Stokes hypothesis. The local Reynolds number R in Eqs. (4.19)-(4.24) is based on a reference length $\delta_r^*=\sqrt{\nu x_r^*/U_\infty^*}$, which is the order of the boundary-layer thickness. Velocities are normalized with respect to the free-stream velocity U_∞^* and lengths are normalized with respect to δ_r^*. Hence,

$$R = \frac{U_\infty^* \delta_r^*}{\nu^*} = \sqrt{\frac{U_\infty^* x_r^*}{\nu^*}}$$

The boundary conditions at the wall are

$$u = v = w = T = 0 \text{ at } y = 0 \tag{4.26}$$

For sonic, subsonic, and supersonic waves the boundary conditions away from the wall have the general form[64]

$$u, v, w, T, p, \text{ are bounded as } y \to \infty \tag{4.27}$$

We assume that μ is a function of the temperature only; hence

$$\mu = T \frac{d\mu_b}{dT}(T_b) = T\mu_b'(T_b) \tag{4.28}$$

Moreover, the linearized equation of state takes the form

$$p/p_b = T/T_b + \rho/\rho_b \tag{4.28b}$$

Since the mean flow is assumed to be quasi-parallel, we seek solutions in the form of 3D traveling Tollmien-Schlichting waves as

$$[u,v,p,T,w] = [\zeta_1(y), \zeta_3(y), \zeta_4(y), \zeta_5(y), \zeta_7(y)] \exp[i(\int \alpha dx + \beta z - \omega t)] \tag{4.29}$$

where α and β are the streamwise and spanwise wavenumbers, respectively, and ω is the frequency. Substituting Eqs. (4.28) and (4.29) into Eqs. (4.19)-(4.24), we obtain

$$D\zeta_3 + i\alpha\zeta_1 - \frac{DT_b}{T_b}\zeta_3 + i(\alpha u_b - \omega)\left(\gamma M_\infty^2 \zeta_4 - \frac{\zeta_5}{T_b}\right) + i\beta\zeta_7 = 0 \tag{4.30}$$

$$\begin{aligned} i(\alpha u_b - \omega)\zeta_1 + \zeta_3 Du_b + i\alpha T_b\zeta_4 - \frac{T_b}{R}\{ &- \mu_b(r\alpha^2 + \beta^2)\,\zeta_1 - \alpha\beta\mu_b(m+1)\zeta_7 \\ &+ i(m+1)\alpha\mu_b D\zeta_3 + \mu_b' D\zeta_1 + i\alpha\mu_b'\zeta_3 + \mu_b D^2\zeta_1 + D(\mu_b' Du_b)\zeta_5 + \mu_b' Du_b\, D\zeta_5\} = 0 \end{aligned} \tag{4.31}$$

$$\begin{aligned} i(\alpha u_b - \omega)\zeta_3 + T_b D\zeta_4 - \frac{T_b}{R}\{ &i(m+1)\,\alpha\mu_b D\zeta_1 + im\alpha\mu_b'\zeta_1 - (\alpha^2 + \beta^2)\mu_b\zeta_3 \\ &+ r\mu_b' D\zeta_3 + im\beta\mu_b'\zeta_7 + i\alpha\mu_b' Du_b\zeta_5 + r\mu_b D^2\zeta_3 + i(m+1)\beta\mu_b\, D\zeta_7\} = 0 \end{aligned} \tag{4.32}$$

$$\begin{aligned} i(\alpha u_b - \omega)\zeta_7 + i\beta T_b\zeta_4 - \frac{T_b}{R}\{ &- (m+1)\,\alpha\beta\mu_b\zeta_1 + i\beta\mu_b'\zeta_3 \\ &+ i(m+1)\beta D\zeta_3 - \mu_b(\alpha^2 + r\beta^2)\zeta_7 + \mu_b' D\zeta_7 + \mu_b\, D^2\zeta_7\} = 0 \end{aligned} \tag{4.33}$$

$$\begin{aligned} i(\alpha u_b - \omega)\zeta_5 + \zeta_3 DT_b - i(\gamma - 1)T_b M_\infty^2(\alpha u_b - \omega)\zeta_4 - \frac{T_b}{R}[2Du_b(D\zeta_1 + i\alpha\zeta_3) \\ + \mu_b'\,(Du_b)^2\zeta_5] - \frac{T_b}{RPr}[-\mu_b(\alpha^2 + \beta^2)\zeta_5 + D(\mu_b D\zeta_5) + D(\mu_b' DT_b\zeta_5)] = 0 \end{aligned} \tag{4.34}$$

$$\zeta_1 = \zeta_3 = \zeta_5 = \zeta_7 = 0 \text{ at } y = 0 \tag{4.35}$$

$$\zeta_n \text{ are bounded as } y \to \infty \tag{4.36}$$

where the prime denotes the derivative with respect to the argument and $D = d/dy$.

In this work, we consider the case of spatial stability so that ω is real. Since the basic flow is two-dimensional, β is constant. In this work, we assume that β is real and α complex so that

$$\alpha = \alpha_r + i\alpha_i \tag{4.37}$$

Moreover, we compute ω from the non-dimensional frequency F as

$$\omega = RF \tag{4.38}$$

and compute the wave angle ψ as

$$\psi = \tan^{-1}(\beta/\alpha_r)$$

The eigenvalue problem is solved using the finite-difference code DBVPFD[40] coupled with a Newton-Raphson iteration technique. This scheme produces results that are as accurate as those obtained by using SUPORT[41] with far less computational time. For the case of no suction, our results are in total agreement with those of Mack[34,57], El-Hady and Nayfeh[62], and Malik[63] . For the case of self-similar suction distributions, $R = 1500$, and $M_\infty = 4.5$, we reproduced the results of Malik[35].

4.4. Results and Discussion

For certain M_∞, P_∞, Pr, and v_w, the velocity profile is determined using the formulation described in Section II. The stability of the calculated profile is then analyzed as described in Section III. A great deal of the physics of the stability problem, however, can be understood by studying the effect of suction on the mean-flow characteristics. Whereas the incompressible Blasius profile does not have an inflection point, an important characteristic of the compressible Blasius flow is the existence of a generalized inflection point inside the boundary layer. The generalized inflection point is defined as the point where $D(\rho_b Du_b) = 0$. In the absence of suction, there is one generalized inflection point inside the compressible boundary layer. Suction creates another generalized inflection point near the wall. In Figure 4.1 we show the variation of the locations of the generalized inflection points with the level of the self-similar suction distribution when $M_\infty = 2.0, 4.5, 5.0,$ and $6.0,$ respectively. As the suction level increases, the two generalized inflection points move closer to each other until they meet and then disappear, as shown in Figure 4.1. The influence of T_∞ on the locations of the generalized inflection points is shown in Figure 4.2. The suction level needed to eliminate the generalized inflection points when $T_\infty = 62\ K°$ is larger than that needed when $T_\infty = 121\ K°$. In Figure 4.3, we show the minimum suction level needed to eliminate the generalized inflection points as a function of Mach number. This level increases rapidly as the Mach number increases. Therefore, the suction

level needed to stabilize the inviscid mechanism increases rapidly as the Mach number increases. The viscous instability, however, can be gauged by the displacement thickness. The variation of the displacement thickness with suction level for different Mach numbers is shown in Figure 4.4. Although the displacement thickness decreases rapidly with suction, its rate of reduction decreases as V_w increases.

All of the previous results are for the case of self-similar velocity profiles. An infinite suction velocity at the leading edge of the plate is needed to obtain such profiles. In Figure 4.5, we compare a self-similar suction distribution with a uniform-suction distribution having the same level at $x = 1$. Using these suction distributions in the non-similar boundary-layer solver, we obtained the skin-friction distributions shown in Figure 4.6. It is clear that the self-similar suction distribution described in Figure 4.5 results in a constant shear coefficient along the plate, thereby providing some confidence in the non-similar solver. The uniform-suction distribution results in a gradually increasing shear coefficient, which asymptotes the shear coefficient produced by the self-similar suction distribution.

After calculating the mean profiles and for certain R, F, and ψ, we solved Eqs. (4.30)-(4.36) for the eigenvalue α and the eigenfunctions ζ_n. In this paper, we present results for both first- and second-mode waves.

a. First-Mode Waves

The most important feature of the stability of supersonic and hypersonic boundary layers is the existence of more than one mode of instability. For the first mode, oblique waves are more unstable than 2D waves. In Figures 4.7 and 4.8, we show the effect of suction on the variation of the growth rate with wave angle for two Mach numbers. It is clear that suction decreases the growth rates of 2D and all 3D waves. Moreover, suction is most effective in reducing the growth rates of 3D waves having wave angles equal or nearly equal to that of the most amplified wave. However, suction has a small influence on the wave angle for which the first mode grows the most. It is clear from Figure 4.9 that suction has a stabilizing effect on first-mode waves. It decreases the growth rates and the range of frequencies receiving amplification. Suction also slightly shifts the most amplified frequency to a higher frequency. Moreover, for a given frequency, suction decreases the growth rate of first-mode waves at all streamwise locations, as shown in Figure 4.10.

The variation of the maximum growth rate with Mach number for various levels of suction is shown in Figure 4.11. The wind-tunnel temperature corresponds to a stagnation temperature of 311 $K°$. If T_∞ gets below 50 $K°$ it is set equal to 50 $K°$. In the absence of suction, the maximum growth rate decreases with Mach number. As shown in Figure 4.11, suction is more effective at low Mach numbers because it is very effective in reducing the viscous instability, which is dominant at low Mach numbers. However, suction

is not as effective in stabilizing the inviscid mechanism, which is dominant at higher Mach numbers, because high levels of suction are needed to eliminate the generalized inflection point at high Mach numbers. For suction levels larger than approximately 0.2, the maximum growth rate increases with M_∞ for low Mach numbers. For high Mach numbers, however, the maximum growth rate decreases slightly with M_∞. This can be attributed to the fact that the inviscid instability gets more dominant as M_∞ increases. For low M_∞ high levels of suction can eliminate the influence of viscosity, leaving only the inviscid mechanism, whereas at low levels of suction both the viscous and inviscid mechanisms continue to coexist. This is the reason why we see different behaviors for low and high levels of suction at relatively low M_∞. At M_∞ equal or larger than 3.8, Mack found that the viscous instability disappears for first-mode waves, and hence viscosity is stabilizing, which may explain the similar behavior for all levels of suction at high Mach numbers. Hence, at high M_∞, suction is not as effective in stabilizing first-mode waves.

In Figure 4.12, we show that the influence of the suction level on the growth rate of first-mode waves at R = 1500, $\psi = 60°, F = 11.5x10^{-6}$ for $M_\infty = 2.6$ and 3.0. The suction levels needed to completely stabilize the flow at $M_\infty = 2.6$ and 3.0 are $V_w = 0.7$ and 0.9, respectively. In both cases the suction velocity needed to stabilize the disturbance is slightly larger than the one needed to eliminate the generalized inflection points. For all the cases investigated, the growth rate at constant frequency varies approximately linearly with the suction level. Based on this, one expects that linear

perturbation methods, such as that of Ref. 12, can be used to predict the stability of flows over suction strips.

Next we investigate the effect of suction on the eigenfunctions of first-mode waves. In Figures 4.13a and 4.13b, we show that, whereas in the absence of suction the temperature disturbance has a peak near the generalized inflection point (GIP), the u disturbance has a peak at the upper generalized inflection point when $V_w = 0.3$. The lower generalized inflection point does not create another peak. As the suction velocity increases, the peak of the u disturbance moves toward the wall following the upper inflection point. At $V_w = 0.66$ the generalized inflection point is eliminated but Figure 4.13d shows that the peaks do not vanish at this level of suction. Furthermore, Figure 4.12 shows that the flow is still slightly unstable at this level of suction in spite of the fact that the source of the inviscid instability is eliminated.

The previous calculations are for self-similar boundary layers. In Figure 4.14, we show the variation of the growth rate with streamwise location for two levels of uniform-suction distribution. Suction decreases the growth rates at all locations. Furthermore, it increases the critical Reynolds number and decreases the Reynolds number corresponding to Branch II of the neutral stability curve.

b. Second-Mode Waves

At Mach numbers above 3.0, a second mode of instability emerges. As the Mach number increases this mode becomes more unstable than the first mode. Malik[35] showed that the maximum growth rate of second-mode waves at $M_\infty = 4.5$ and R = 1500 decreases with suction and the frequency of the most amplified wave is considerably shifted to the right. Figure 4.15 shows a set of results similar to those of Malik. It is clear that for some frequencies suction increases the growth rate. Keeping F constant, we show in Figure 4.16 the variation of the growth rate with suction velocity at $M_\infty = 6.0$. As the suction level increases from zero, the growth rate increases until it reaches a maximum at $V_w = 0.22$. As V_w increases further, the growth rate decreases monotonically. The maximum growth rate, however, monotonically decreases with suction velocity as shown in Figure 4.17. In fact the maximum growth rate decreases approximately linearly with suction velocity. The corresponding frequencies are plotted in Figure 4.18. They increase approximately linearly with suction velocity when $V_w > 0.1$.

Next, we plot in Figure 4.19 the variation of the growth rate with wave angle for $V_w = 0$ and 0.1. Even in the case of suction the most unstable second mode is still two-dimensional. The second mode is stabilized for all wave angles by suction.

In Figure 4.20, we show the variation of the maximum growth rate with M_∞ for different levels of suction. The Mach number at which unstable second-mode waves exist increases with suction level. Without suction, this

Mach number is $M_\infty = 3.8$, in agreement with Mack[39,57] . With suction, this Mach number increases to $M_\infty = 4.0$ when $V_w = 0.1$ and to $M_\infty = 4.2$ when $V_w = 0.3$. In addition to shifting the Mach number at which second-mode waves become unstable, suction is very effective in decreasing the maximum growth rate of second-mode waves for lower supersonic and hypersonic Mach numbers, Mach numbers below 5.5. For example, at $M_\infty = 5.0$, the growth rate drops from 0.0043 to 0.0034 when $V_w = 0.1$ and to 0.0025 when $V_w = 0.3$, respectively. However, at higher Mach numbers suction loses its effectiveness. For example, at $M_\infty = 7.0$ the maximum growth rate drops from 0.0025 to 0.0024 when $V_w = 0.1$ and to 0.00216 when $V_w = 0.3$. Figure 4.21 shows the effect of suction on the variation of the frequency corresponding to the maximum growth rate with Mach number for the conditions in Figure 4.20. It is obvious that these frequencies increase by suction at all Mach numbers.

In Figures 4.22a-4.22c, we show the effect of suction on the temperature disturbance; i.e., ζ_5 . In the absence of suction, Figure 4.22a shows that the temperature disturbance has four peaks: the upper two peaks lie on both sides of the generalized inflection point (GIP). When $V_w = 0.3$ the second of these peaks moves downward to the new location of the upper generalized inflection point, as shown in Figure 4.22b. However, it seems that the lower generalized inflection point does not affect the locations of the peaks. When V_w increases to 0.6, Figure 4.22c shows that the upper generalized inflection point considerably moves down and the second peak from the top increases and shifts downward with this generalized inflection point. The third peak from the top is nearly damped out.

Next we investigate the effect of uniform-suction distributions on second-mode waves. Figure 23 shows the variation of the growth rate with streamwise location for different suction levels when $M_\infty = 4.5$. The resulting curves shift considerably to the right as the suction level increases, resulting in a large increase in the critical Reynolds number. The growth rates corresponding to the self-similar suction distribution shown in Figure 4.5 are also plotted in Figure 4.23. Comparing the latter growth rates with the growth rates corresponding to a constant suction of $1.5x10^{-4}$, we note that the self-similar suction distribution is more stabilizing for low R where the suction level is large, and less stabilizing for high R where the suction level is small. Figure 24 shows that suction considerably reduces the N factors. Moreover, the start of the growth of disturbances moves downstream as the suction level increases. The effect of uniform-suction distributions on the variation of the growth rate of second-mode waves with frequency is shown in Figure 4.25. The band of unstable frequencies shifts to the right, as in the self-similar case. The results in Figures 4.23-4.25, however, are for $M_\infty = 4.5$. At this Mach number suction is effective in stabilizing second-mode waves. On the other hand, suction loses its effectiveness for higher Mach numbers. For example, when $M_\infty = 6.0$, Figure 4. 26 shows the variation of the growth rate along the plate for different levels of uniform-suction distributions. Whereas a $v_w = 2x10^{-}4$ reduces the maximum growth rate by 50% when $M_\infty = 4.5$, it reduces the maximum growth rate by only 8% when $M_\infty = 6.0$. Moreover, the peak growth rate widens up as the suction level increases, resulting in a larger area underneath the curve.

To find the effect of suction on the N factor we search for the most dangerous frequency, the frequency that results in an $N = 9.0$ in the shortest distance. In Figure 4.27, we show the variation of the N-factor with streamwise distance for several frequencies. It seems that $F = 30x10^{-6}$ is the most dangerous frequency at $M_\infty = 6.0$. At this relatively low frequency, the first and second modes merge with each other, as shown in Figure 4.28. The growth rates of first-mode waves, however, are very small at this Mach number and suction has no significant effect on them. As shown in Figure 4.28 suction is not very effective in reducing the growth rates of second-mode waves. More importantly, it is clear from Figure 4.29 that suction is not effective in reducing the overall N factor of the disturbance. The effect of suction is restricted to slightly delaying the growth of the disturbance. In the absence of suction, the N factor reaches 9.0 at $R = 5420$, while for the cases of $v_w = 0.5x10^{-4}$, $1.0x10^{-4}$, and $1.5x10^{-4}$, the N factor reaches 9 at R = 5530, 5660, and 5790, respectively. If transition is to occur when N = 9, then a constant suction velocity of $0.5x10^{-4}$, $1.0x10^{-4}$ and $1.5x10^{-4}$ will delay transition by only 4%, 9%, and 14 %, respectively. At $M_\infty = 7.0$, Figure 4.30 shows that the effectiveness of suction significantly decreases. When $V_w = 0.4$, the maximum growth rate decreases by only 20%. When $V_w = 0.8$, the maximum growth rate decreases by 44%.

From the previous results it is obvious that the coexistence of inviscid and viscous instability mechanisms significantly alters the effect of suction on the stability of supersonic and hypersonic boundary layers. If a suction level was enough to stabilize the boundary layer at a certain Mach number, it is not safe

to assume that the same level is enough to stabilize the flow at higher Mach numbers. In general, suction loses its effectiveness in reducing the growth rates of second-mode waves at high Mach numbers. The present results also show that suction has different effects on first- and second-mode waves, especially when a single wave with a fixed frequency is being considered.

Chapter 5

Summary, Conclusions, and Recommendations

We present an analysis of the effects of cooling and suction on the stability of subsonic flows over two-dimensional roughness elements and the effect of suction on the stability of supersonic and hypersonic flows over flat plates, all within the framework of a quasi-parallel, compressible, linear, spatial stability theory. Included in the theory are disturbances due to velocity, pressure, temperature, and transport properties. The mean flows over the two-dimensional roughness elements are calculated using the interacting boundary-layer equations while the flow over the flat plate is calculated by solving either the non-similar or the self-similar boundary-layer equations, depending on the distribution of the suction velocity.

The eigenvalue problem arising from the linearized disturbance equations with the appropriate boundary conditions are solved numerically using a variable-step finite-difference subroutine that solves the two-point

boundary-value problem. For three-dimensional disturbances this subroutine was coupled with a Newton-Raphson iteration scheme to improve convergence. The non-similar boundary-layer equations are solved using central differences in the normal direction and three-points backward differences in the streamwise direction. Results are presented for various suction and temperature distributions.

5.1. Conclusions

A main conclusion that can be drawn from the numerical results is that the coexisting of more than one instability mechanism can significantly complicate the effects of suction and cooling on the stability of boundary-layer flows. In addition, the following conclusions can be drawn:

5.1.1. Influence of Cooling on 2-D Humps and Backward-Facing Steps

(a) While wall cooling slightly reduces the separation bubble on the side of a step or a hump, suction considerably reduces the separation region, especially when a strip with high suction velocity is placed across the separation bubble.

(b) Cooling stabilizes the flow in the attached region, whereas it destabilizes the flow in the separated region due to the movement of the generalized inflection point toward the wall and the increase in the negative flow.

(c) Since the reduction in the separation bubble by cooling is small, the variation of the N factor with wall temperature has a relative minimum. Hence, there exists an optimum wall temperature at which cooling is most effective.

(d) Cooling the wall everywhere except in the separation region has a minor effect on the growth rates and the N factor.

(e) Increasing the Mach number results in a decrease in the optimum wall temperature and in a slight reduction in the effectiveness of cooling.

5.1.2. Influence of Suction on the Flow over 2-D Backward-Facing Steps

(a) While suction reduces vorticity in the attached regions, it increases vorticity in the detached regions. This combined with the movement of the generalized inflection point toward the wall results in a destabilizing effect in the separation region. The attached flow, however, is stabilized by suction.

(b) Due to the large reduction in the separation bubble by suction, the overall N factor decreases monotonically as the suction level increases.

(c) For the same total flow rate, properly distributed suction strips are more effective in stabilizing the flow than a continuous-suction distribution.

(d) For the subsonic flows investigated, both suction and cooling slightly alter the most dangerous frequency.

5.1.3. Influence of Suction on Supersonic and Hypersonic Flow

(a) The coexistence of inviscid and viscous instability mechanisms complicates the effect of suction on the stability of supersonic and hypersonic boundary layers over flat plates. Suction is more effective in stabilizing the viscous mechanism. Suction loses its effectiveness in stabilizing the inviscid mechanism as the Mach number increases.

(b) For low suction levels the maximum growth rate of first-mode waves decreases as the Mach number increases, whereas for high suction levels the maximum growth rate increases with M_∞ for low Mach numbers, and decreases as M_∞ increases for high Mach numbers. In general, the stabilizing

effect of suction on first-mode waves decreases significantly as the Mach number increases.

(c) Suction slightly alters the wave angles corresponding to the maximum growth rates. Moreover, suction stabilizes first-mode waves for all wave angles.

(d) Suction stabilizes first-mode waves at all frequencies and Reynolds numbers. Nevertheless, the frequency and the Reynolds number corresponding to the maximum growth rate increase slightly as suction increases.

(e) The frequency band corresponding to growing second-mode disturbances significantly shifts to the right as the suction level increases. A similar trend is true for the Reynolds numbers corresponding to growing second-mode waves. This is true for non-similar and self-similar velocity profiles.

(f) Whereas for relatively low Mach numbers suction is effective in stabilizing second-mode waves, it looses its effectiveness for high Mach numbers. The reduction in the N factor becomes insignificant for Mach numbers greater than 6.0 and the effect of suction is restricted to slightly delaying the growth of disturbances.

(g) The most growing second mode continues to two-dimensional when suction is applied.

5.2. Recommendations

The results obtained throughout Chapters 2 , 3, and 4 point to the danger of extrapolation of controls designed for the case of one instability mechanism to the case with more than one instability mechanism.

More specific recommendations for future work are listed below.

5.2.1. Flows Over Roughness Elements

- investigation of the effect of suction and cooling on the receptivity and Goertler, and secondary instabilities.
- extension of the present analysis to supersonic flows.
- investigation of the effect of suction and cooling on other separated and inflectional flows.
- investigation of the effect of suction and cooling on the stability of flows over roughness elements on swept wings where the cross-flow instability plays an important role.
- conduction of detailed experiments in order to validate the present results.

5.2.2. Smooth Surfaces

- investigation of the influence of suction strips and their optimum distributions.

- taking into consideration real gas effects, flow dissociation, etc.

- performance of detailed experiments to validate the theoretical results.

- investigation of the effects of suction on supersonic flows over swept wings.

- analysis of the combined effects of suction and heat transfer on the stability of flows over two-dimensional flows and swept-back wings.

References

1. Schlichting, H.,"Boundary-Layer Theory," McGraw-Hill Book Co., New York, 1979.

2. Hefner, J. N. and Bushnell, D. M., "An Overview of Concepts for Aircraft Drag Reduction," von Karman Institute, Rhode-st.-Genese Belgium, AGARD-R-654, March 28 - April 1, 1977, pp. 1.1-1.30.

3. Pfenninger, W., "USAF and Navy Sponsored Northrup LFC Research Between 1949 and 1967," AGARD/VKI Special Course for Drag Reduction, 1977, pp. 3.1-3.75.

4. Kosin, R.E., "Laminar Flow Control by Suction as Applied to the X-21 Airplane," J. Aircraft, Vol. 2, 1965, pp 384-390.

5. Young, A. D.(ed.), "Special Course on Concepts for Drag Reduction," von Karman Institute, Rhode-St-Genese, Belgium, AGARD-R-654, March 28 - April 1, 1977.

6. Whitcomb, R. T., "Methods for Reducing Subsonic Drag Due to Lift," Presented at the AGARD/VKI Special course on Concepts for Drag Reduction, Rhode-st.-Genese, Belgium, March 28 - April 1, 1977, pp. 2.1-2.38.

7. Eppler, R. and Fasel, H. (eds.), "Laminar-Turbulent Transition," IUTAM Symposium, Stuttgart, Germany, September 16-22. 1979, Springer-Verlag, New York, 1980.

8. Schubauer, G. B., and Skarmstad, K. H., "Laminar Boundary Layer Oscillation and Transition on a Flat Plate," J. Aero. Sci., Vol. 14, 1947, pp. 69-72.

9. Herbert, Th., "Secondary Instability of Plane Shear Flows - Theory and Applications," in Laminar-Turbulent Transition, ed. V. V. Koszlov, 1985, pp. 9-20.

10. Nayfeh, A. H. and Masad, J. A., "Subharmonic Instability in Boundary-Layers," submitted for publication, Phys. Fluids.

11. Saric, W. S. and Nayfeh, A. H., "Nonparallel Stability of Boundary-Layer Flows," Phys. Fluids, Vol. 18, 1975, pp. 945-950.

12. Smith, A. M. O., "Transition, Pressure Gradient, and Stability Theory," IX International Congress for Applied Mechanics, Brussels, 1956.

13. Van Ingen, J. L., "A Suggested Semiempirical Method for the Calculation of the Boundary-Layer Transition Region," Dept. of Aero. Eng., Univ. of Technology, Delft, Holland, Rep. VTH-71 and 74, 1956.

14. Jaffe, N. A., Okamura, J. J., and Smith, A. M. O., "Determination of Spatial Amplification Factors and Their Application to Predicting Transition," AIAA J., Vol. 8, 1970, pp. 301-308.

15. Nayfeh, A. H., Ragab, S. A., and Al-Maaitah, A. A., "Effect of Bulges on the Stability of Boundary Layers," Phys. Fluids, Vol. 31, 1988, pp. 796-806.

16. Al-Maaitah, A. A., "Effect of Roughness Element on the Stability of Boundary-Layers," VPI&SU, M.S. Thesis, 1987.

17. Goldstein, M. E., "Scattering of Acoustic Waves into Tollmien-Schlichting Waves by Small Streamwise Variation in Surface Geometry," J. Fluid Mech., Vol. 154, 1985, pp. 509-528.

18. Nayfeh, A. H., and Al-Maaitah, A. A.,"Influence of Streamwise Vortices on Tollmien-Schlichting Waves," Phys. Fluids, Vol. 31, 1988, pp. 3543-3549.

19. Malik, M. R., "Wave-Interaction in Three-Dimensional Boundary Layers," AIAA Paper No. 86-1129, 1986.

20. Holmes, B. J., O'bara, C. J., and Yip, L. P., "Natural Laminar Flow Flight Experiments on Modern Airplane Surface," NASA TP 2256, 1984.

21. Holmes, B. J., O'bara, C. J., Martin, G. L., and Domack, C. S., "Manufacturing Tolerances for Natural Laminar Flow Air Frame Surfaces," NASA CP 2413, 1986.

22. O'bara, C. J. and Holmes, B. J., "Flight Measured Laminar Boundary-Layer Transition Phenomena Including Stability Theory Analysis," NASA TP 2414, 1985.

23. Fage, A., "The Smallest Size of Spanwise Surface Corrugation Which Affect Boundary Layer Transition on an Airfoil," British Aeronautical Research Council, 2120, 1943.

24. Klebanoff, P. S. and Tidstrom, K. R., "Mechanism by which a Two-Dimensional Roughness Element Induces Boundary-Layer Transition," Phys. Fluids, Vol. 15, 1972, pp. 1173-1188.

25. Bestek, H., Gruber, K., and Fasel, H., "Numerical Investigation of Unsteady Laminar Boundary Layer Flows Over Backward-Facing Steps," presented

at The Fourth Asian Congress of Fluid Mechanics, Hong Kong, August 19-23, 1988.

26. Burnel, S., Gougat, P. and Martin, F., "The Influence of Local Deformation on the Development of Natural Instability in a Laminar Boundary Layers," NASA TM-76558, 1981.

27. Gouget, P. and Martin, F., "Existence of a Natural Instability not Predicted by Theory and Connected to a Wall Deformation in a Laminar Boundary Layer," NASA TM-76559, 1981.

28. Vijgen, P. M., Dodbele, S. S., Holmes, B. J., and Van Dam, C. P., "Effect of Compressibility on Design and Subsonic Fuselages for Natural Laminar Flow," J. Aircraft, Vol. 25, 1988, pp. 776-782.

29. Hastings, E. C., Schoenster, J. A., O'bara, C. J., and Dodbele, S. S., "Flight Research on Natural Laminar Flow Nacelles: A Progress Report," AIAA Paper No. 86-1629, 1986.

30. Asrar, W. and Nayfeh, A. H., "Nonparallel Stability of Heated Two-Dimensional Boundary Layers," Phys. Fluids, Vol. 28, 1985, pp. 1263-1272.

31. Wazzan, A. R., Okamura, T. T., and Smith, A. M. O., "The Stability of Water Flow Over Heated and Cooled Flat Plates," J. Heat Trans., Vol. 90, 1986, pp. 109-121.

32. Wazzan, A. R., Okamura, T. T., and Smith, A. M. O., "The Stability and Transition of Heated and Cooled Incompressible Laminar Boundary Layers," Proceedings of the 4th International Heat Transfer Conference, edited by U. Grigul and E. Hahne (Elsevier, Amsterdam, 1970), Vol. 2, Paper No. FC1.4.

33. Potter, M. C. and Garber, E., "Stability of Plane Poiseuille Flow with Heat Transfer," Phys. Fluids, Vol. 15, 1972, pp. 387-391.

34. Mack, L. M., "Boundary-Layer Stability Theory," Jet Propulsion Lab, Document 900-277 (Rev. A), Pasadena, CA, 1969.

35. Malik, M. R., "Predictions and Control of Transition in Hypersonic Boundary Layers," AIAA Paper No. 87-1414, 1987.

36. Davis, R. T., "A Procedure for Solving the Compressible Interacting Boundary-Layer Equations for Subsonic and Supersonic Flows," AIAA Paper No. 84-1614, 1984.

37. Davis, R. T. and Werle, M. J., "Progress on Interacting Boundary-Layer Computations at High Reynolds Number," in Numerical and Physical

Aspects of Aerodynamics Flows, edited by T. Cebeci, Springer, Berlin, 1982, pp. 187-198.

38. Ragab, S. A., Nayfeh, A. H., and Krishna, R. C., "Stability of Compressible Boundary Layers over Smooth Backward- and Forward-Facing Steps," submitted for publication, Phys. Fluids.

39. Chang, K. C., Alemdaroglu, N., Mehfa, U., and Cebeci, T., "Further Comparison of Interactive Boundary-Layer and Thin-Layer Navier-Stokes Procedures," J. Aircraft, Vol. 25, 1988, pp. 897-903.

40. Pereyra, V., "PASAV3: An Adaptive Finite Difference Fortran Program for First Order Nonlinear, Ordinary Boundary Value Problem," in Lecture Notes in Computer Science, edited by B. Childs, M. Scott, J. W. Daniel, E. Denman, and P. Nelson, Springer, Berlin, 1976, pp. 67-88.

41. Scott, M. R. and Watts, H. A., "Computational Solution of Linear Two-Point Boundary Value Problems via Orthonormalization," SIAM J. Num. Anal., Vol. 14, 1977, pp. 40-70.

42. Cebeci, T. and Egan, D. A., "Effect of Wave-like Roughness on Transition," AIAA Paper No. 88-0139, 1988.

43. Van Dam, C. P. and Holmes, B. J., "Boundary-Layer Transition Effects on Airplane Stability and Control," J. Aircraft, Vol. 25, 1988, pp. 702-709.

44. Carmichael, B. H., Whites, R. C., and Pfenninger, W., "Low Drag Boundary Layer Suction Experiment in Flight on the Wing Glove of a F-94A Airplane," Northrup Aircraft Rpt. No. NAI-57-1163 (BLC-101), 1957.

45. Carmichael, B. H. and Pfenninger, W., "Surface Imperfection Experiments on a Swept Laminar Suction Wing," Northrup Aircraft Rpt. No. NOR-59-454 (BLC-124), 1959.

46. Carmichael, B. H., "Surface Waviness Criteria for Swept and Unswept Laminar Suction Wings," Northrup Aircraft Rpt. No. NOR-59-438 (BLC-123), 1957.

47. Spence, O. A. and Randall, D. G., "The Influence of Surface Waves on the Stability of a Laminar Boundary Layer with Uniform Suction," British Aeronautical Research Council 2241, 1954.

48. Lin, C. C., "On the Stability of Two-Dimensional Parallel Flows," Q. App. Math., Vol. 3, 1945, pp. 117-142, 218-234, 277-301.

49. Nayfeh, A. H. and Reed, H. L., "Stability of Flows Over Axisymmetric Bodies with Porous Suction Strips," Phys. Fluids, Vol. 28, 1985, pp. 2990-2998.

50. Reed, H. L. and Nayfeh, A. H., "Numerical Perturbation Techniques for Stability of Flat-Plate Boundary Layers with Suction," AIAA J., Vol. 24, 1986, pp. 208-214.

51. Reynolds, G. A. and Saric, W. S., "Experiments on the Stability of Flat-Plate Boundary Layers with Suction," AIAA J., Vol. 24, 1986, pp. 202-207.

52. Saric, W. S. and Reed, H. L., "Effect of Suction and Weak Mass Injection on Boundary-Layer Transition," AIAA J., Vol. 24, 1986, pp. 383-389.

53. Hahn, M. and Pfenninger, W., "Prevention of Transition over a Backward Step by Suction," J. Aircraft, Vol. 20, 1973, pp. 618-622.

54. Srokowski, A. J. and Orszag, S. A., "Mass Flow Requirements for LFC Wing Design," AIAA Paper No. 77-1222, 1977.

55. Hefner, J. N. and Bushnell, D. M., "Application of Stability Theory to Laminar Flow Control," AIAA Paper No. 79-1493, 1979.

56. Lekoudis, S. G., "Stability of Boundary Layers over Permeable Surfaces," AIAA Paper No. 87-203, 1987.

57. Mack, L. M., "Special Course on Stability and Transition of Laminar Flow," AGARD Report No. 709.

58. Nayfeh, A. H., "Stability of Compressible Boundary Layers," Proceedings of the Transonic Symposium, NASA-Langley Research Center, Hampton, VA, April 9-12, 1988.

59. Mack. L. M., "Stability of the Compressible Laminar Boundary Layer According to a Direct Numerical Solution," in AGARD 97, Part I, 1965, pp. 329-345.

60. Wazzan, A. R., Taghavi, H., and Keltner, G, "The Effect of Mach Number on the Spatial Stability and Adiabatic Flat Plate Flow to Oblique Disturbances," Phys. Fluids, Vol. 27, 1984, pp. 331-341.

61. Mack, L. M., "Remarks on Disputed Numerical Results in Compressible Boundary-Layer Stability Theory," Phys. Fluids, Vol. 27, 1984, pp. 342-347.

62. El-Hady, N. M. and Nayfeh, A. H., "Nonparallel Stability of Compressible Boundary-Layer Flows," AIAA Paper No. 80-0277, 1980.

63. Malik, M. R., "Numerical Methods for Hypersonic Boundary Layer Stability," HTC Report No. 88-6, 1988.

64. Lees, L. and Lin, C. C., "Investigation of the Stability of the Laminar Boundary Layer in Compressible Fluid," NASA Technical Note, No. 1115, 1946.

Attention Patron:

Page 78 repeated in numbering

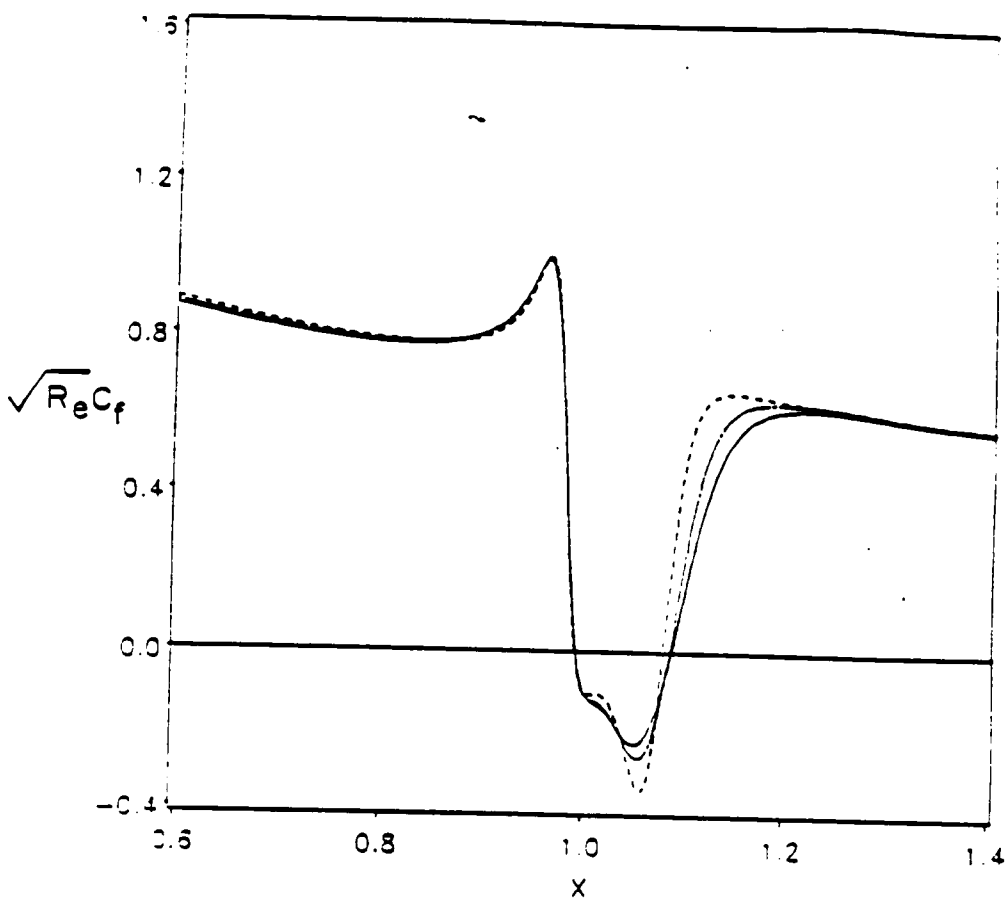

Figure 2.1. Effect of wall cooling on the shear coefficient for a flow over a backward-facing step when the step height = 0.003, step slope = - 4.34695, M_∞ = 0.5, Re = 1.0x10^6, and Pr = 0.72: ___ T_w/T_{ad} = 1.0, ___ _ T_w/T_{ad} = 0.8, and - - - T_w/T_{ad} = 0.55 .

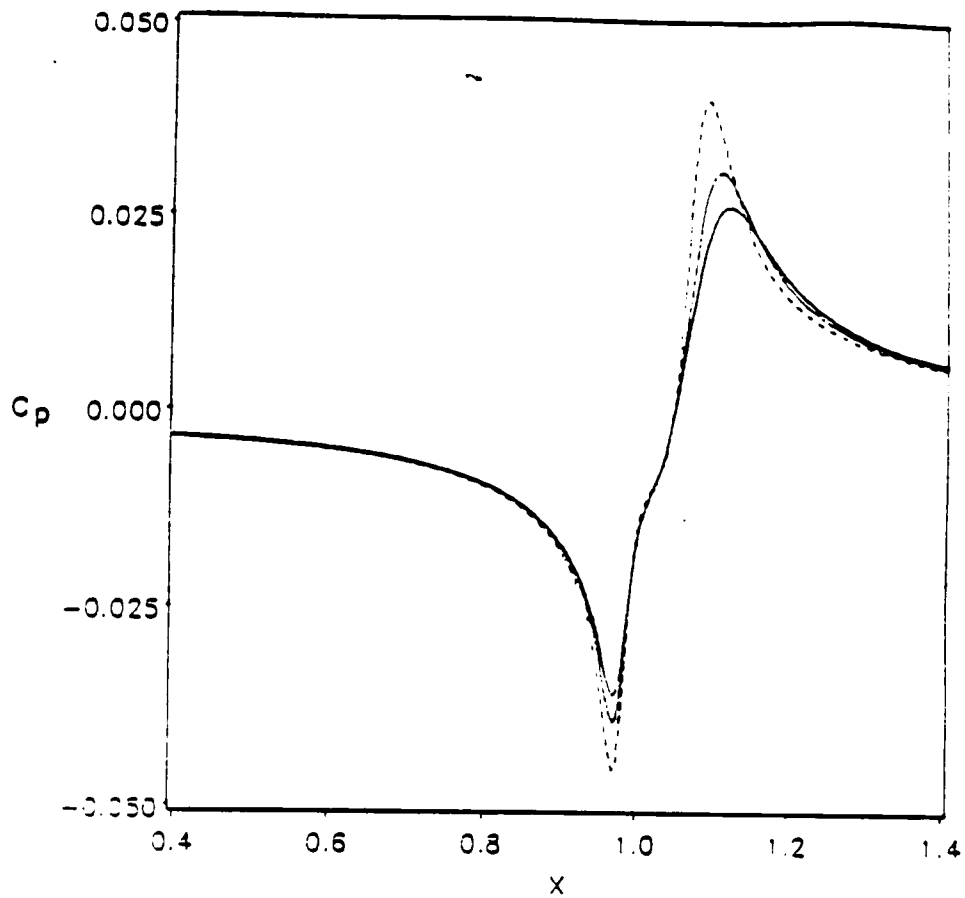

Figure 2.2. Effect of wall cooling on the pressure coefficients for a flow over a backward-facing step when the step height = 0.003, step slope = -4.34695, $M_\infty = 0.5$, $Re = 1.0 \times 10^6$, and Pr = 0.72: ___ $T_w/T_{ad} = 1.0$, ___ _ $T_w/T_{ad} = 0.8$, and - - - $T_w/T_{ad} = 0.55$.

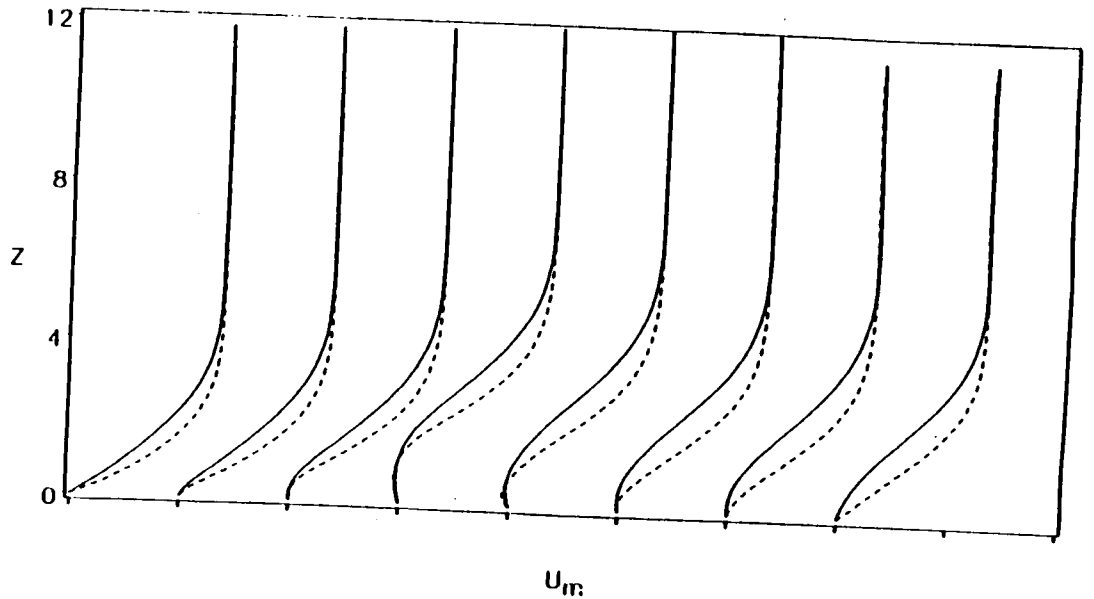

Figure 2.3. Effect of wall cooling on the streamwise velocity profiles along the plate when the step height = 0.003, step slope = -4.34965, $M_\infty = 0.5$, $Re = 1.0x10^6$, and Pr = 0.72. The profiles correspond to the following values of R starting from left to right: 985, 992, 997, 1012, 1027, 1037, 1042, and 1051. The separation bubble for the cooled wall starts at R = 997 and ends at R = 1037: ___ $T_w/T_{ad} = 1.0$, and - - - $T_w/T_{ad} = 0.55$.

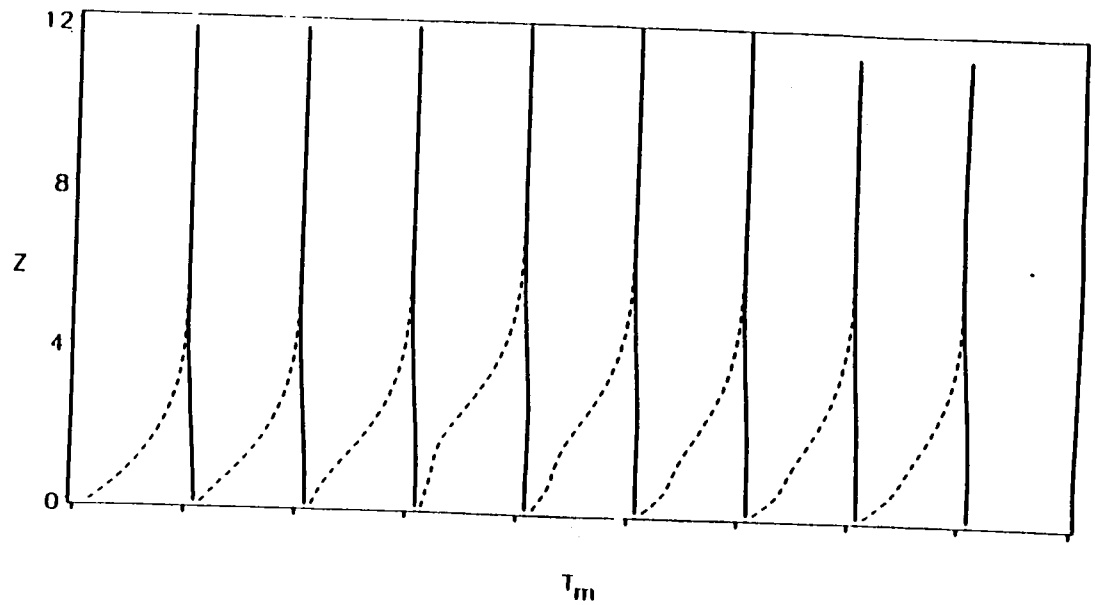

Figure 2.4. Effect of wall cooling on the temperature profiles along the plate when the step height = 0.003, step slope = -4.34965, $M_\infty = 0.5$, $Re = 1.0x10^6$, and Pr = 0.72. The profiles correspond to the following values of R starting from left to right: 985, 992, 997, 1012, 1027, 1037, 1042, and 1051. The separation bubble for the cooled wall starts at R = 997 and ends at R = 1037: ___ $T_w/T_{ad} = 1.0$, and - - - $T_w/T_{ad} = 0.55$.

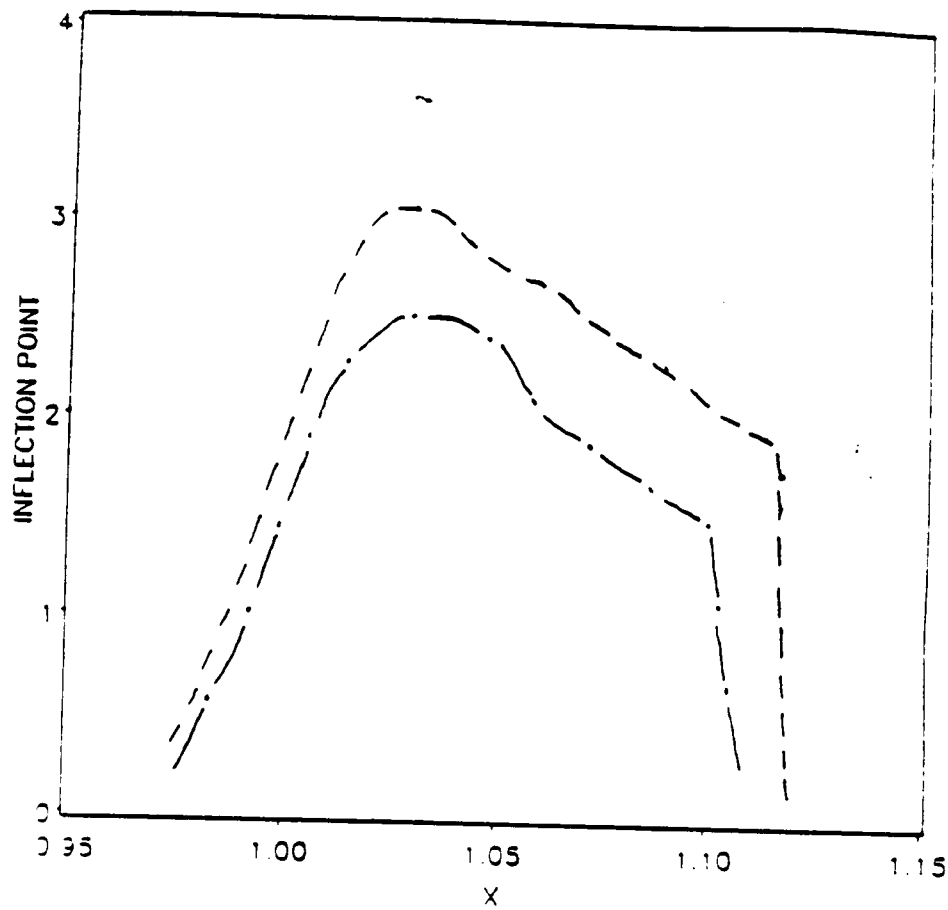

Figure 2.5. Variation of the inflection point across the separation region for adiabatic and cooled-wall conditions when the step height = 0.003, step slope = – 4.34695 , M_∞ = 0.5, Re = 1.0x10^6, and Pr = 0.72: - - - T_w/T_{ad} = 0.8, and ___ T_w/T_{ad} = 1.0.

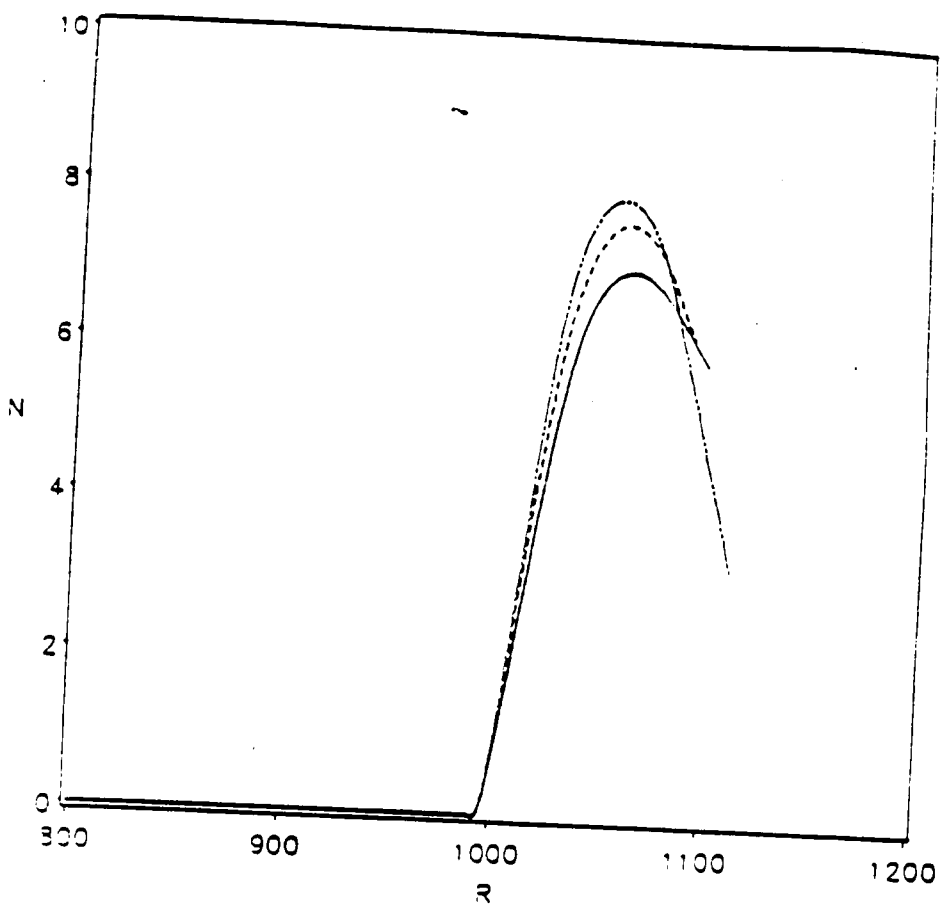

Figure 2.6. The influence of the frequency on the N factor when $T_w = 0.55\ T_{\infty}$, step height = 0.003, step slope = - 4.34965, $M_{\infty} = 0.5$, $Re = 10x10^{-6}$, and Pr = 0.72: ___ $F = 40x10^{-6}$, – – – $F = 60x10^{-6}$, and — ___ $F = 50x10^{-6}$.

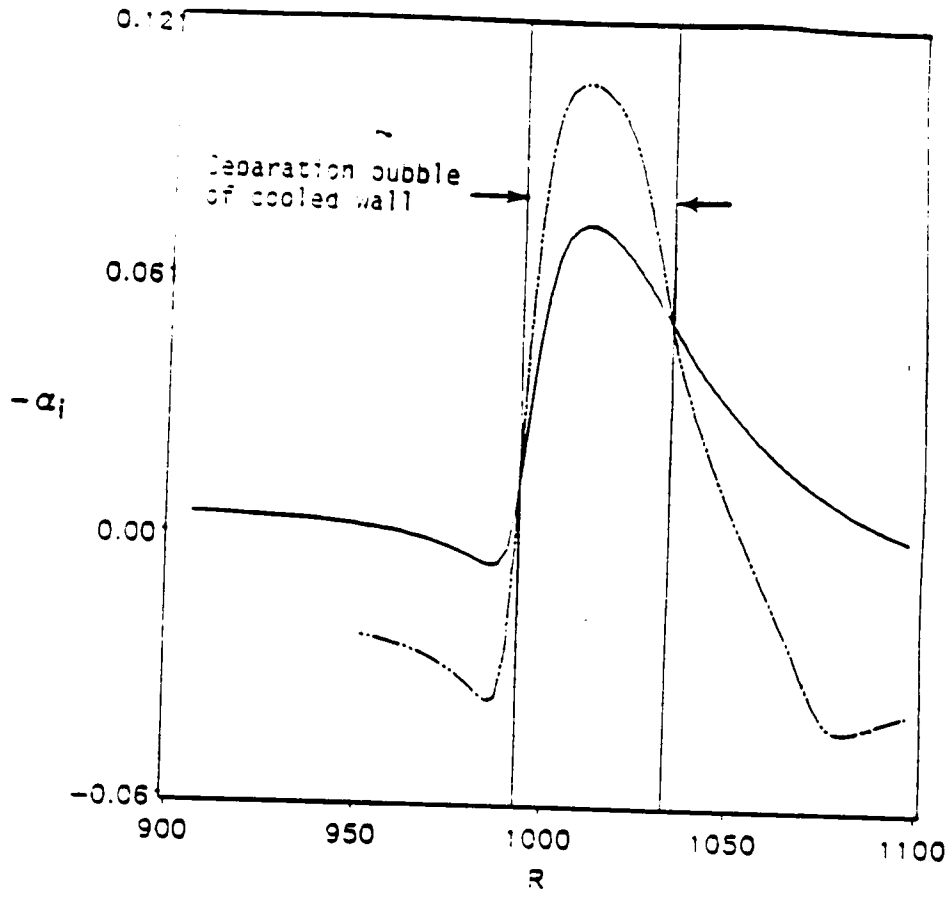

Figure 2.7. The growth rates for the flow over cooled and adiabatic walls when the step height = 0.003, step slope = - 4.34965, $M_\infty = 0.5$, $Re = 10x10^6$, Pr = 0.72, and $F = 50x10^{-6}$: ____ $T_w/T_{wd} = 1.0$ and ____ _ _ $T_w/T_{wd} = 0.55$.

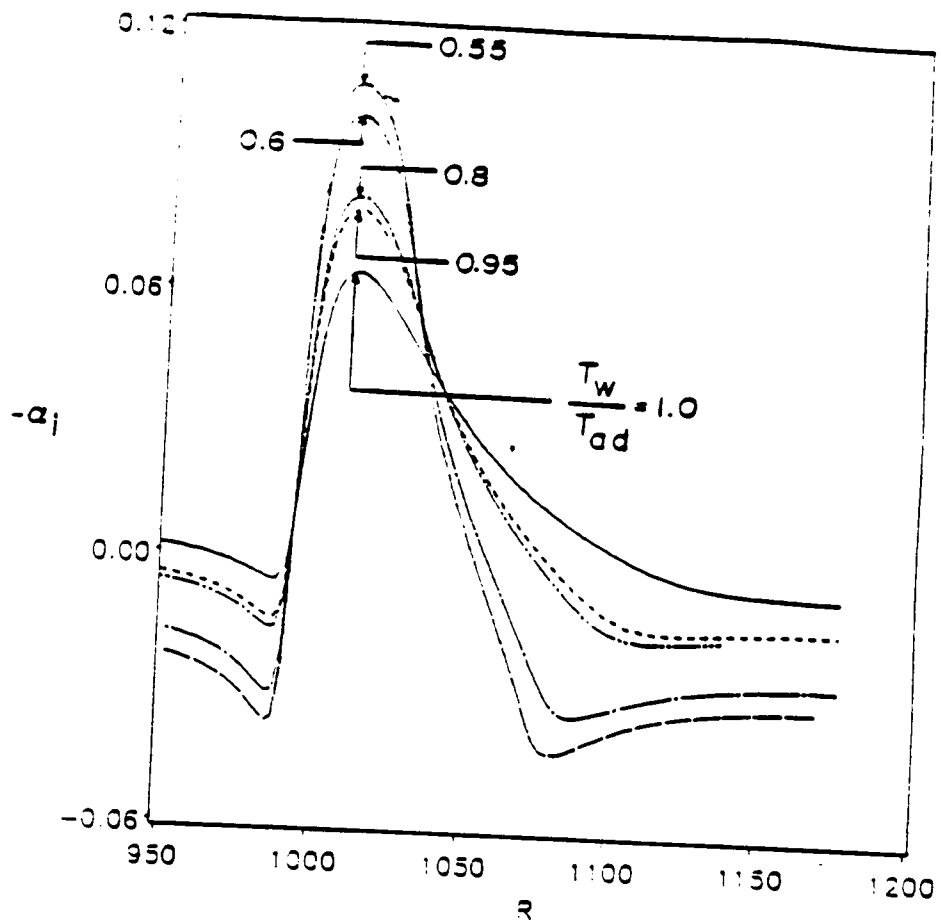

Figure 2.8. Variation of the growth rates with wall temperature: step height = 0.003, step slope = - 4.34695, M_∞ = 0.5, Re = 1.0×10^6, Pr = 0.72, and F = 50×10^{-6}.

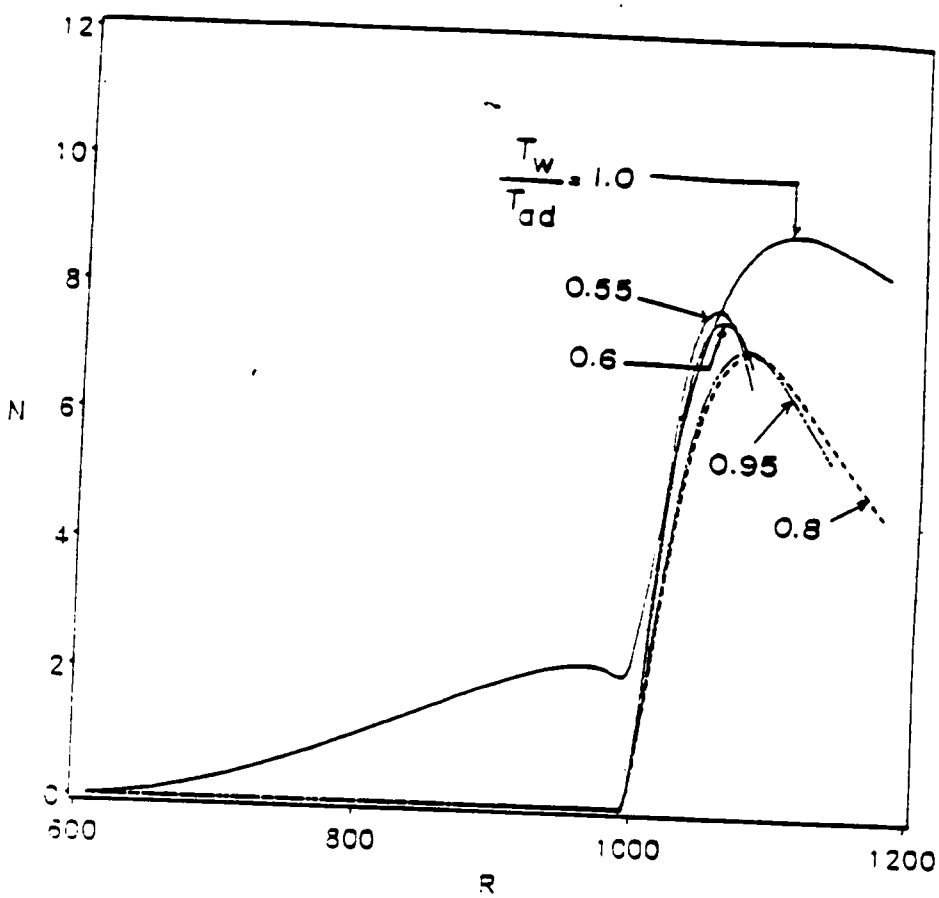

Figure 2.9. Variation of the amplification factor with wall temperature: step height = 0.003, step slope = - 4.34695, M_∞ = 0.5, Re = 1.0×10^6, Pr = 0.72, and F = 50×10^{-6}.

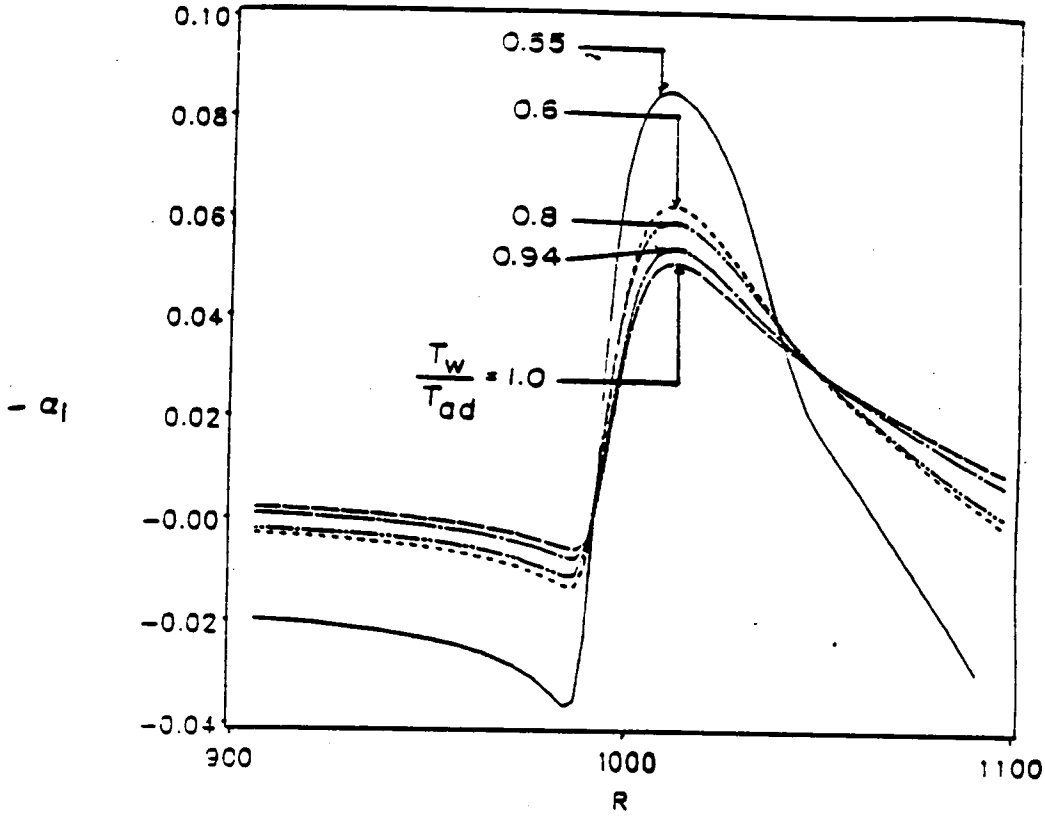

Figure 2.10. Variation of the growth rates with wall temperature: step height = 0.003, step slope = - 4.34695, M_∞ = 0.8, Re = 1.0×10^6, Pr = 0.72, and F = 50×10^{-6}.

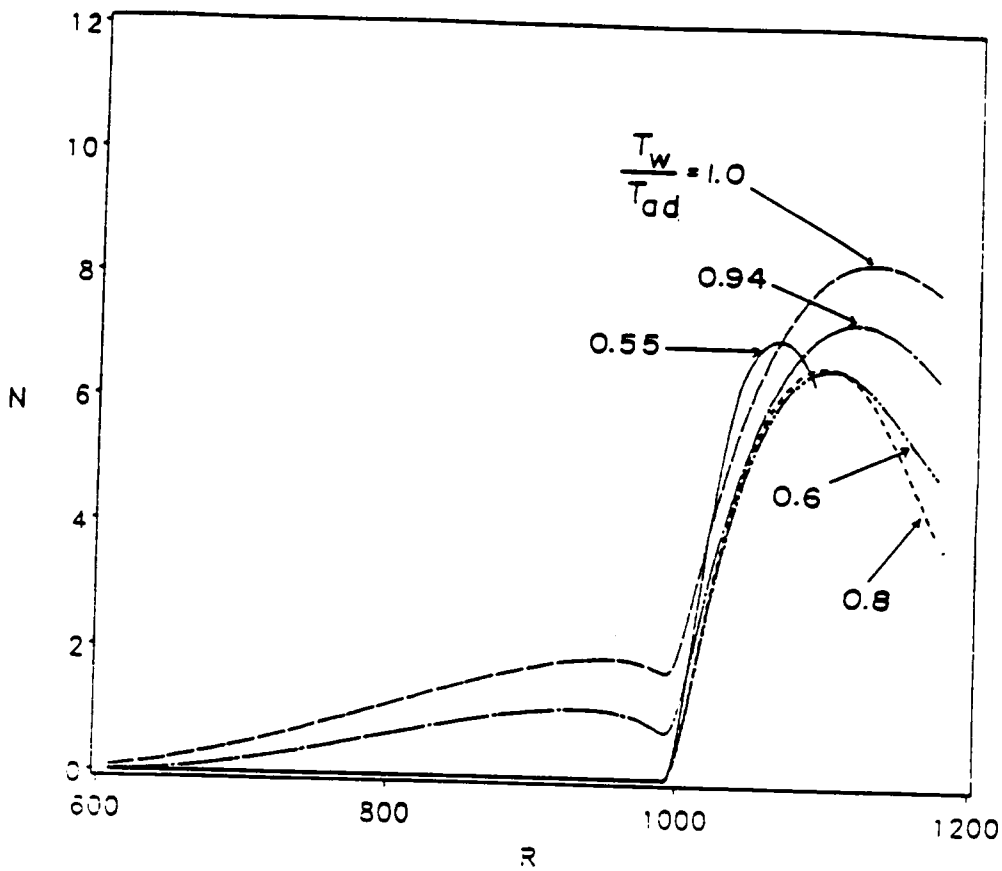

Figure 2.11. Variation of the amplification factor with wall temperature: step height = 0.003, step slope = - 4.34695, M_∞ = 0.8, Re = 1.0×10^6, Pr = 0.72, and F = 50×10^{-6}.

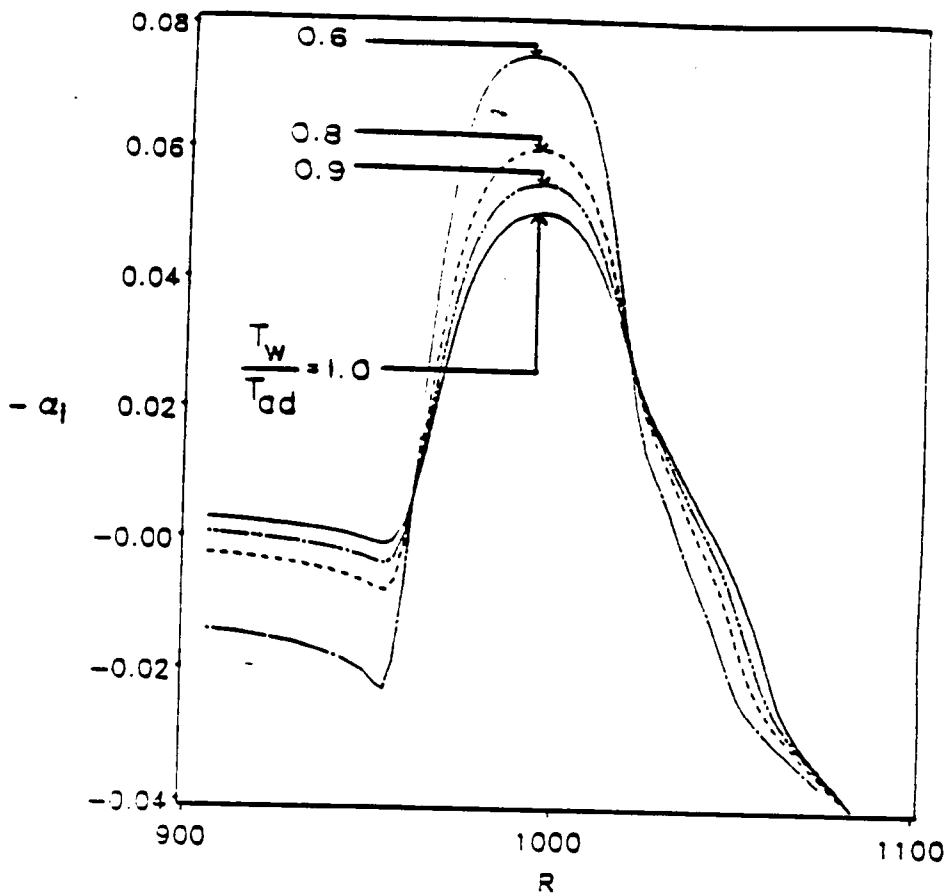

Figure 2.12. Variation of the growth rates with wall temperature for a cubic hump: hump height = 0.003, $x_w = 0.2$, $M_\infty = 0.8$, $Re = 1.0x10^6$, $Pr = 0.72$, and $F = 50x10^{-6}$.

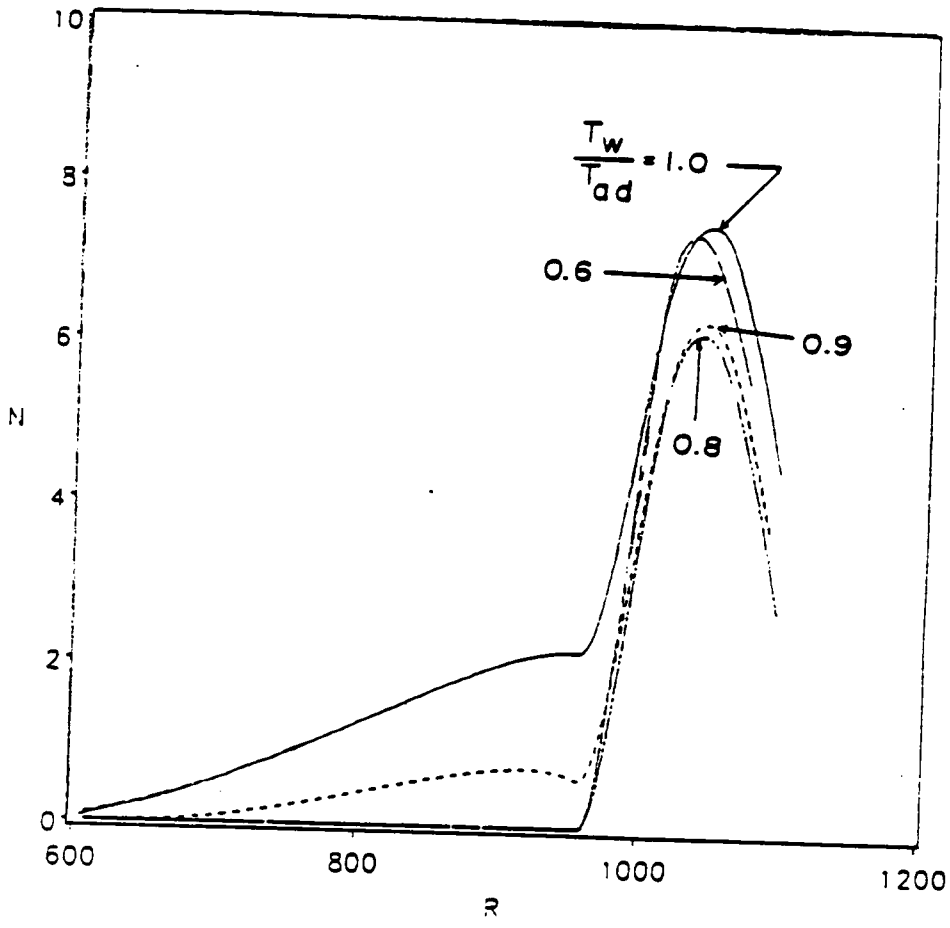

Figure 2.13. Variation of the amplification factor with wall temperature for a cubic hump: hump height = 0.003, x_w = 0.2, M_∞ = 0.8, Re = 1.0×10^6, Pr = 0.72, and $F = 50 \times 10^{-6}$.

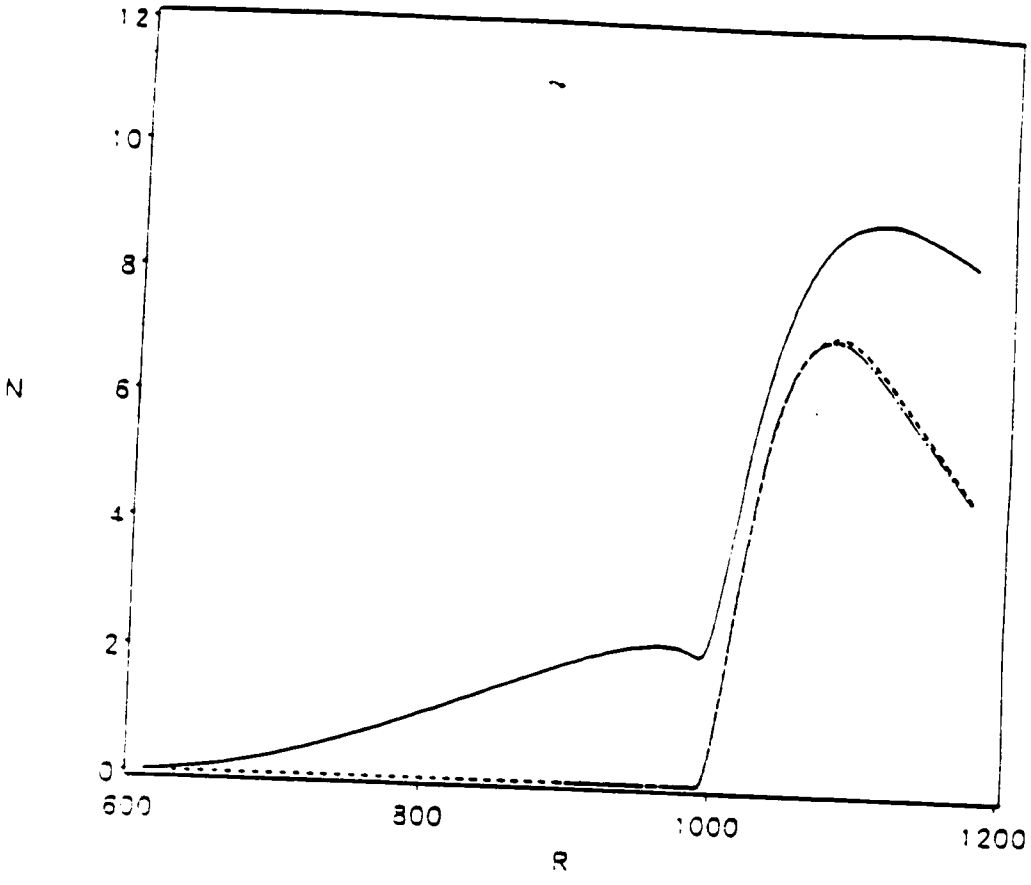

Figure 2.14. Effect of an adiabatic separation region on the amplification factor: step height = 0.003, step slope = - 4.34695, M_∞ = 0.5, Re = 1.0×10^6, Pr = 0.72, and F = 50×10^{-6}: ___ adiabatic wall, __ T_w/T_{ad} = 0.8, - - - cooled everywhere except in separation region.

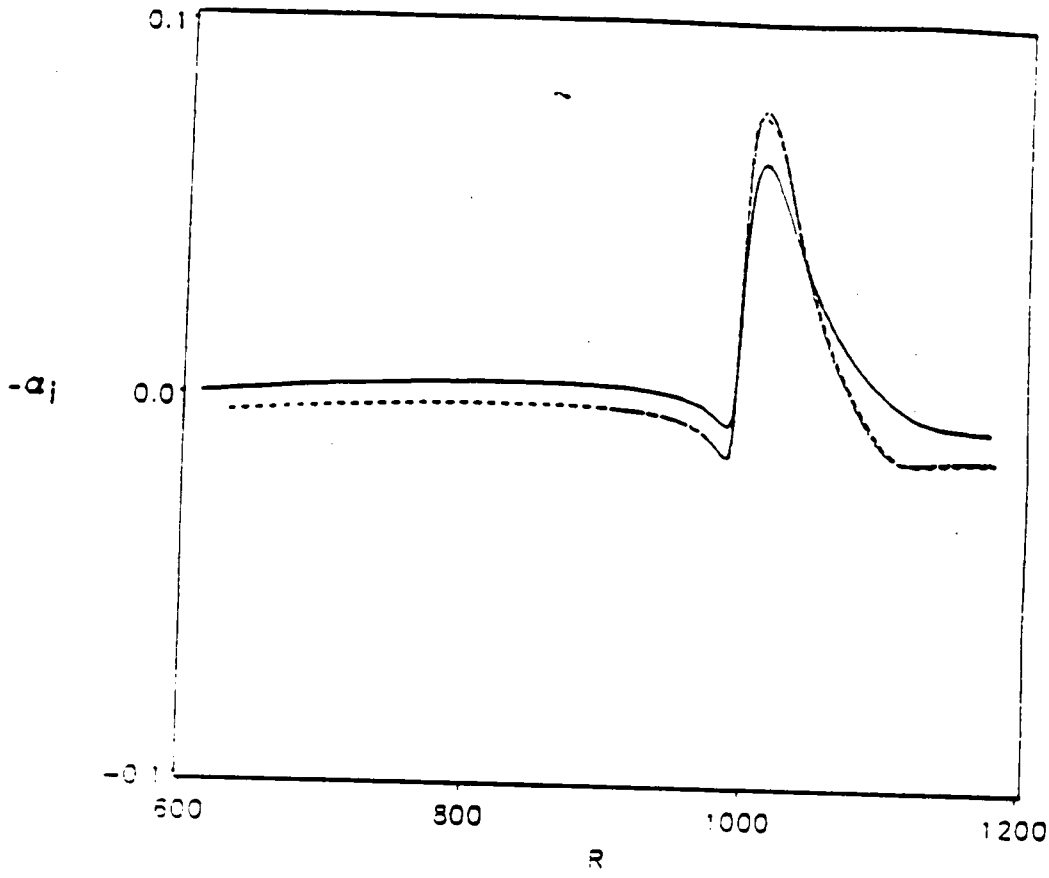

Figure 2.15. Effect of an adiabatic separation region on the growth rates: step height = 0.003, step slope = - 4.34695, M_∞ = 0.5, Re = 1.0×10^6, Pr = 0.72, and F = 50×10^{-6} : ___ adiabatic wall, __ $T_w/T_{ad} = 0.8$, - - - cooled everywhere except in separation region.

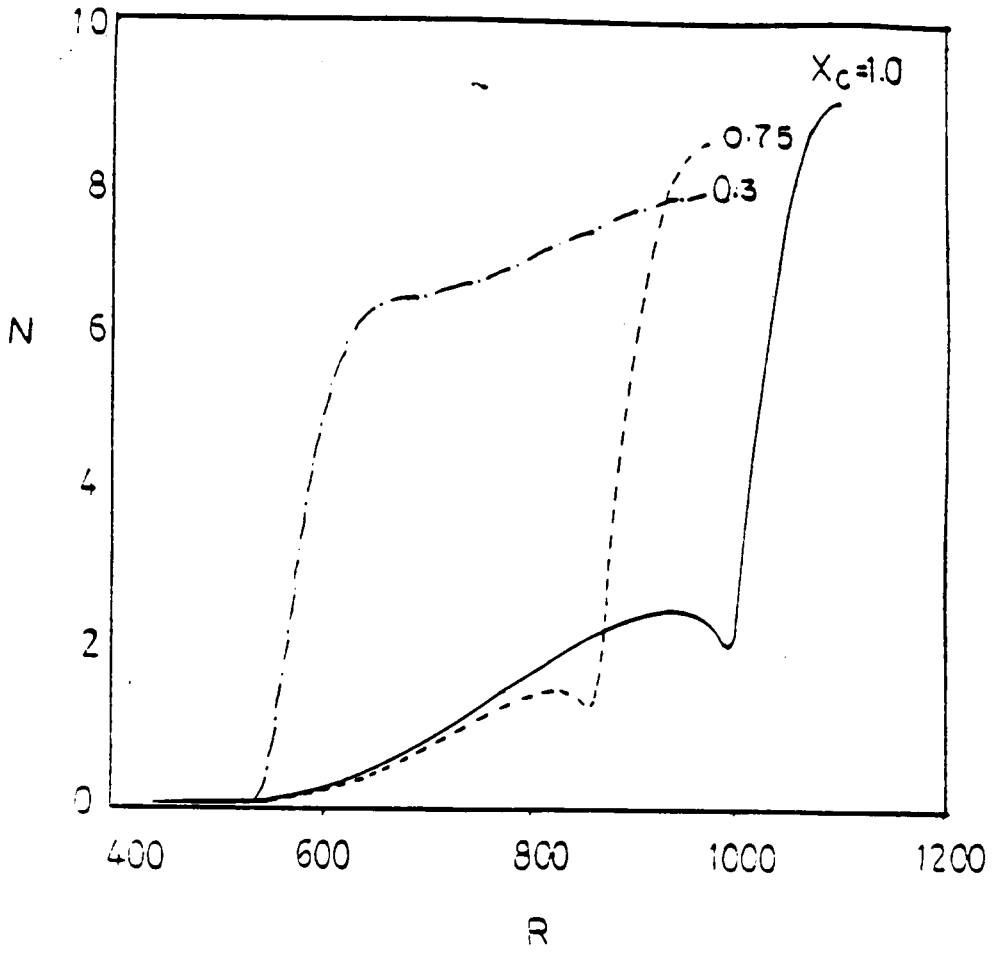

Figure 2.16. Effect of step location on the amplification factor: step height = 0.003, step slope = - 4.34695, M_∞ = 0.5, Re = 1.0×10^6, Pr = 0.72, and F = 50×10^{-6}.

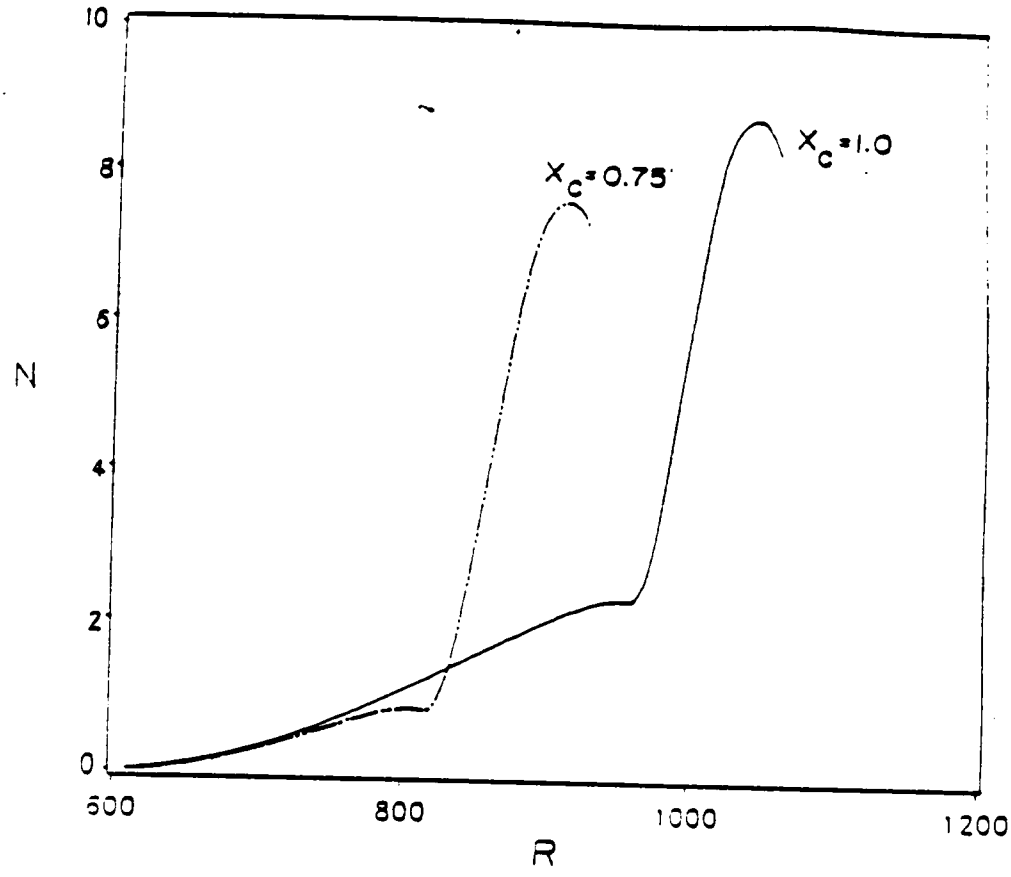

Figure 2.17. Effect of hump location on the amplification factor: hump height = 0.003, hump width = 0.2, M_∞ = 0.5, Re = 1.0×10^6, Pr = 0.72, and $F = 50 \times 10^{-6}$.

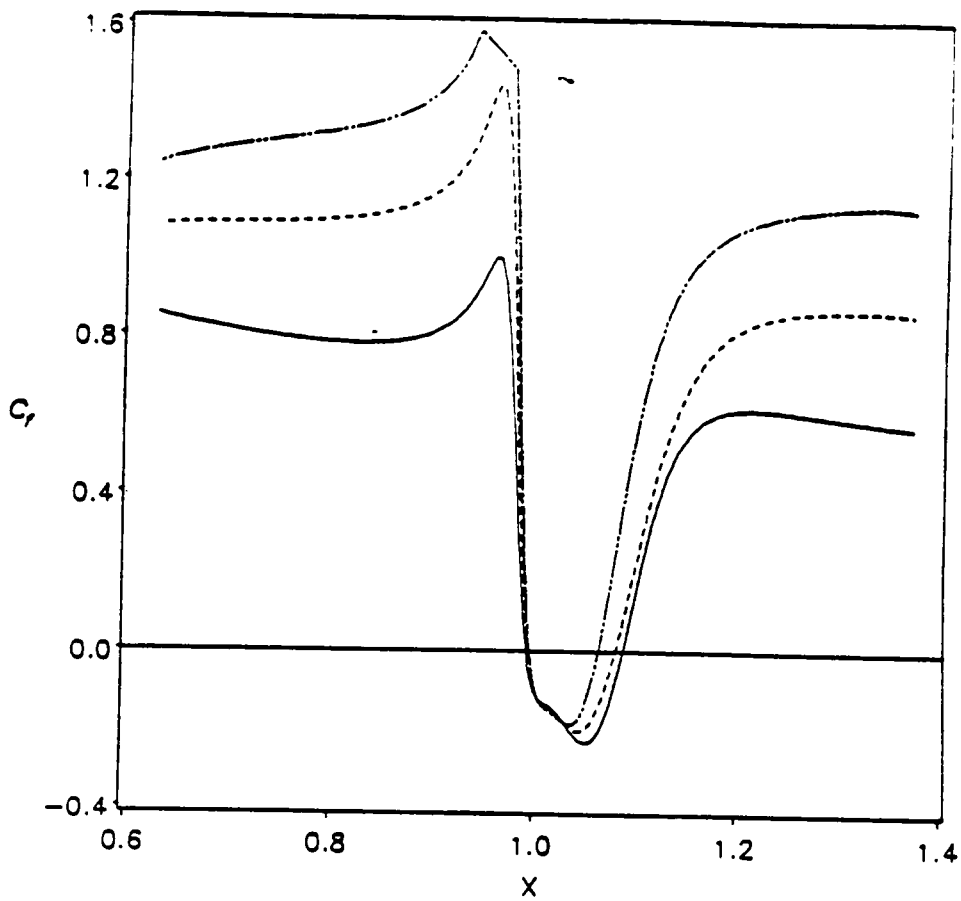

Figure 3.1. Effect of wall suction on the shear coefficient for a flow over a backward-facing step when the step height = 0.003, step slope = - 4.35, M_∞ = 0.8, Re = $1.0x10^6$, and Pr = 0.72: ___ $v_w = 0.0$, - - - $v_w = 3.0x10^{-4}$, and __.__ $v_w = 5.10x10^{-4}$.

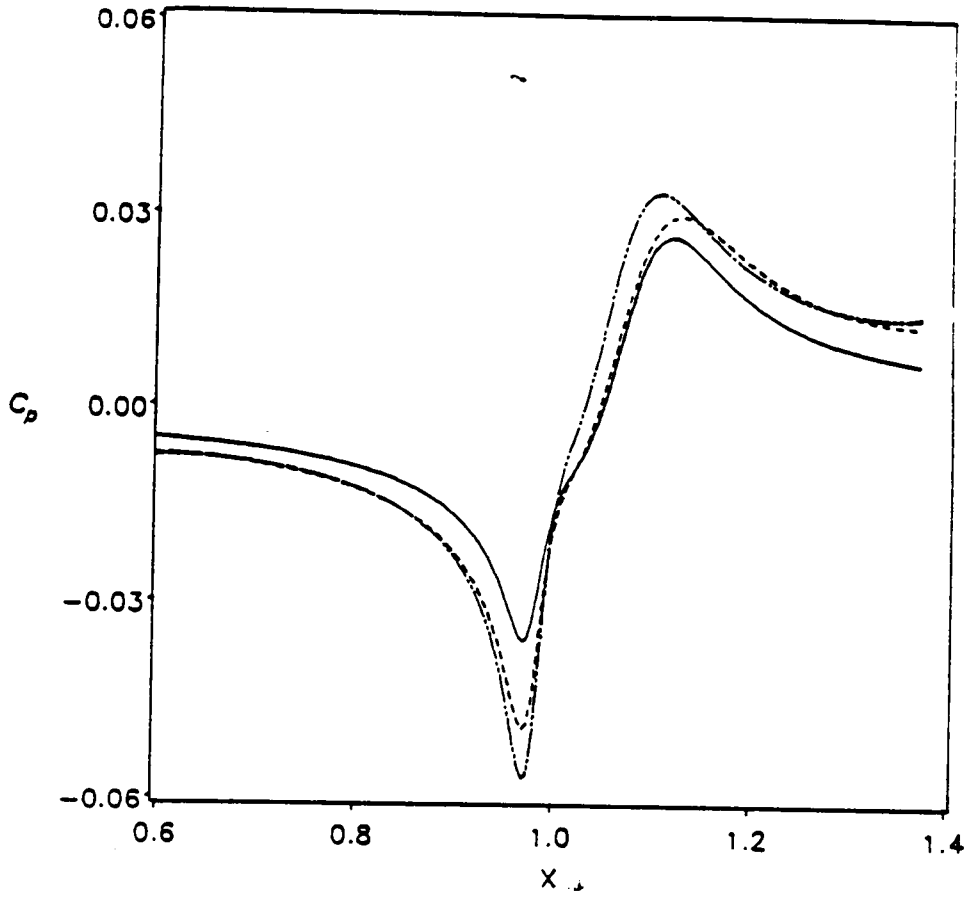

Figure 3.2. Effect of wall suction on the pressure coefficients for a flow over a backward-facing step when the step height = 0.003, step slope = -4.35, $M_\infty = 0.8$, $Re = 1.0 \times 10^6$, and Pr = 0.72: ___ $v_w = 0.0$, - - - $v_w = 3.0 \times 10^{-4}$, and __·__ $v_w = 5.0 \times 10^{-4}$.

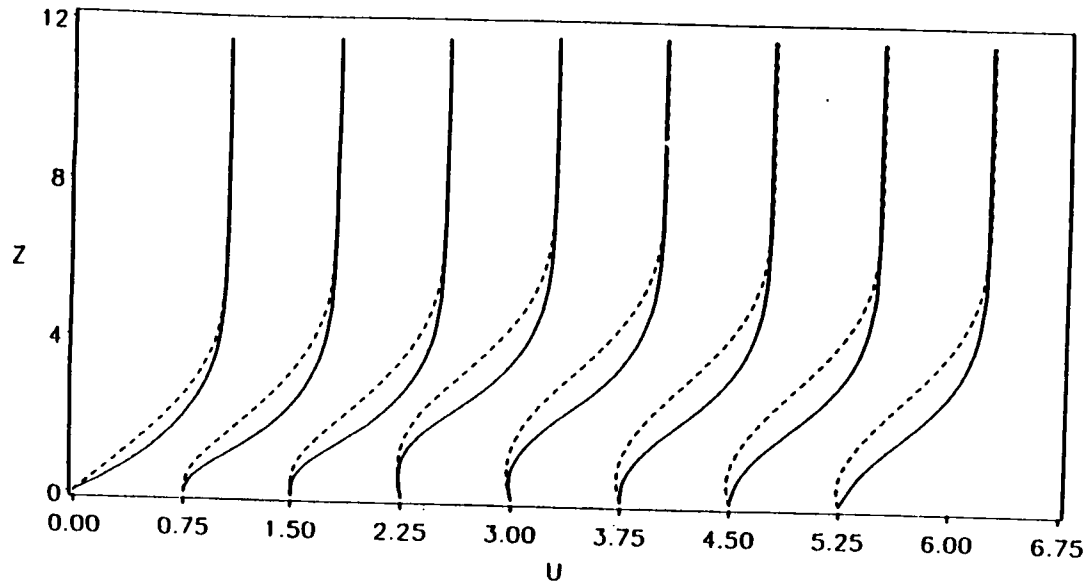

Figure 3.3. Effect of wall suction on the streamwise velocity profiles along the plate when the step height = 0.003, step slope = -4.35, $M_\infty = 0.5$, $Re = 1.0x10^6$, and Pr = 0.72. The profiles correspond to the following values of R starting from left to right: 897, 1000, 1010, 1020, 1030, 1034, and 1042; - - - $v_w = 0.0$ and ___ $v_w = 5.0x10^{-4}$.

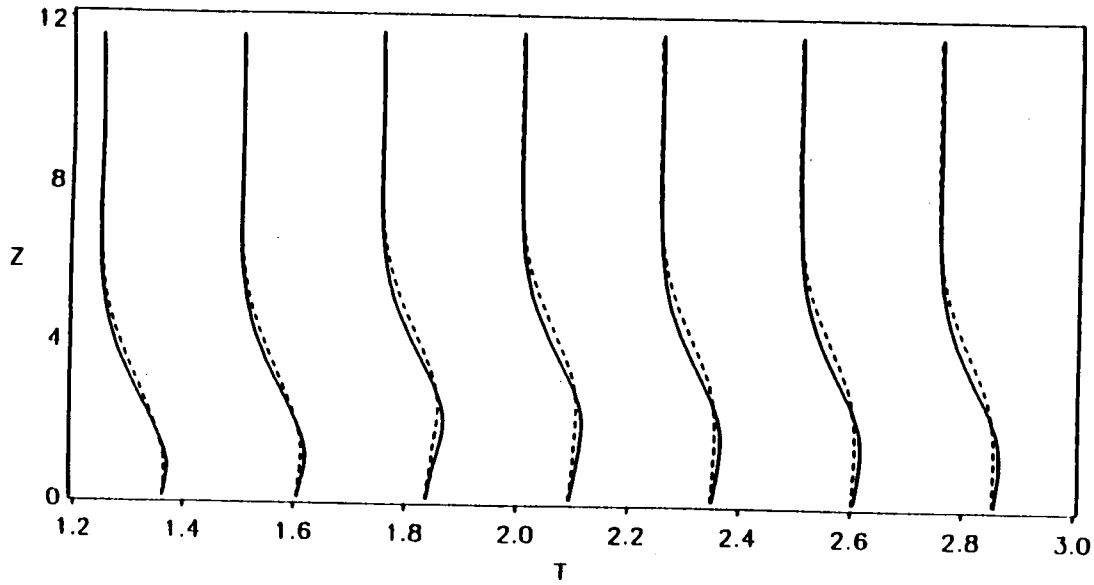

Figure 3.4. Effect of wall suction on the temperature profiles along the plate when the step height = 0.003, step slope = -4.35, $M_\infty = 0.8$, $Re = 1.0x10^6$, and Pr = 0.72. The profiles correspond to the following values of R starting from left to right: 897, 1000, 1010, 1020, 1030, 1034, and 1042; - - - $v_w = 0.0$ and $v_w = 5.0x10^{-4}$.

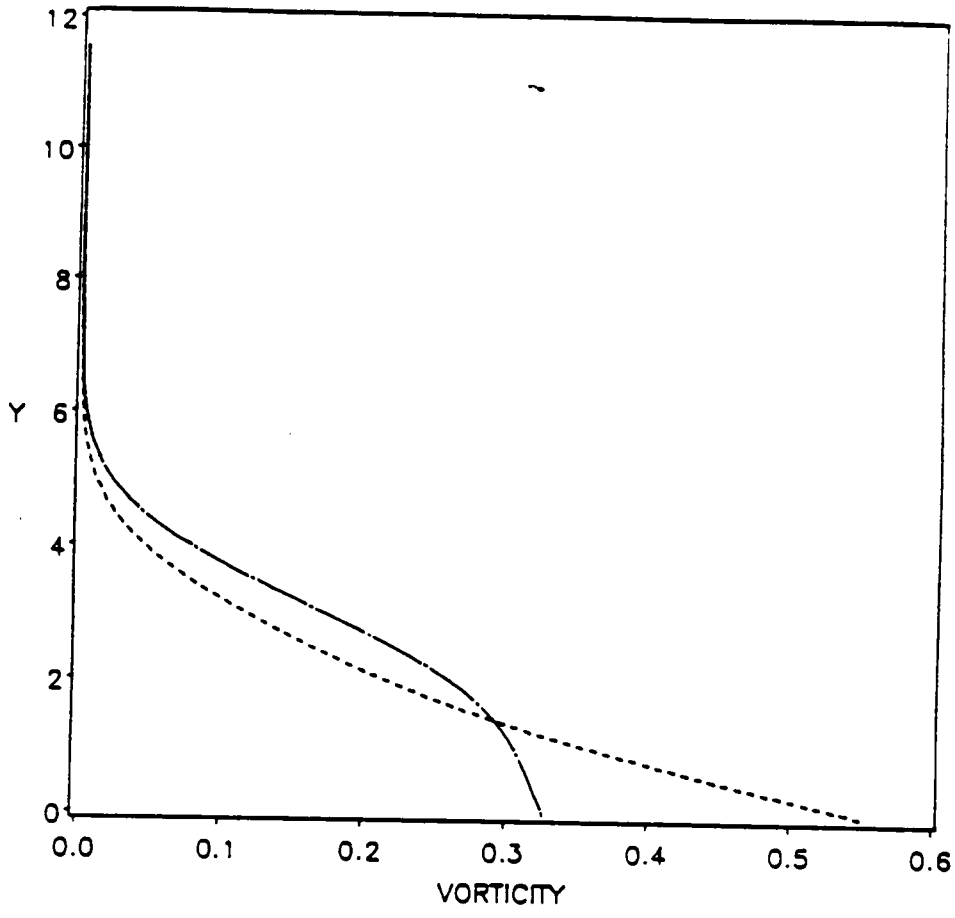

Figure 3.5. Influence of suction on the first derivative of the velocity profile at x = 0.8 when the step height = 0.003, step slope = - 4.35, $M_\infty = 0.8$, $Re = 1.0 \times 10^6$, and Pr = 0.72: __.__ $v_w = 0.0$ and - - - $v_w = 5.0 \times 10^{-4}$.

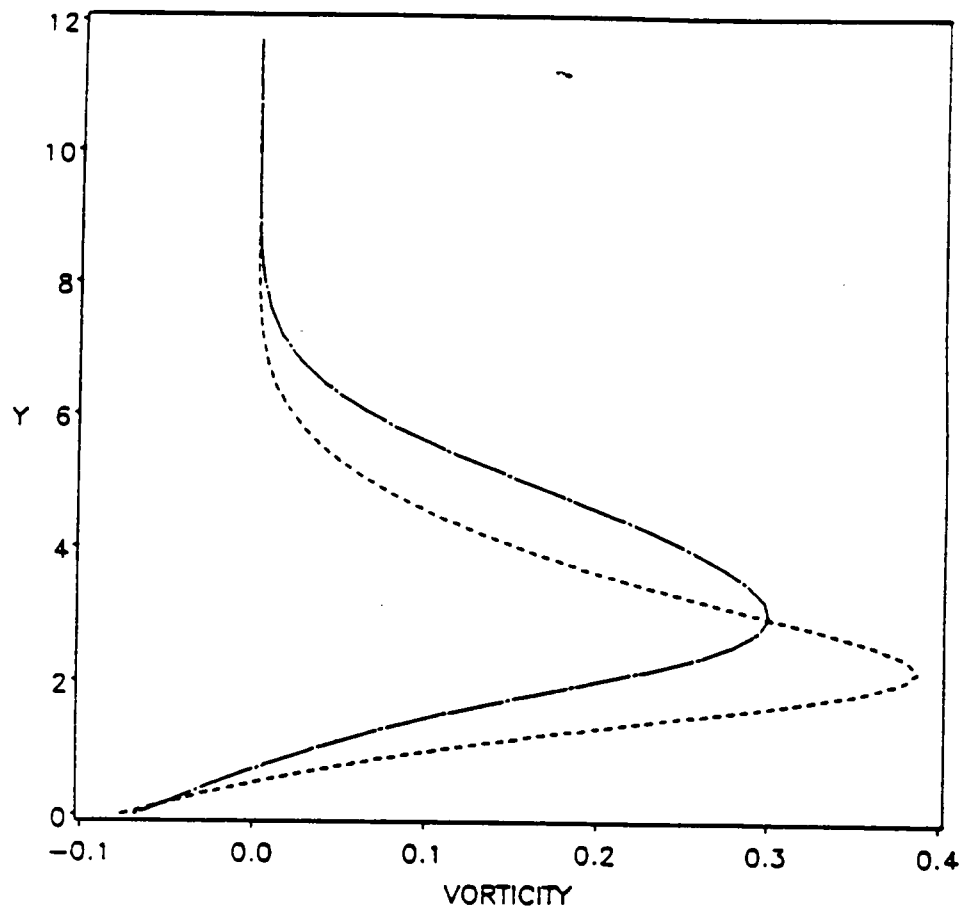

Figure 3.6. Influence of suction on the first derivative of the velocity profile at x = 1.04 when the step height = 0.003, step slope = - 4.35, $M_\infty = 0.8$, $Re = 1.0x10^6$, and Pr = 0.72: __.__ $v_w = 0.0$ and - - - $v_w = 5.0x10^{-4}$.

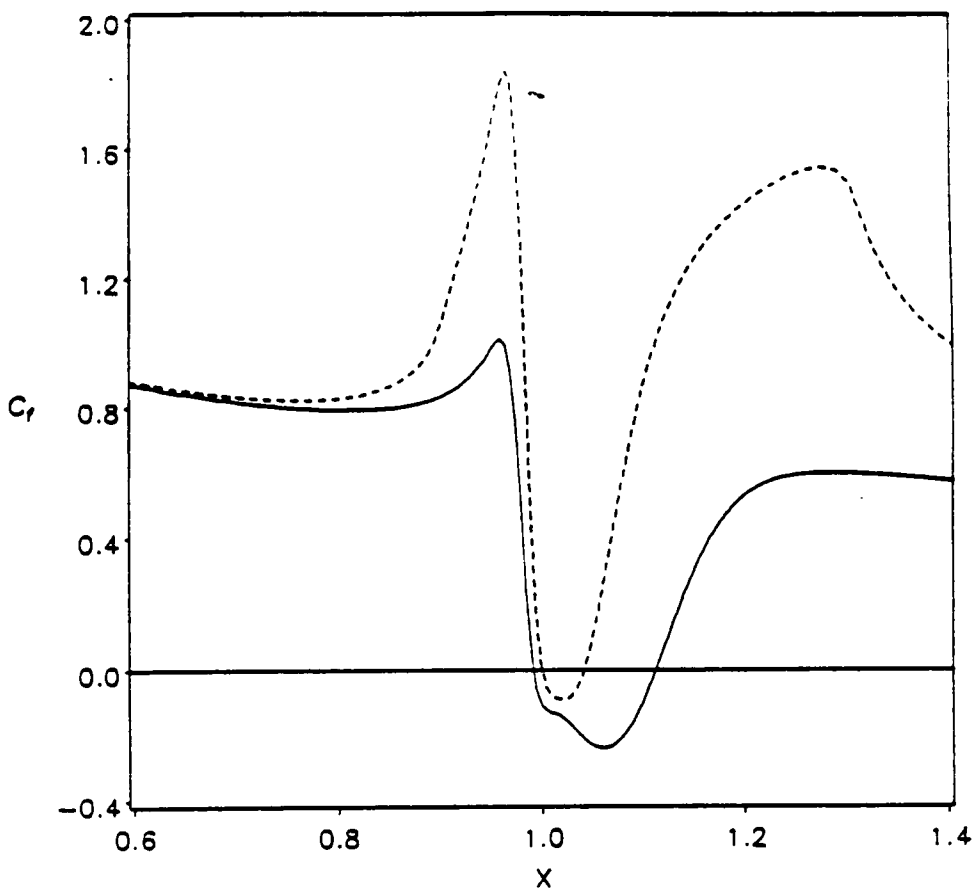

Figure 3.7. Effect of a concentrated suction strip on the shear coefficient. The strip starts at x = 0.9 and ends at x = 1.3, $v_w = 1.0x10^{-3}$, step height = 0.003, step slope = - 4.35, $M_\infty = 0.8$, $Re = 1.0x10^{6}$, Pr = 0.72: ___ without suction and - - - with suction.

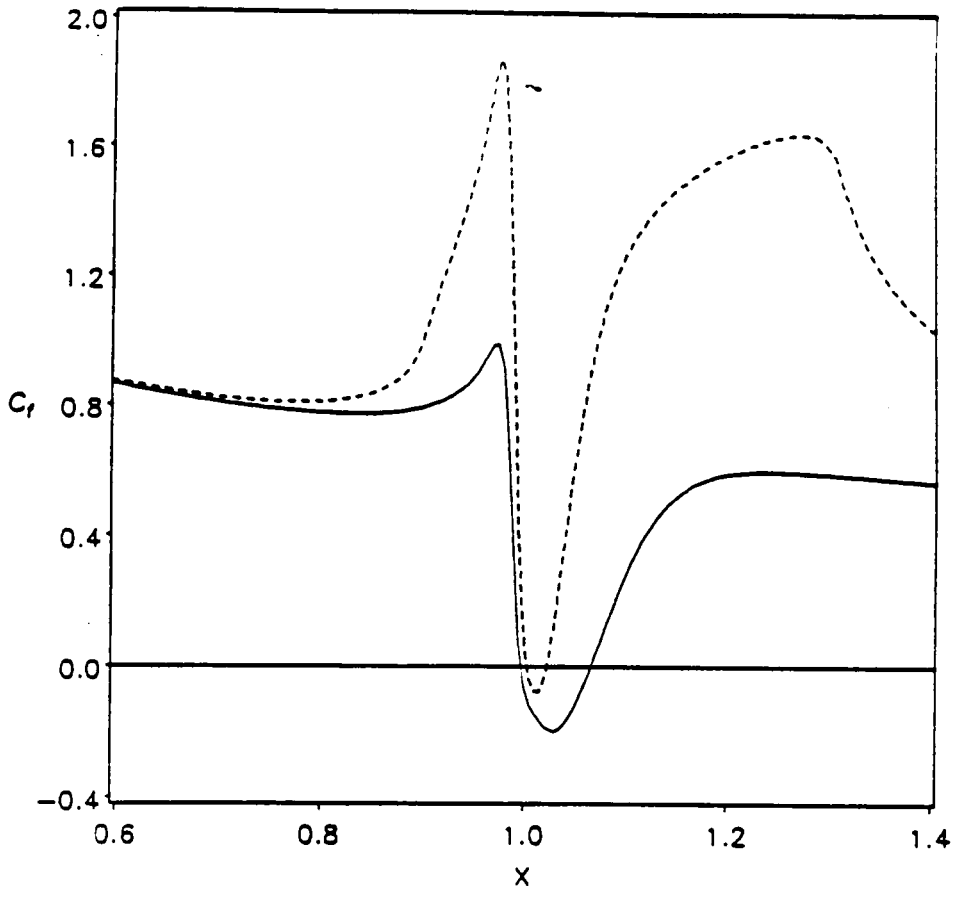

Figure 3.8. Effect of a concentrated suction strip on the shear coefficient. The strip starts at x = 0.9 and ends at x = 1.3, $v_w = 1.0x10^{-3}$, step height = 0.002, step slope = - 4.35, $M_\infty = 0.8$, $Re = 10x10^{6}$, Pr = 0.72: ___ without suction and - - - with suction.

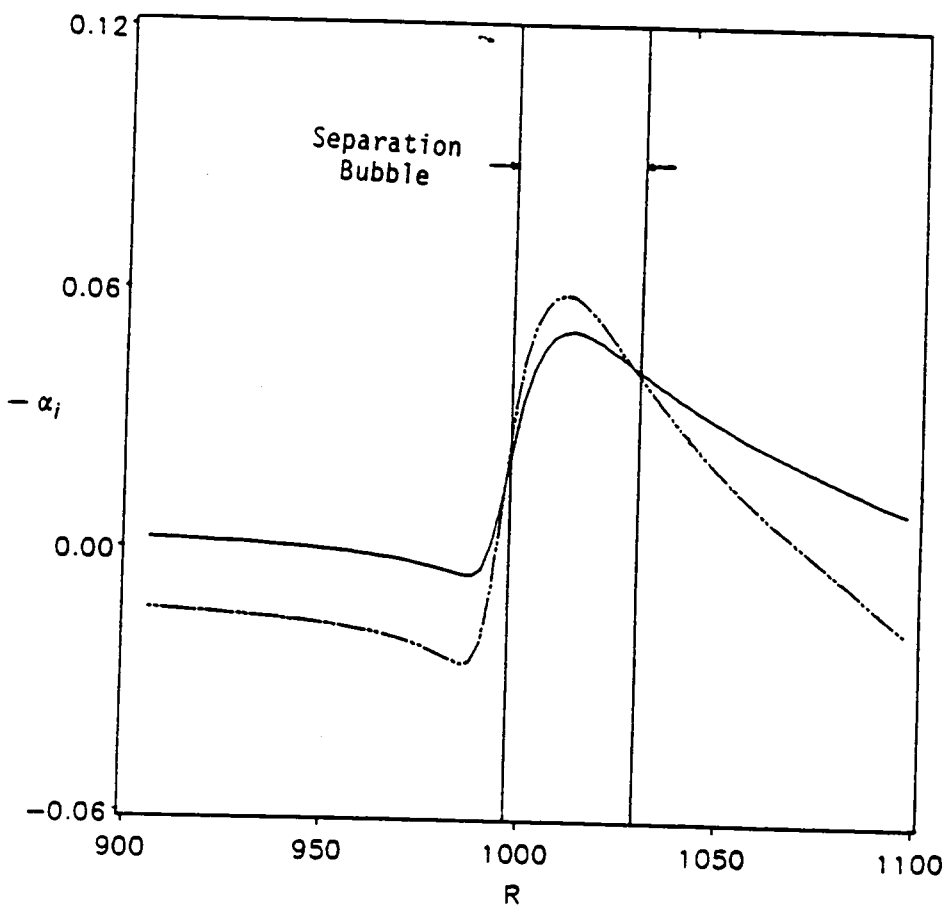

Figure 3.9. The growth rates for the flow over steps with and without continuous suction when the step height = 0.003, step slope = - 4.35, M_∞ = 0.8, Re = 1.0×10^6, Pr = 0.72, and F = 50×10^{-6}: ___ $v_w = 0.0$ and __·__ $v_w = 5.0 \times 10^{-4}$.

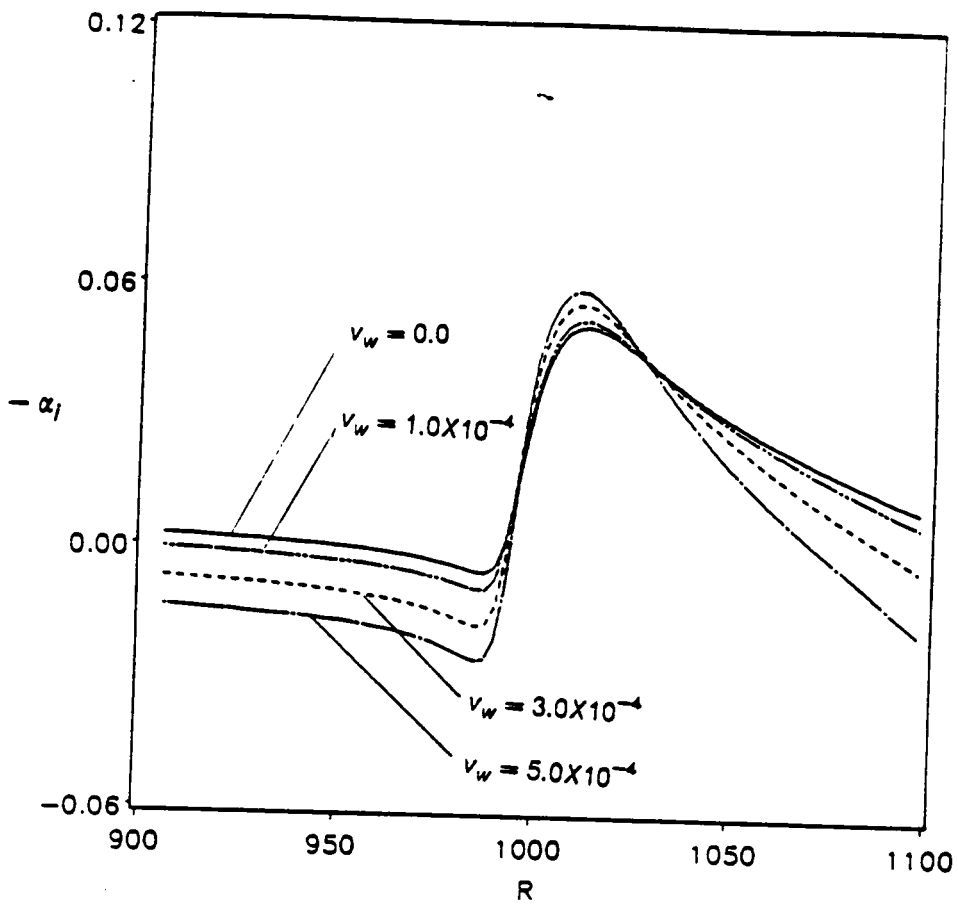

Figure 3.10. The variation of the growth rates with streamwise location for different continuous suction levels: step height = 0.003, step slope = - 4.35, M_∞ = 0.8, Re = $1.0x10^6$, Pr = 0.72, and F = $50x10^{-6}$.

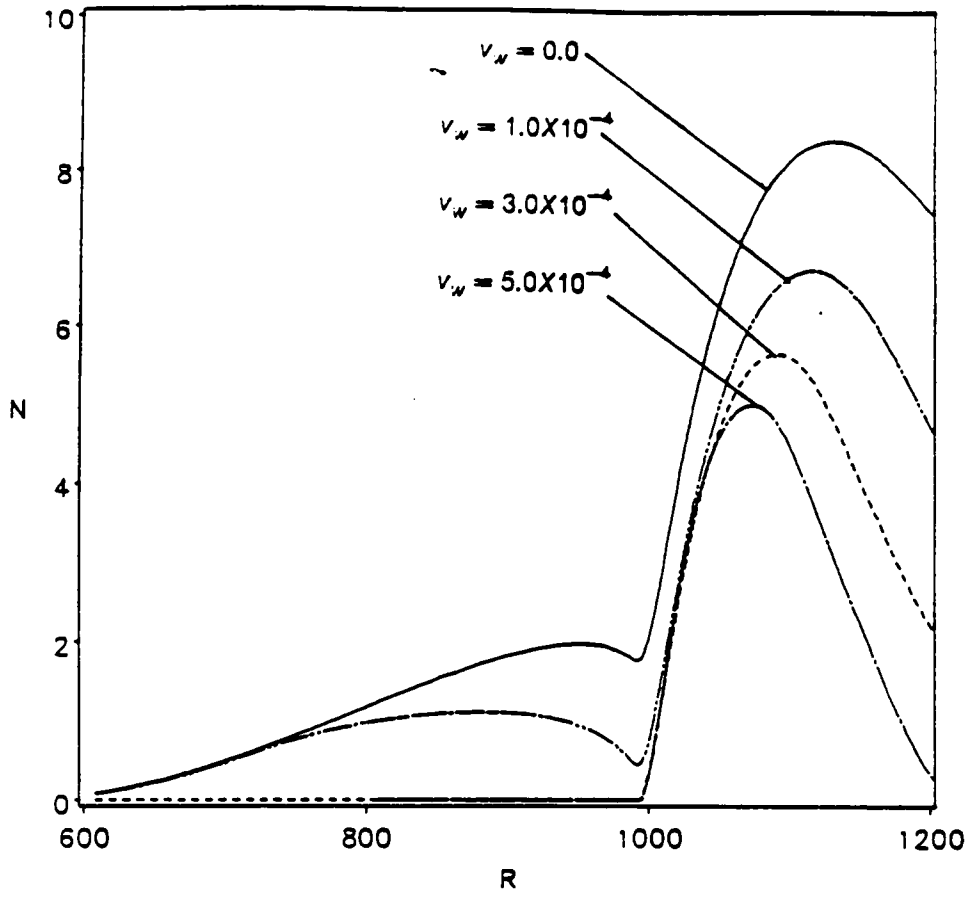

Figure 3.11. The variation of the amplification factor with streamwise location for different continuous suction levels: step height = 0.003, step slope = -4.35, M_∞ = 0.8, Re = $1.0x10^6$, Pr = 0.72, and F = $50x10^{-6}$.

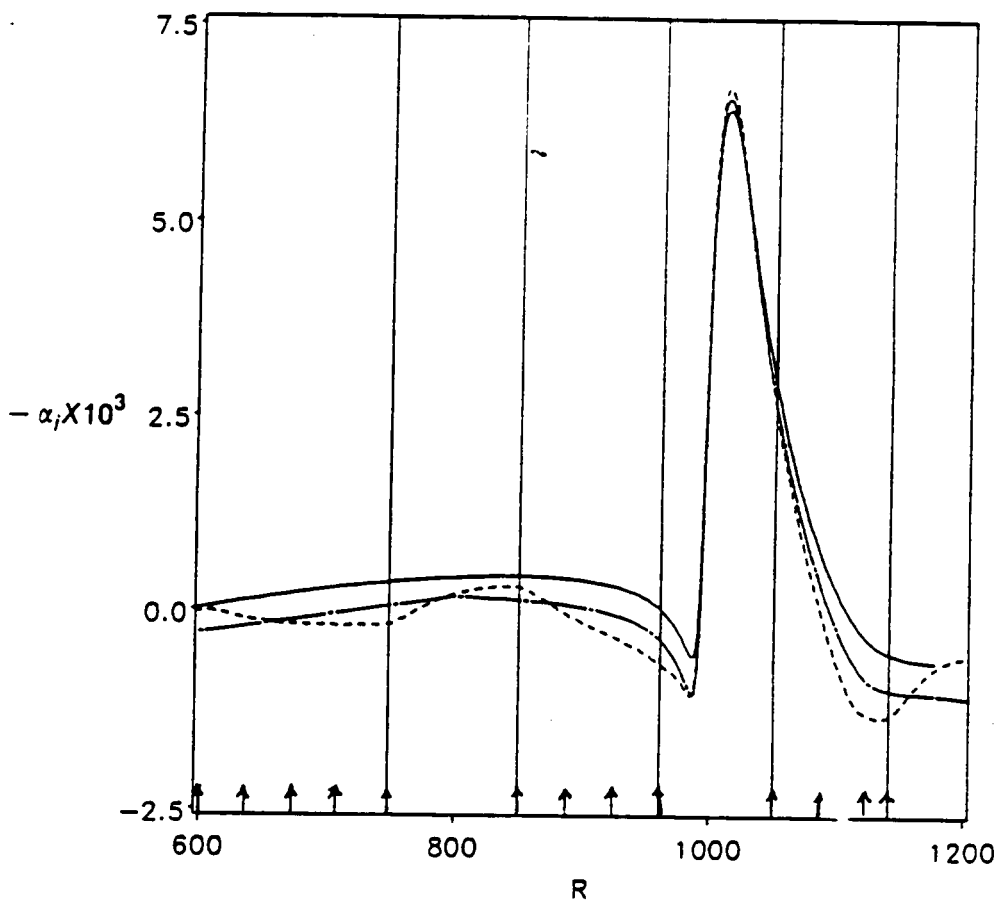

Figure 3.12. The effect of suction strips and continuous suction on the growth rates for the flow over a step with a height of 0.003, step slope = - 4.35, $M_\infty = 0.5$, $Re = 1.0x10^6$, $Pr = 0.72$, and $F = 50x10^{-6}$. The suction strips are centered at R = 678, 907, and 1097 with a length of 0.2 L* each. In the case of strips v_w = 2.33 x 10^{-4} and in the case of continuous suction $v_w = 1.0x10^{-4}$: ___ no suction, __.__ continuous suction, and - - - suction strips.

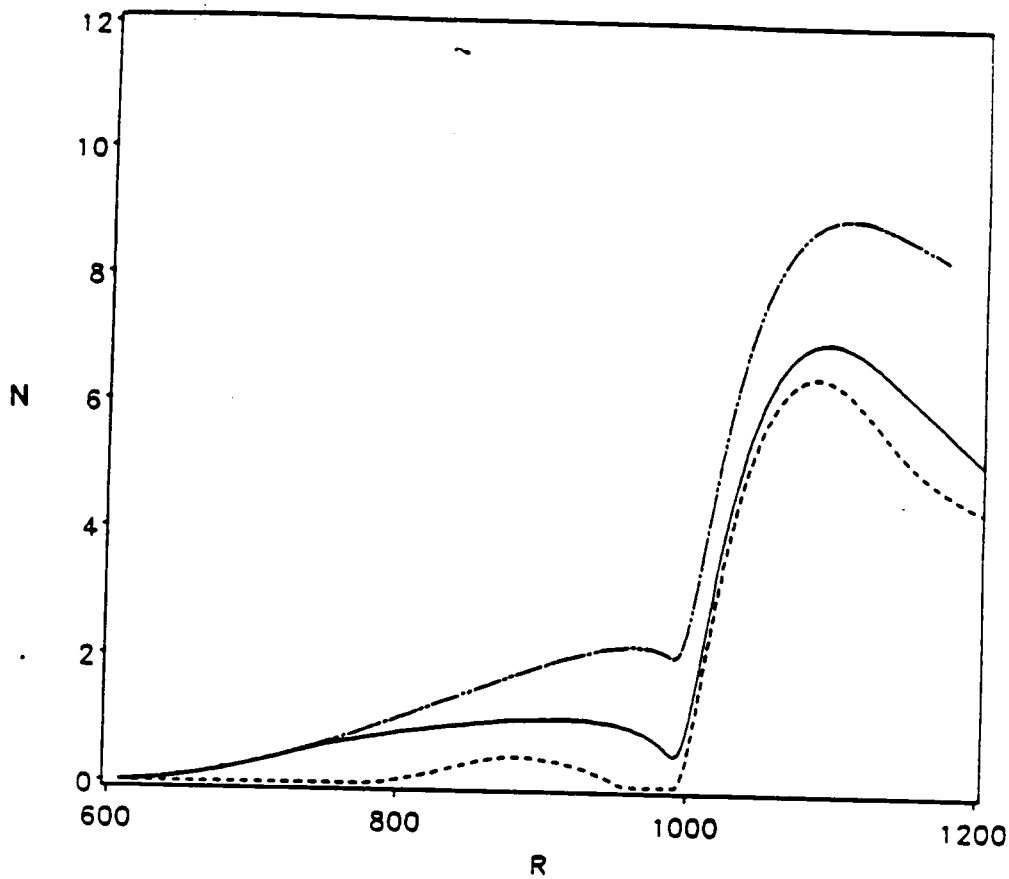

Figure 3.13. Comparison of the variation of the amplification factor with streamwise location for the cases of continuous suction, suction strips, and no suction. Flow conditions are the same as in Figure 12: __.__ no suction, ____ continuous suction, and - - - suction strips.

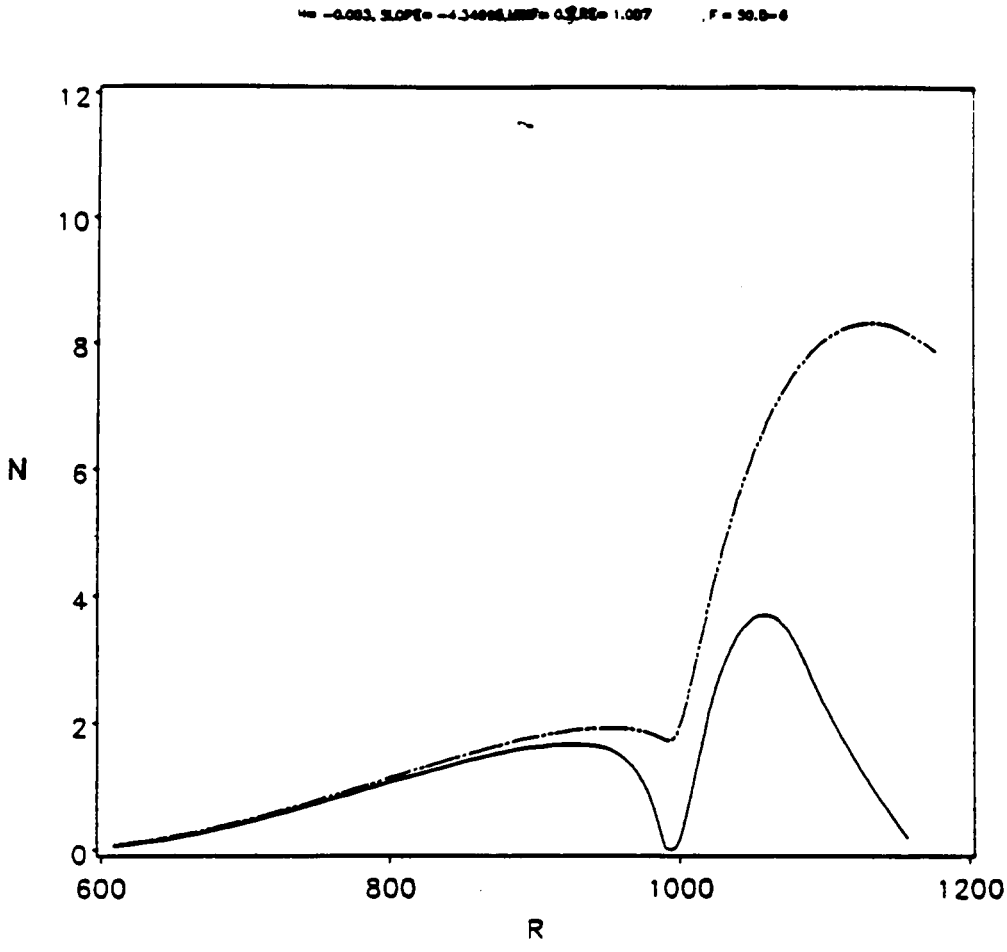

Figure 3.14. Effect of the concentrated strip suction described in Figure 7 on the amplification factor. Flow conditions are the same as in Figure 7, $F = 50 \times 10^{-6}$; __..__ no suction and ___ suction strip.

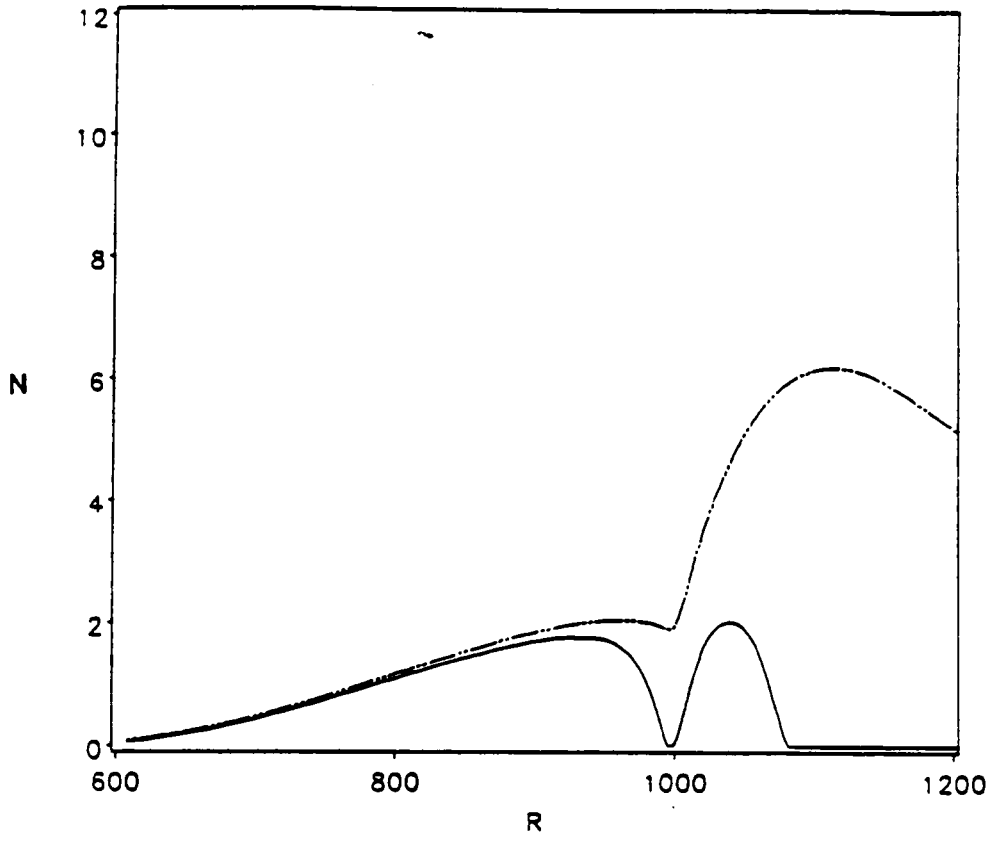

Figure 3.15. Effect of the concentrated strip suction described in Figure 8 on the amplification factor. Flow conditions are the same as in Figure 8, $F = 50x10^{-6}$; __..__ no suction and ___ suction strip.

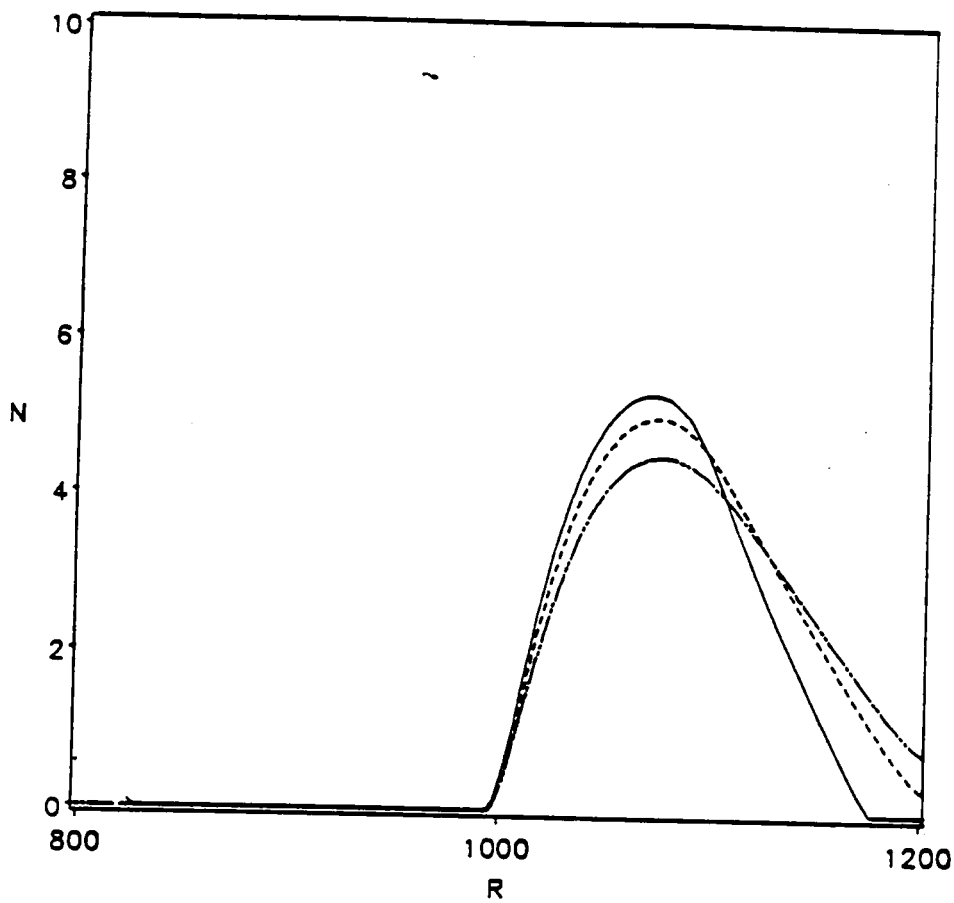

Figure 3.16. The variation of the amplification factor with streamwise location for flows over steps with continuous wall suction for different frequencies when the step height = 0.003, step slope = - 4.35, M_∞ = 0.5, Re = $1.0x10^6$, $V_w = 5x10^{-4}$, and Pr = 0.72: __··__ $F = 40x10^{-6}$, ___ $F = 50x10^{-6}$, and - - - $F = 60x10^{-6}$.

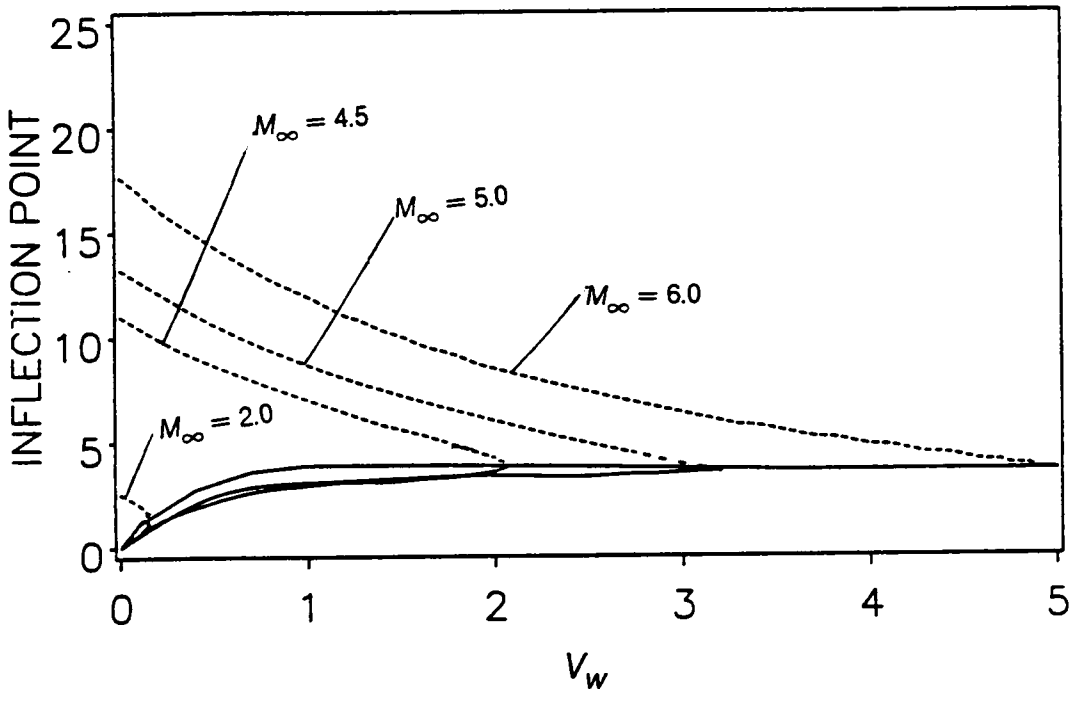

Figure 4.1. Variation of the location of the generalized inflection points with suction level for several Mach numbers for Pr = 0.72 and wind-tunnel temperature: ___ lower inflection point and – – – upper infection point.

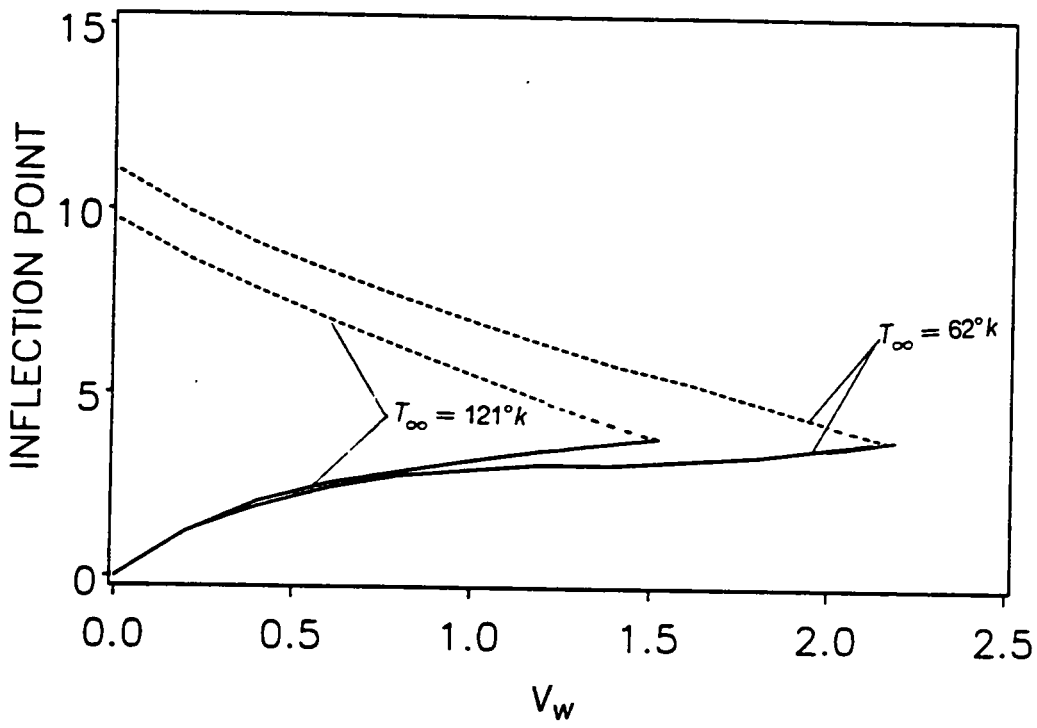

Figure 4. 2. Effect of T_∞ on the variation of the location of the generalized inflection points with suction level when $M_\infty = 4.5$ and Pr = 0.70: ___ lower inflection point and – – – upper infection point.

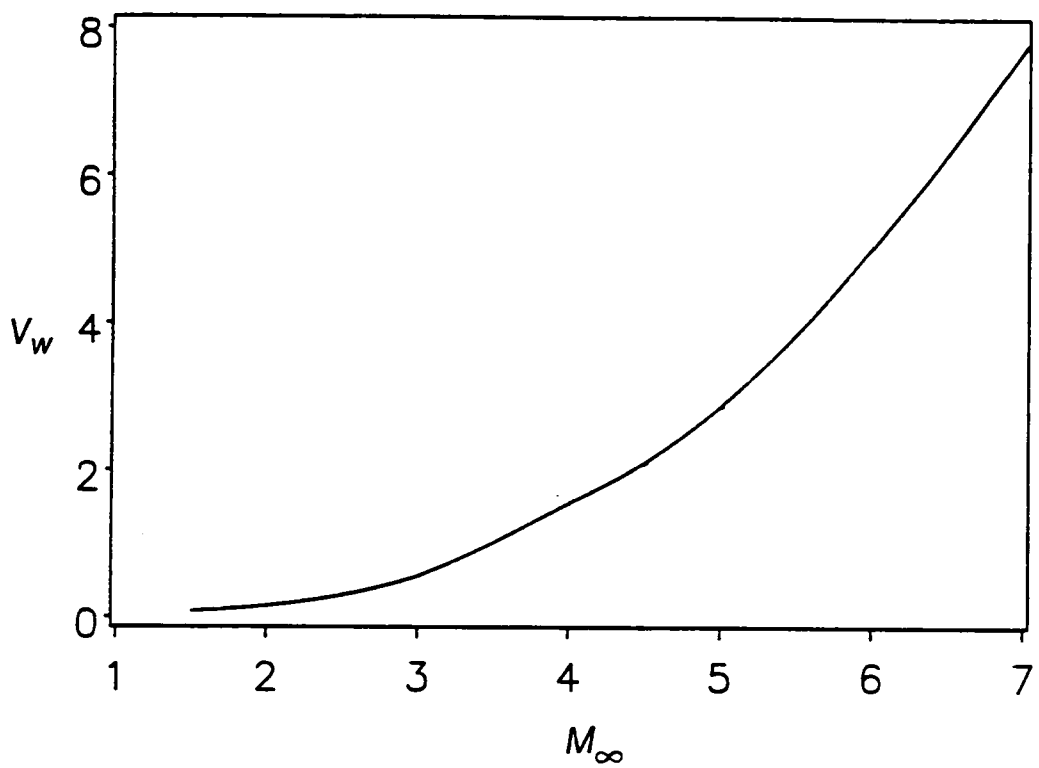

Figure 4. 3. The suction velocity needed to eliminate the generalized inflection points as a function of Mach number for wind-tunnel temperature and Pr = 0.72.

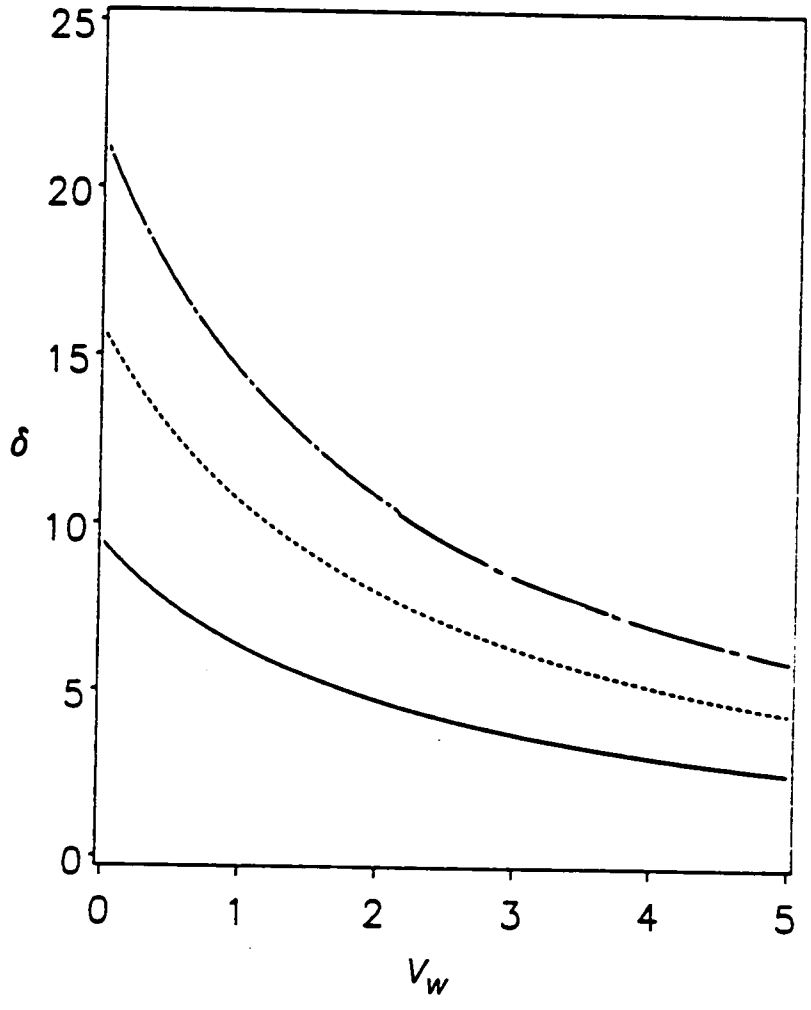

Figure 4. 4. Variation of the displacement thickness with suction velocity for wind-tunnel temperature and Pr = 0.72: ___ $M_\infty = 4.5$, - - - $M_\infty = 6.0$, and ___ _ ___ $M_\infty = 7.0$.

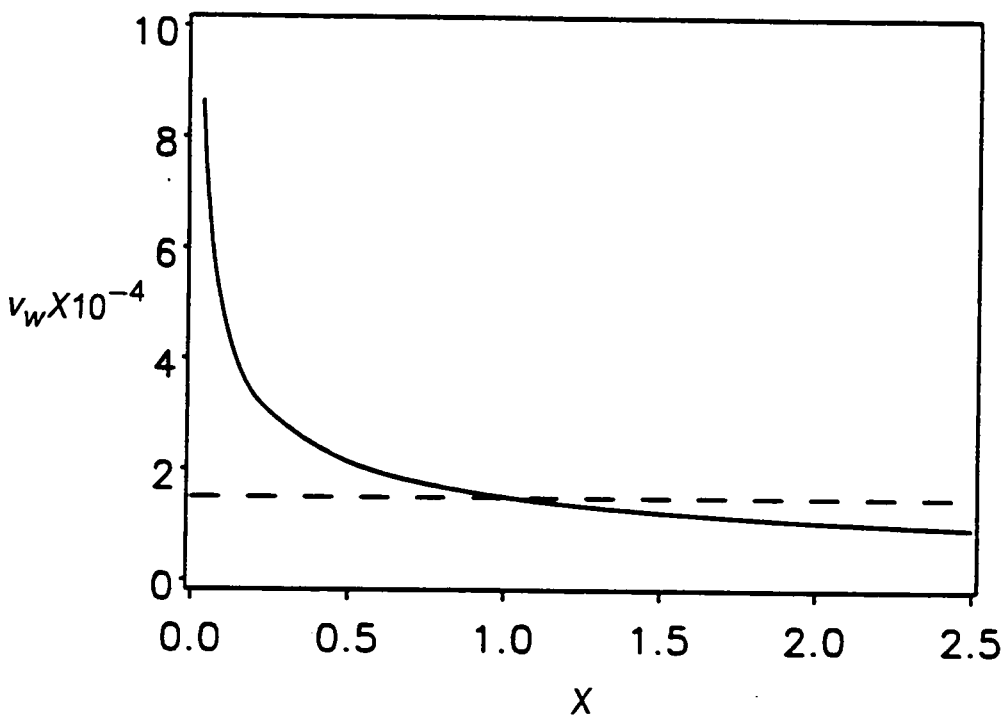

Figure 4. 5. Comparison of the suction distribution which results in a self-similar mean profile with a uniform-suction distribution for $M_\infty = 4.5$, $T_\infty = 121K°$, $Pr = 0.70$, and Re = $2.5x10^6$. ___ self-similar distribution and - - - uniform distribution.

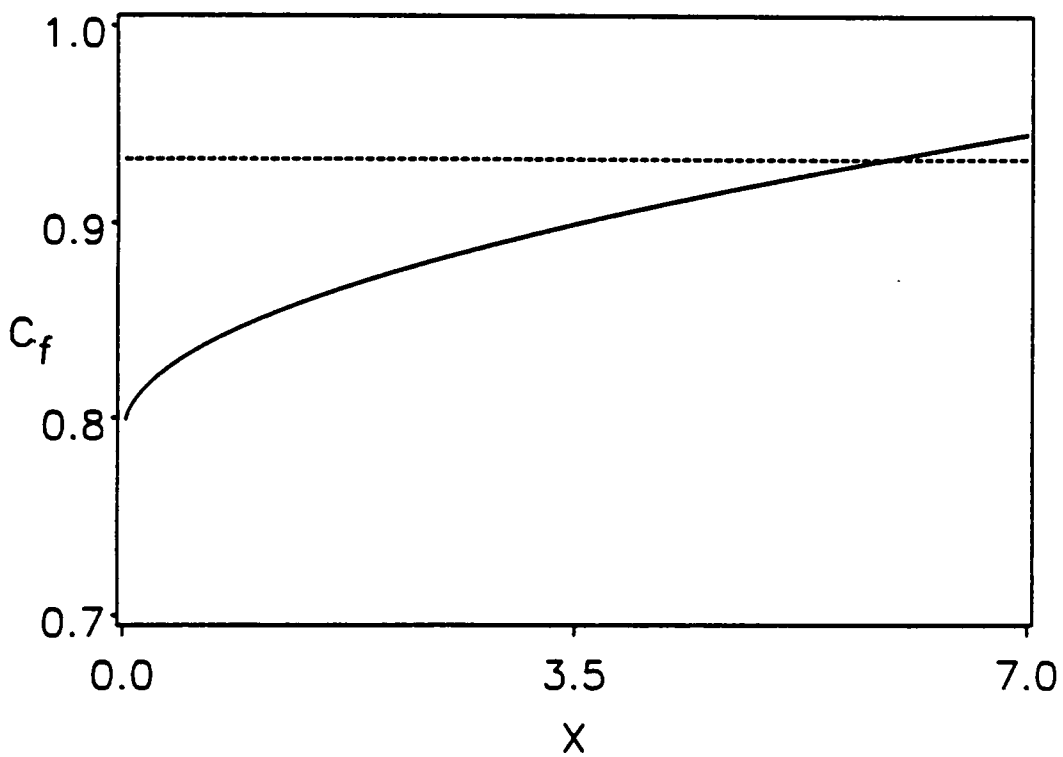

Figure 4. 6. Comparison of the shear coefficients obtained using two suction distributions when $M_\infty = 4.5$, $T_\infty = 121K°$, Pr = 0.70, and Re = $2.5x10^6$: ___ $v_w = 1.5x10^{-4}$ and - - - $V_w = 0.1$.

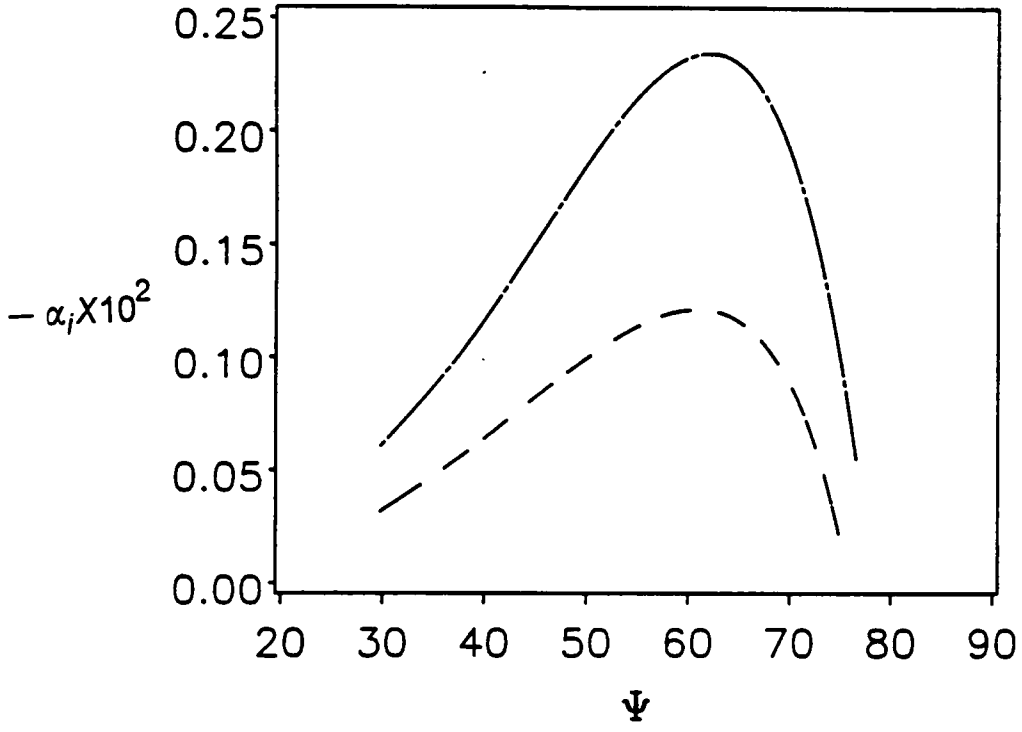

Figure 4. 7. Effect of suction on the variation of the growth rate of first-mode waves with wave angle for M_∞ = 2.1, R = 1500, T_∞ = 178$K°$, F = 13.550x10^{-6}, and Pr = 0.72: __.__ V_w = 0.0 and - - - V_w = 0.3. Self-similar boundary layer.

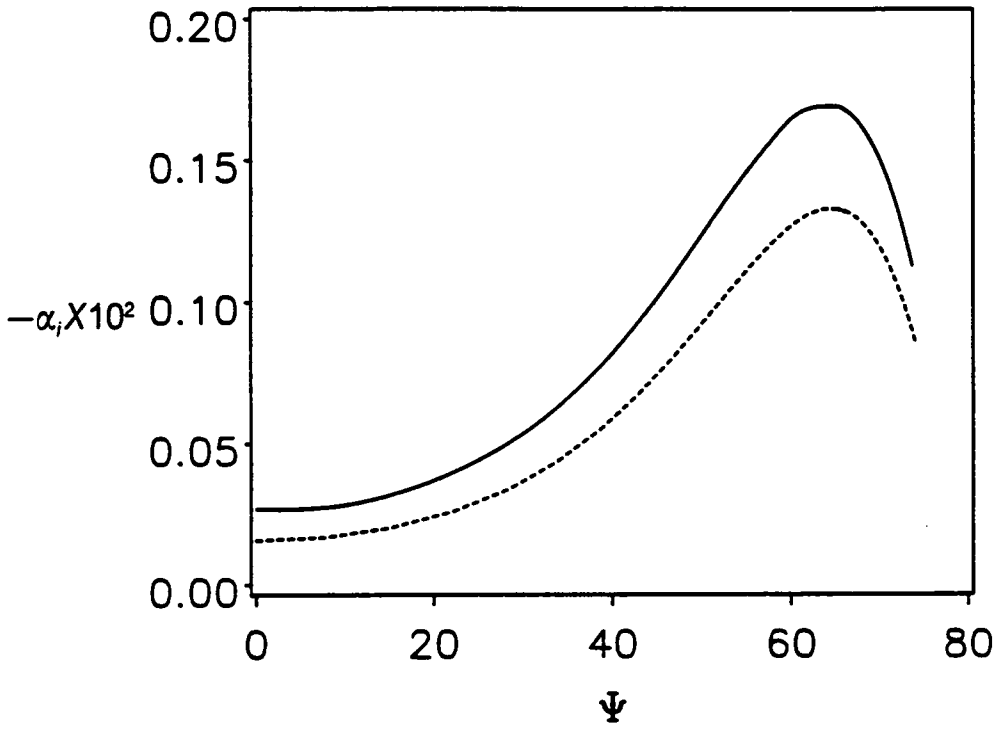

Figure 4. 8. Effect of suction on the variation of the growth rate of first-mode waves with wave angle for M_∞ = 4.5, R = 1500, $T_\infty = 62K°$, F = $20.0x10^{-6}$, and Pr = 0.72, ___ V_w = 0.0 and - - - V_w = 0.3. Self-similar boundary layer.

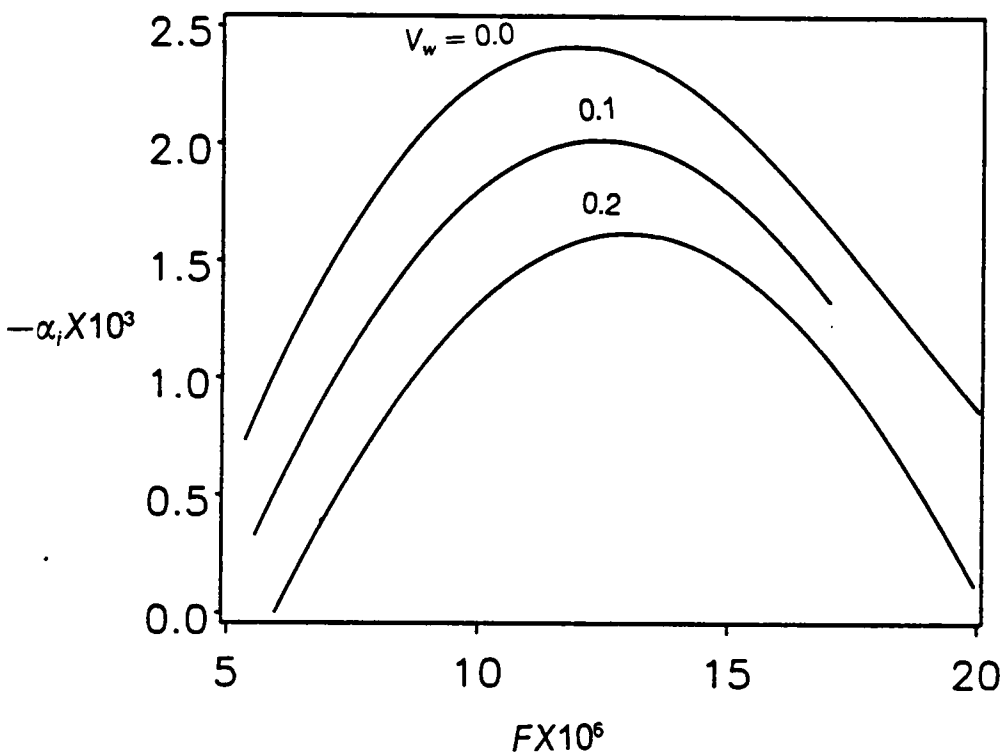

Figure 4. 9. Effect of suction on the variation of the growth rate of first-mode waves with frequency for three levels of suction for M_∞ = 2.1, R = 1500, $T_\infty = 165K°$, $\psi = 60°$, and Pr = 0.72. Self-similar boundary layer.

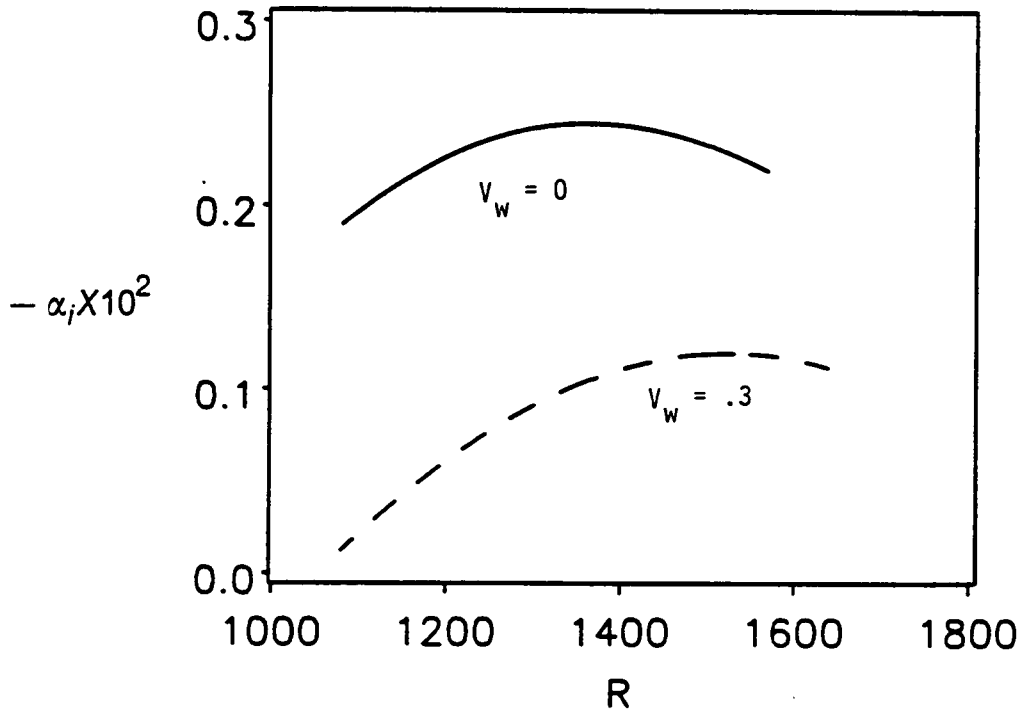

Figure 4. 10. Effect of suction on the variation of the growth rate with streamwise location for M_∞ = 2.1, $T_\infty = 178K°$, F = 13.550x10^{-6}, $\psi = 60°$, and Pr = 0.72. Self-similar boundary layer.

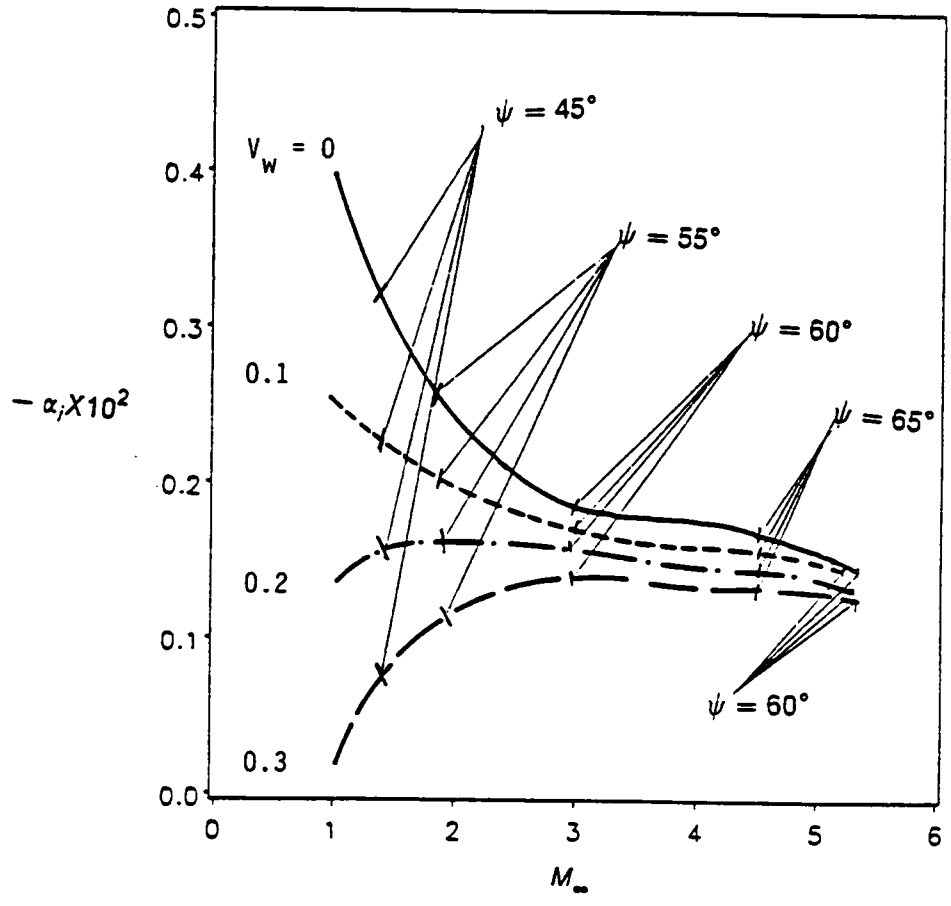

Figure 4. 11. Effect of suction on the variation of the maximum growth rate of first-mode waves with Mach number for R = 1500, Pr = 0.72, and wind-tunnel temperature. Self-similar boundary layer.

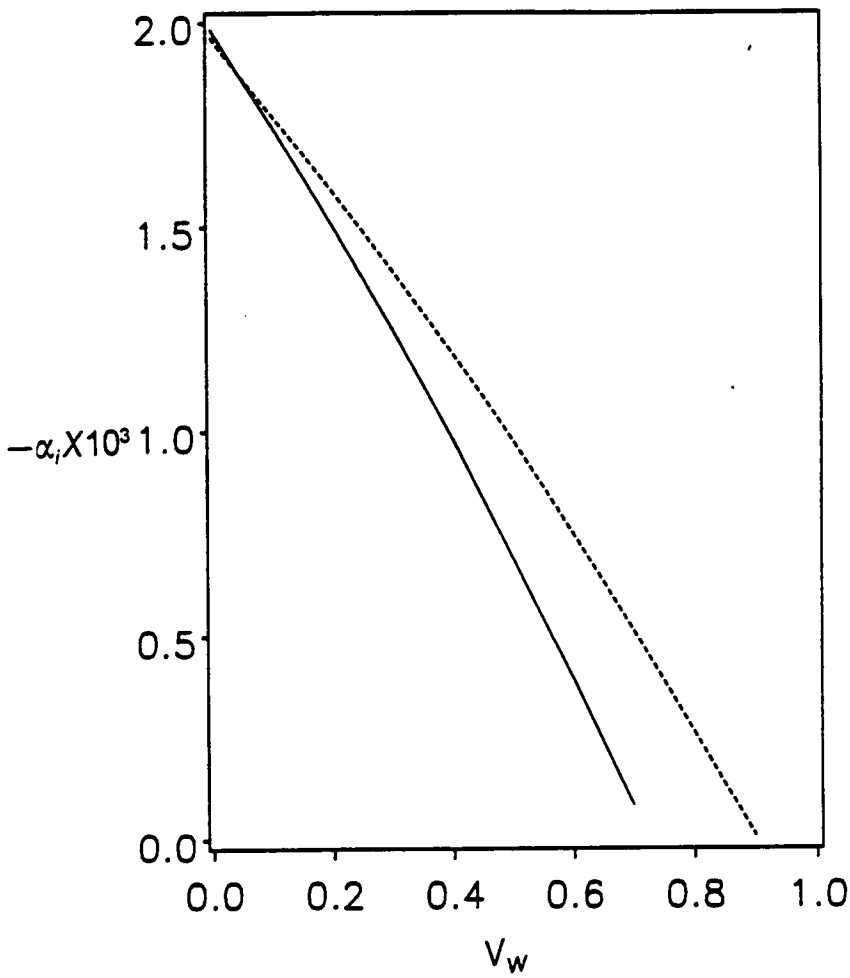

Figure 4. 12. Effect of suction on the growth rate of first-mode waves when $T_\infty = 123K°$, F = 11.50x10^{-6}, R = 1500, Pr = 0.72, and $\psi = 60°$: ___ $M_\infty = 2.6$ and - - - $M_\infty = 3.0$. Self-similar boundary layer.

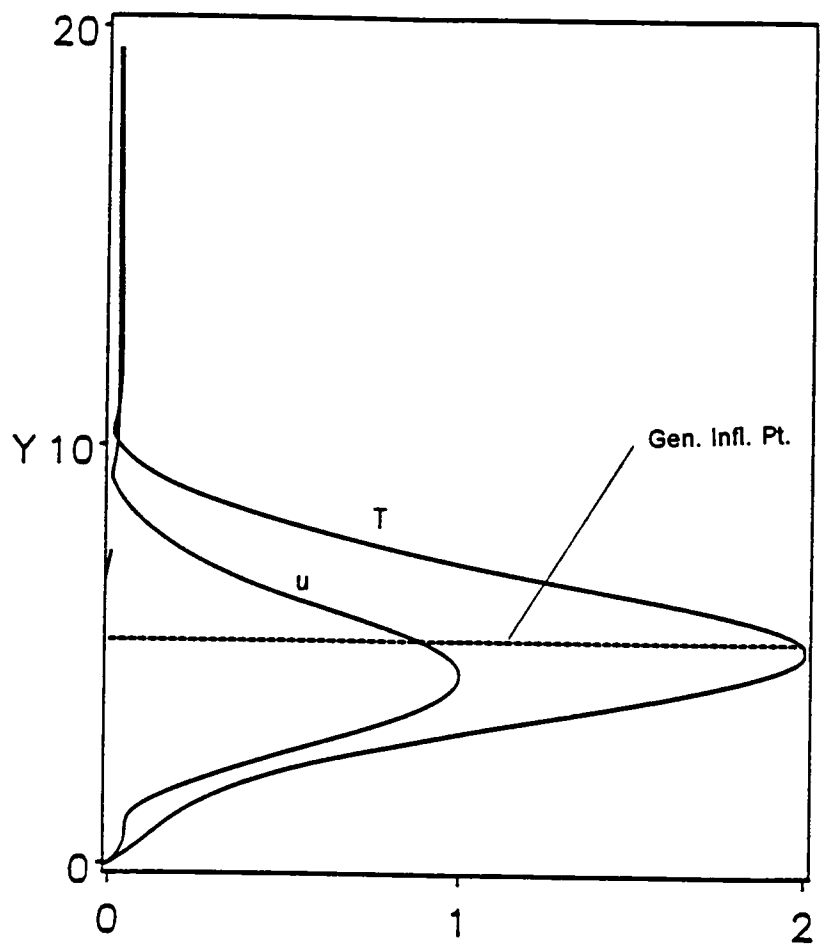

Figure 4. 13. Effect of suction on the eigenfunctions of first-mode waves when $M_\infty = 3.0$, $T_\infty = 123K°$, $R = 1500$, and $F = 11.15x10^{-6}$; (a) $V_w = 0.0$,

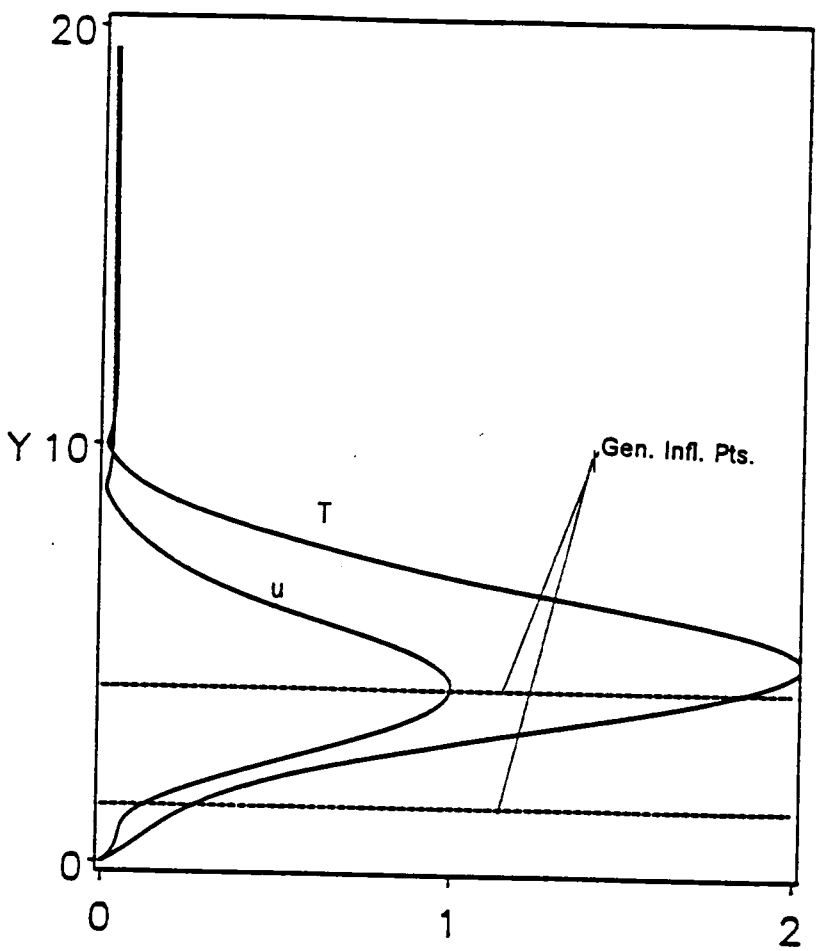

Figure 4.13. Effect of suction on the eigenfunctions of first-mode waves when $M_\infty = 3.0$, $T_\infty = 123\ K°$, $R = 1500$, and $F = 11.15x10^{-6}$: $(b) V_w = 0.3$,

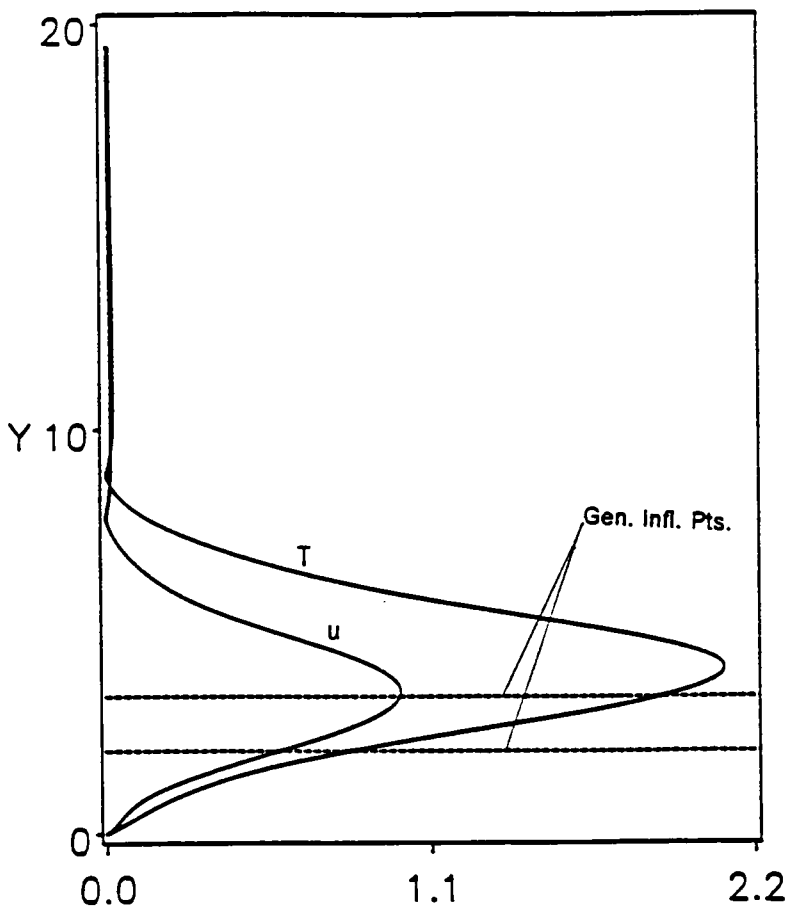

Figure 4.13. Effect of suction on the eigenfunctions of first-mode waves when $M_\infty = 3.0$, $T_\infty = 123\,K°$, $R = 1500$, and $F = 11.15x10^{-6}$: (c)$V_w = 0.5$

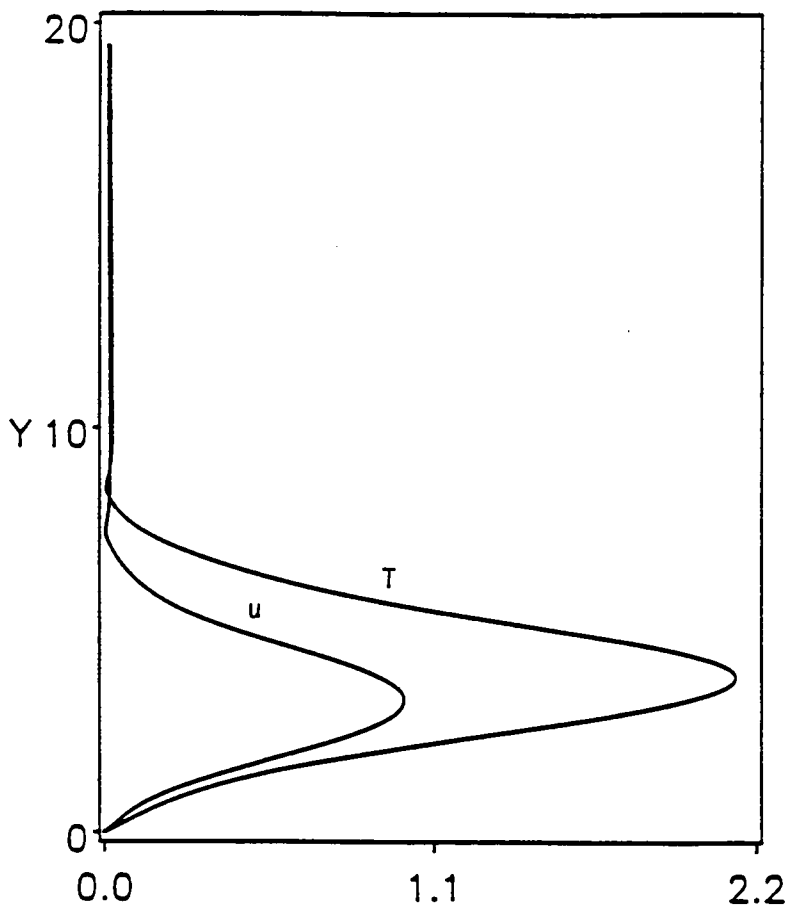

Figure 4.13. Effect of suction on the eigenfunctions of first-mode waves when $M_\infty = 3.0$, $T_\infty = 123\,K°$, $R = 1500$, and $F = 11.15x10^{-6}$: (d)$V_w = 0.66$.

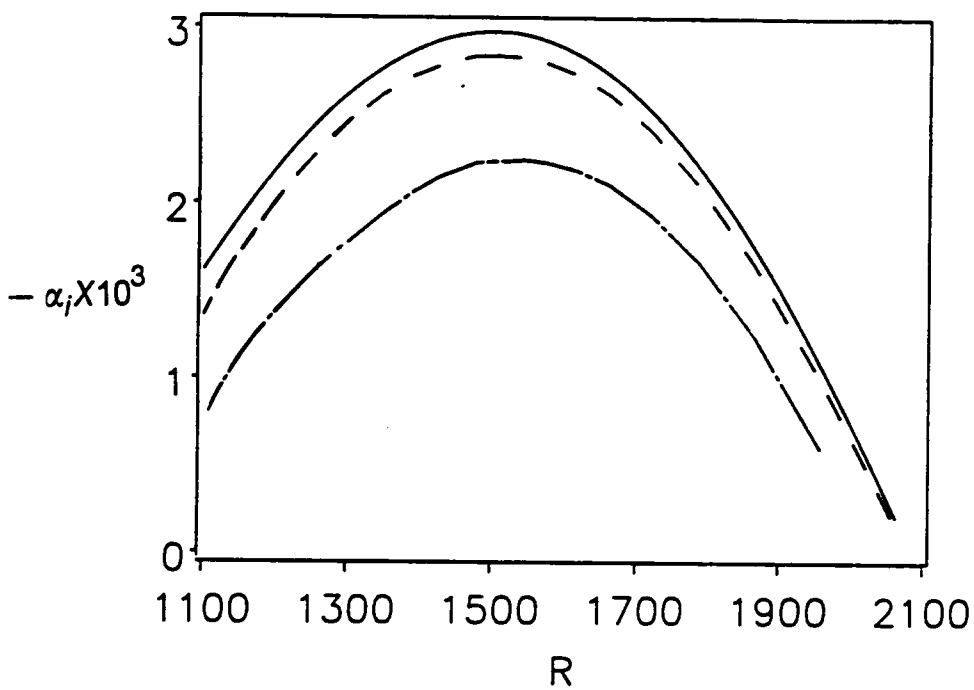

Figure 4. 14. Variation of the growth rate of first-mode waves with streamwise location for two uniform-suction distributions when $M_\infty = 1.5$, $T_\infty = 121\ K°$, $\psi = 55°$, and Pr = 0.70: ___ $v_w = 0.0$, - - - $v_w = 1x10^{-5}$, and ___ _ ___ $v_w = 1x10^{-4}$.

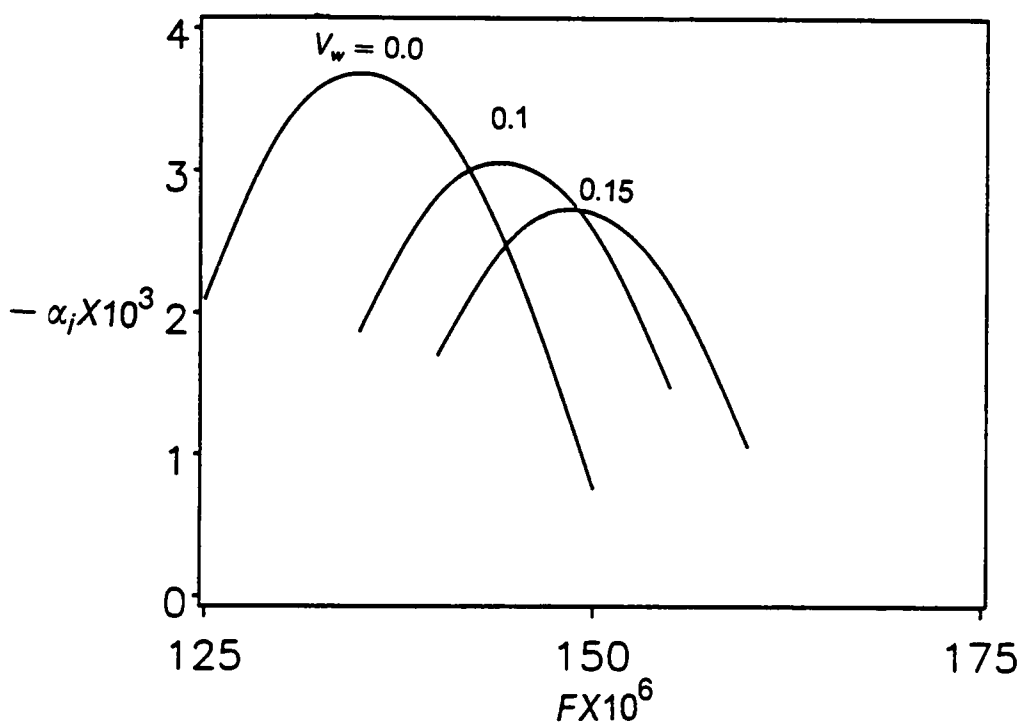

Figure 4. 15. Effect of suction on the variation of the growth rate of second-mode waves with frequency for $M_\infty = 4.5$, $T_\infty = 70\ K°$, R = 1500, Pr = 0.72, and $\psi = 0.0°$. Self-similar boundary layer.

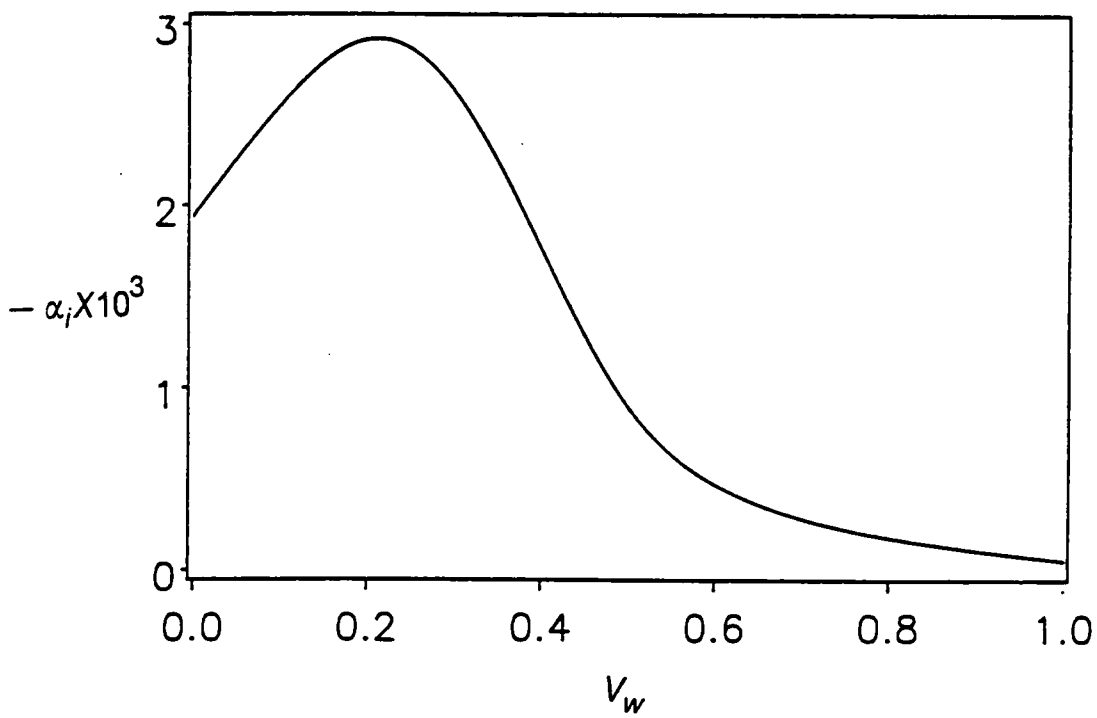

Figure 4. 16. Effect of suction on the growth rate of second-mode waves for M_∞ = 6.0, T_∞ = 52 $K°$, F = 93.550x10^{-6}, R = 1500, Pr = 0.72, and ψ = 0.0° . Self-similar boundary layer.

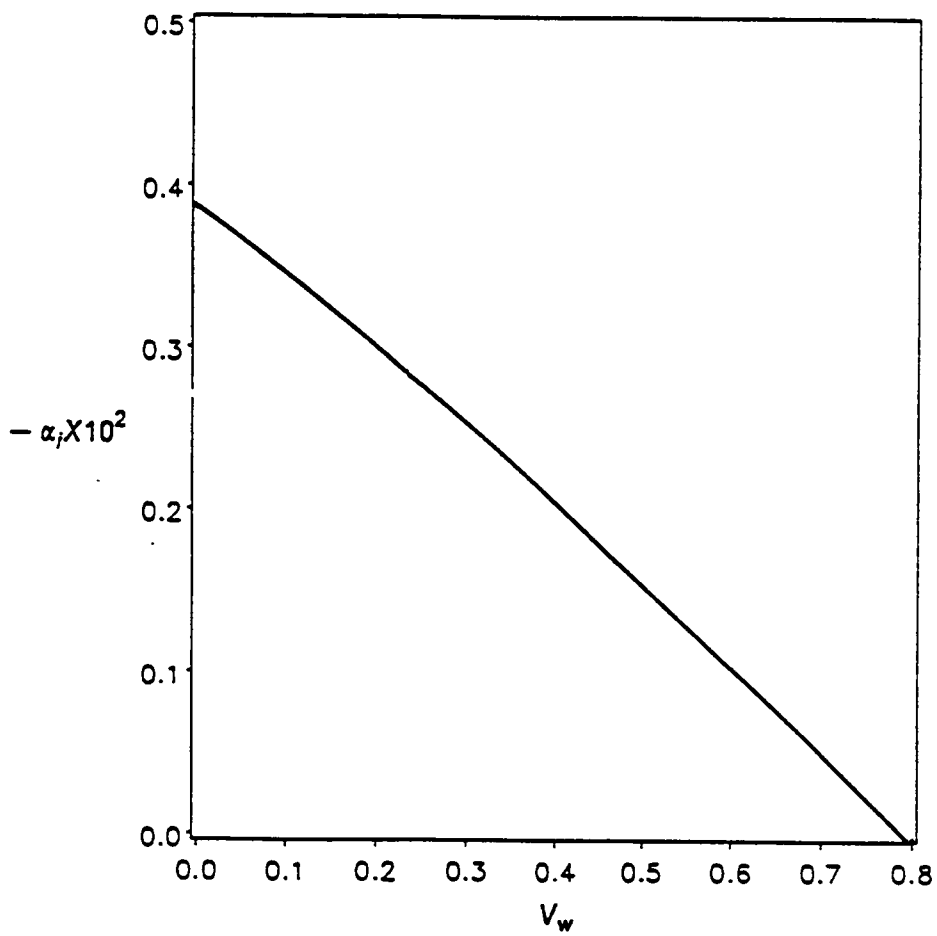

Figure 4. 17. Variation of the maximum growth rate of second-mode waves with suction velocity for M_∞ = 5.0, T_∞ = 59 $K°$, R = 1500, Pr = 0.72, and ψ = 0.0° . Self-similar boundary layer.

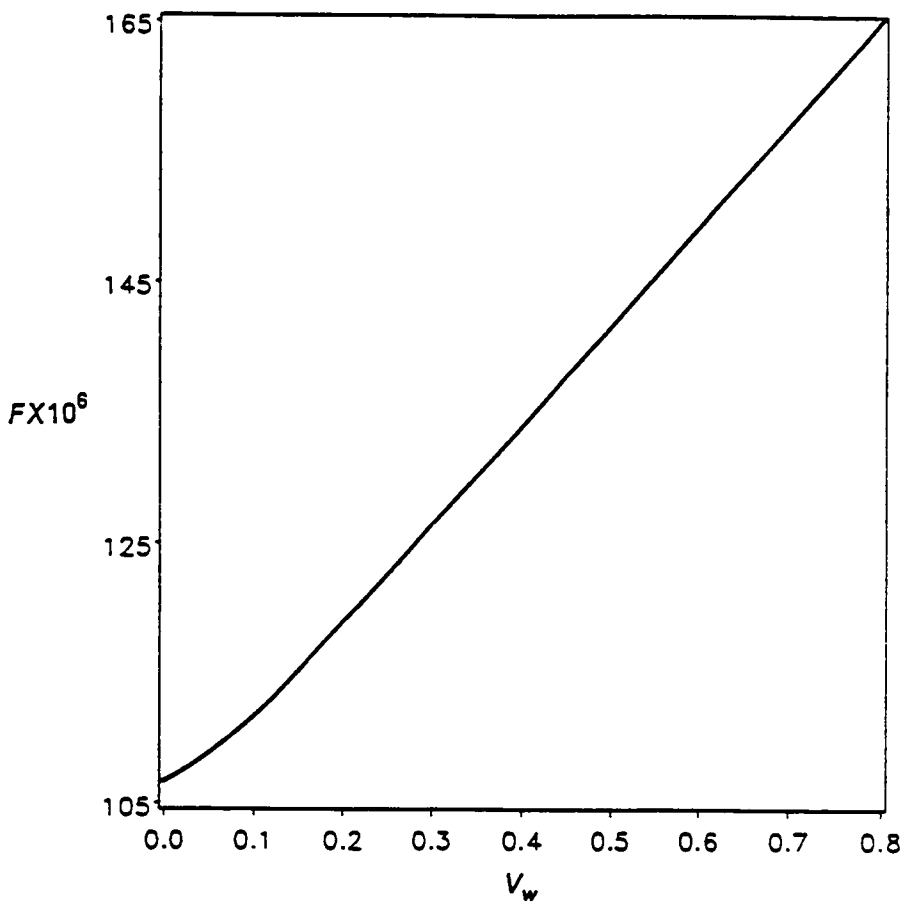

Figure 4. 18. Variation of the frequencies corresponding to the maximum growth rate with suction velocity for M_∞ = 5.0, T_∞ = 59 $K°$, R = 1500, Pr = 0.72, and ψ = 0.0° . Self-similar boundary layer.

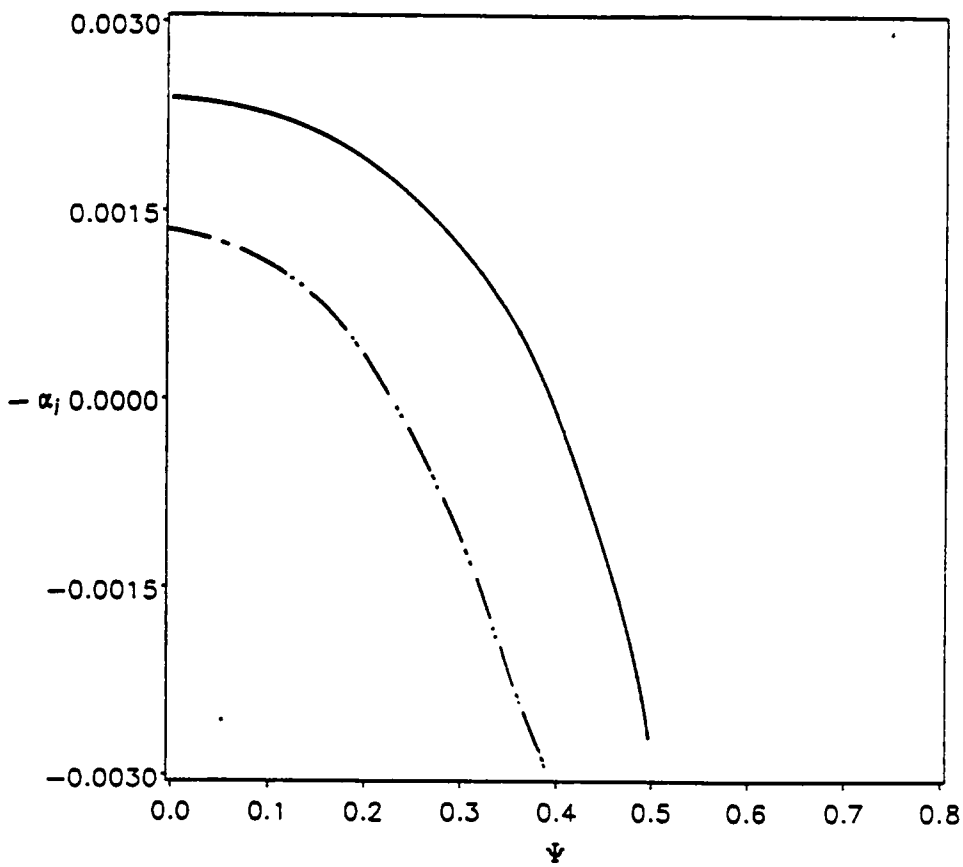

Figure 4. 19. Effect of suction on the variation of the growth rate of second-mode waves with wave angle for M_∞ = 4.5, T_∞ = 121 $K°$, R = 1500, Pr = 0.72, and F = 153.33x10.$^{-6}$: ___ V_w = 0.0 and _.._ V_w = 0.1. Self-similar boundary layer.

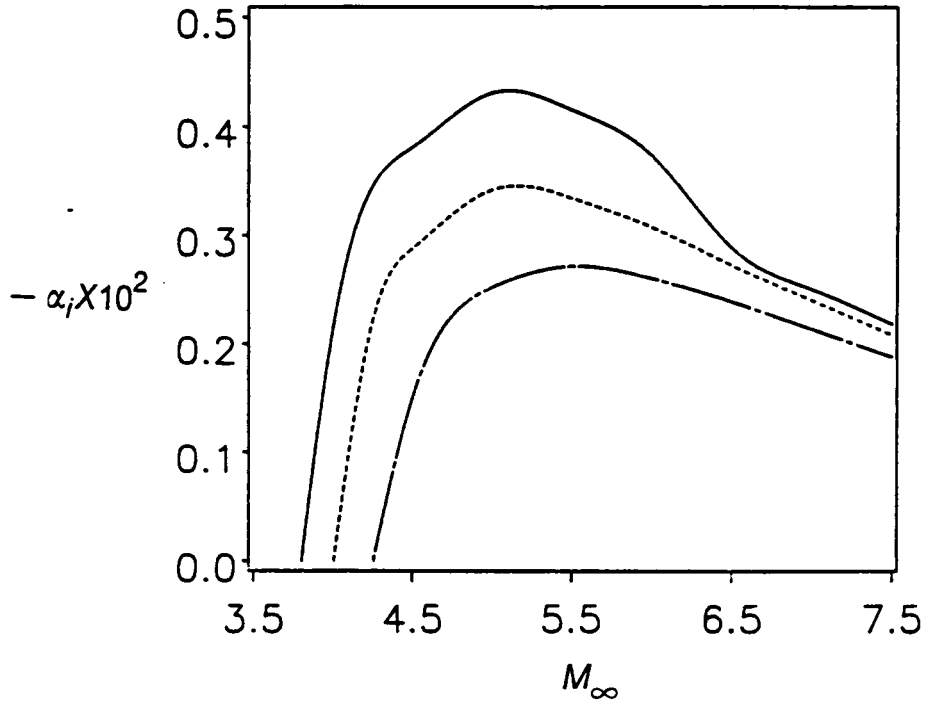

Figure 4. 20. Effect of suction on the variation of the maximum growth rate of second-mode waves with Mach number for wind-tunnel temperature, R = 1500, $\psi = 0.0°$, and Pr = 0.72: ___ V_w = 0.0, - - - V_w = 0.1, and ___ V_w = 0.3. Self-similar boundary layer.

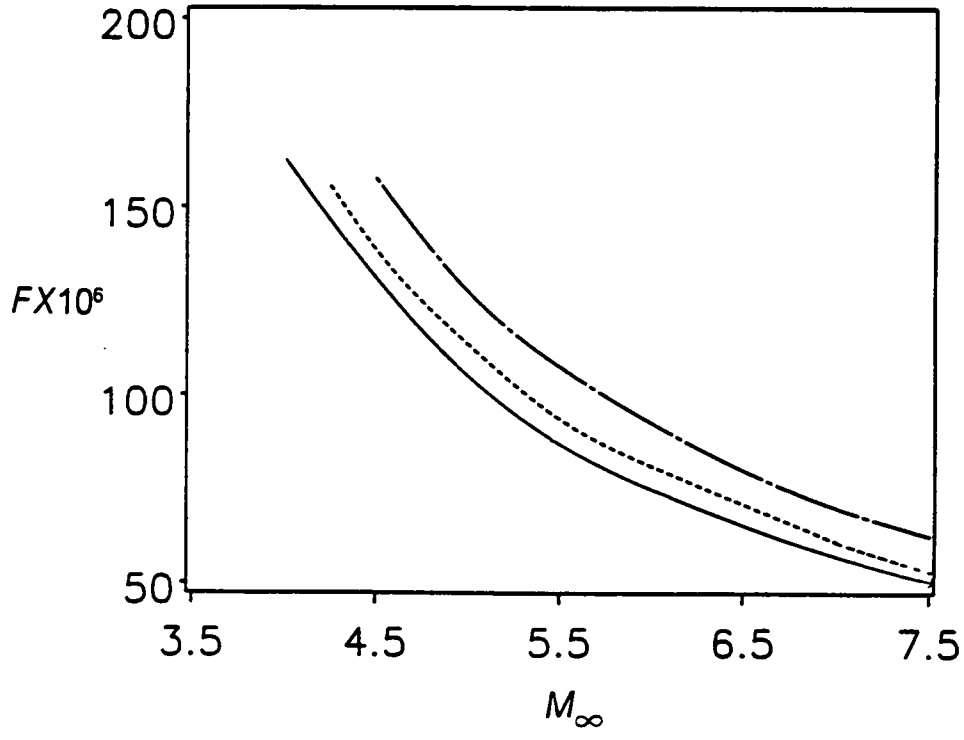

Figure 4. 21. Effect of suction on the variation of the frequencies corresponding to the maximum growth rates with Mach number for wind-tunnel temperature, R = 1500, ψ = 0.0° and Pr = 0.72: ___ V_w = 0.0, - - - V_w = 0.1, and __ _ __ V_w = 0.3. Self-similar boundary layer.

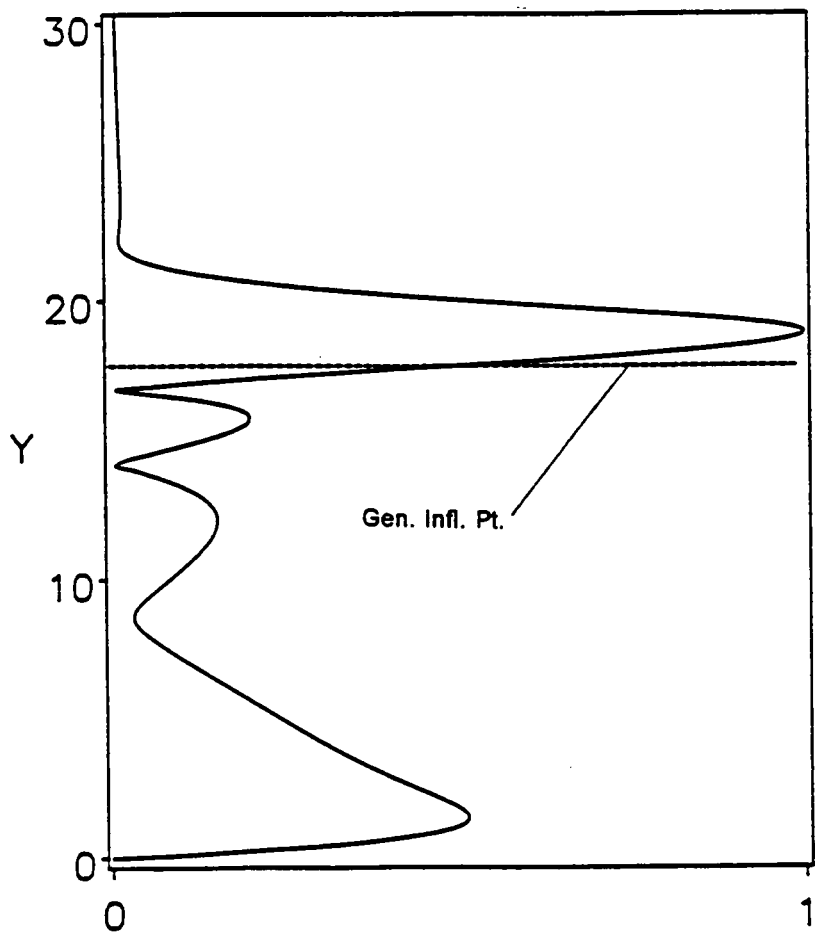

Figure 4. 22. Effect of suction on the eigenfunctions of the temperature disturbance for $M_\infty = 6.0$, Pr = 0.72, $T_\infty = 50K°$, $F = 66.0x10^{-6}$, R = 1500: (a) $V_w = 0.0$

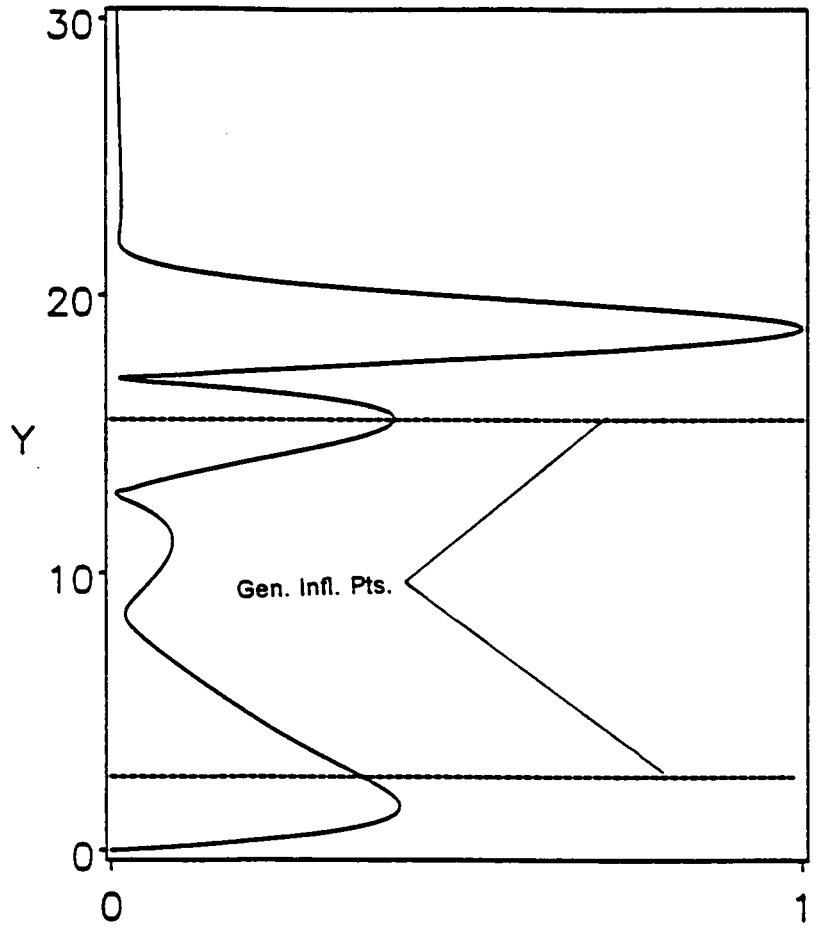

Figure 4.22. Effect of suction on the eigenfunctions of the temperature disturbance for $M_\infty = 6.0$, Pr = 0.72, $T_\infty = 50\ K°$, $F = 66.0x10^{-6}$, R = 1500: (b) $V_w = 0.3$.

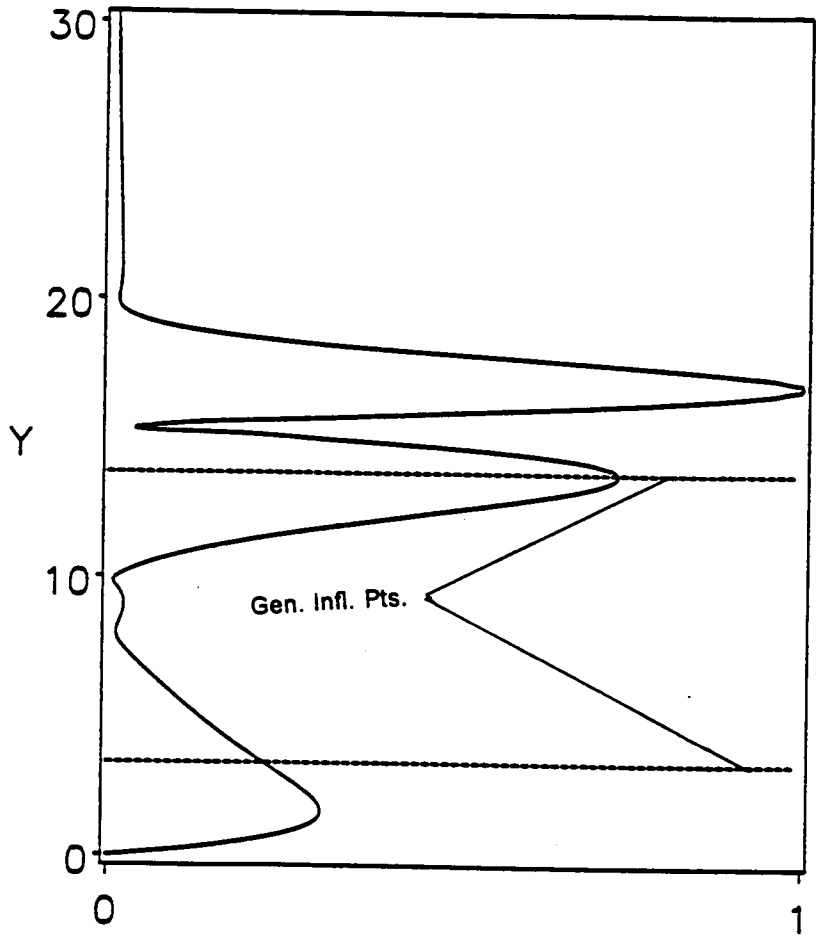

Figure 4.22. Effect of suction on the eigenfunctions of the temperature disturbance for $M_\infty = 6.0$, Pr = 0.72, $T_\infty = 50\ K°$, $F = 66.0x10^{-6}$, R = 1500: (c) V_w = 0.6.

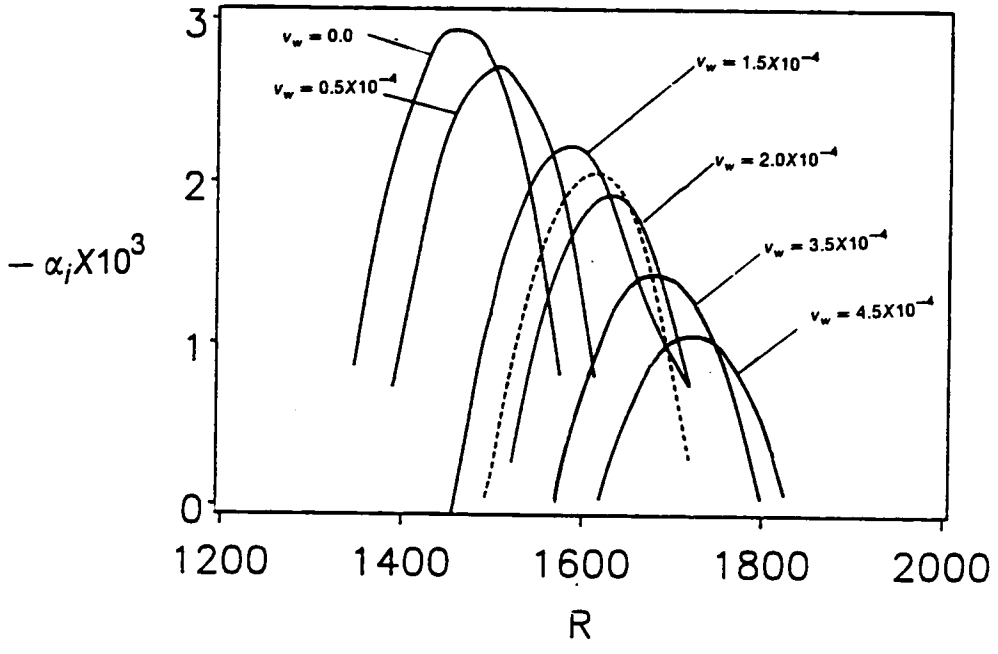

Figure 4. 23. Variation of the growth rate of second-mode waves with Reynolds number for different levels of constant suction for $M_\infty = 4.5$, Pr = 0.70, $T_\infty = 121$ and F = $153.33x10^{-6}$: ___ non-similar boundary layer and - - - self-similar boundary layer.

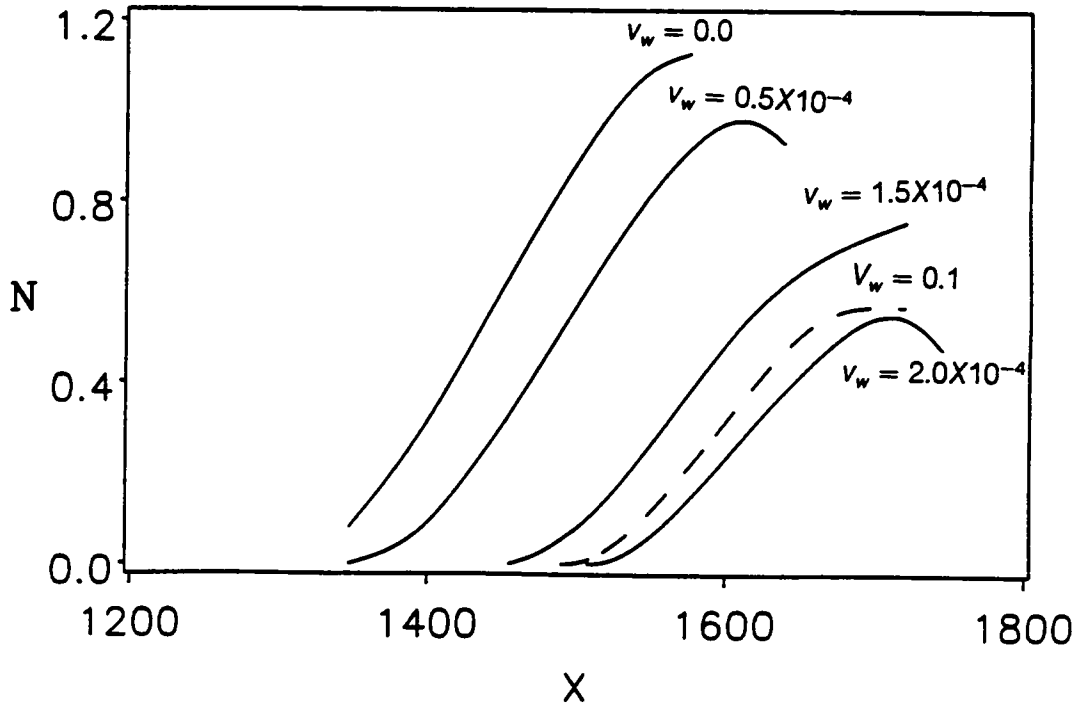

Figure 4. 24. Influence of suction on the variation of the N factor with streamwise location; same conditions as in Figure 4.23.

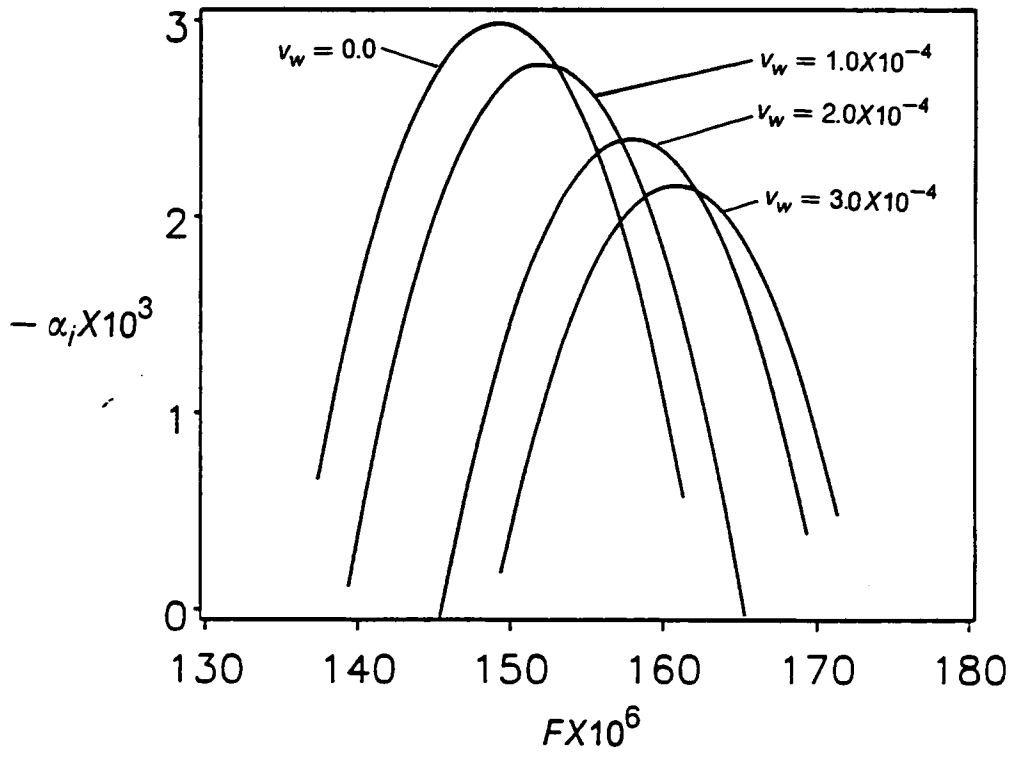

Figure 4. 25. Influence of suction on the variation of the growth rate of second-mode waves with frequency for R = 1500, M_∞ = 4.5, Pr = 0.70, $T_\infty = 121K°$. Non-similar boundary layer.

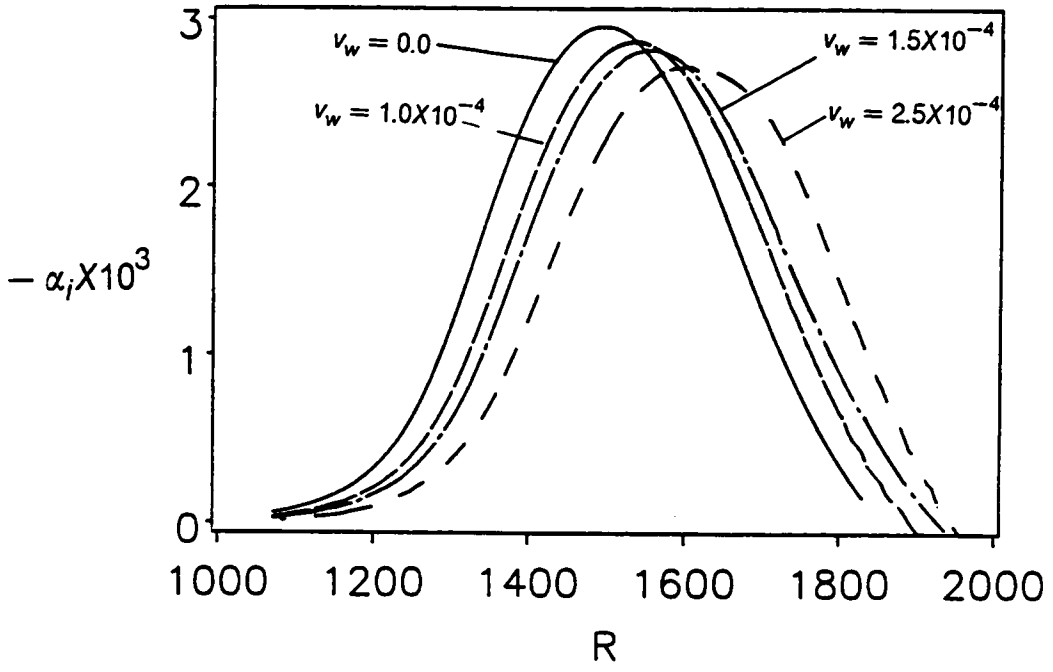

Figure 4. 26. Influence of suction on the variation of the growth rate of second-mode waves with Reynolds number for $M_\infty = 6.0$, Pr = 0.70, $T_\infty = 62K°$, R = 1500, and F = $66x10^{-6}$. Non-similar boundary layer.

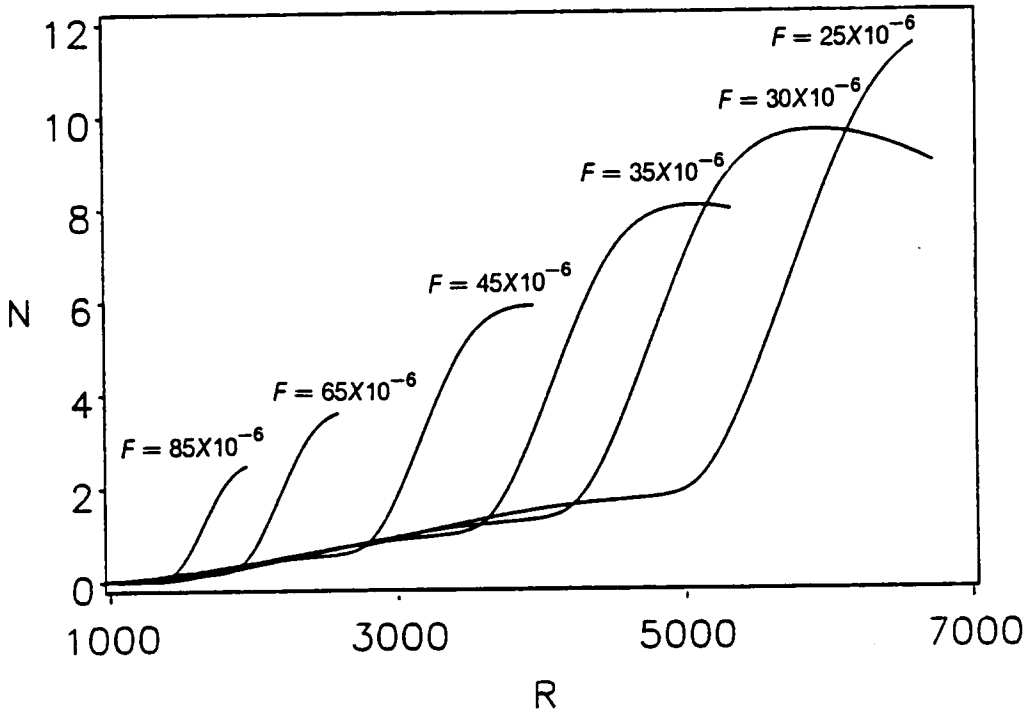

Figure 4. 27. Variation of the N factor with streamwise distance for several frequencies when $M_\infty = 6.0$, Pr = 0.70, $T_\infty = 62K^0$ and no suction is applied.

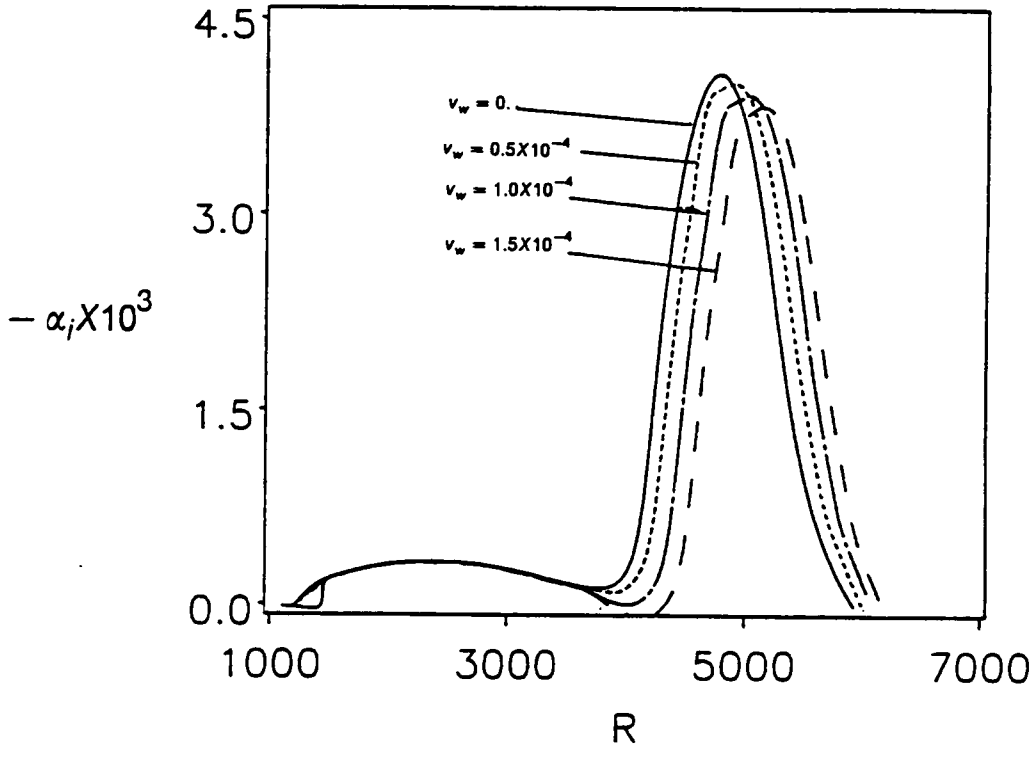

Figure 4. 28. Effect of constant suction on the variation of the growth rate with streamwise distance for the most dangerous frequency; $F = 30x10^{-6}$, $M_\infty = 6.0$, and Pr = 0.70. Non-similar boundary layer.

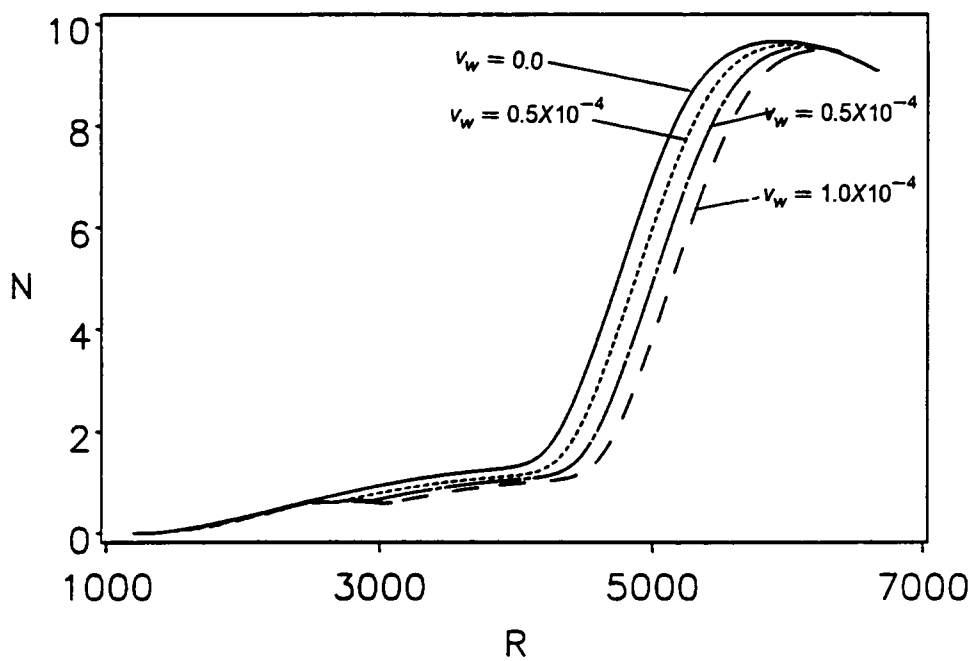

Figure 4. 29. Influence of uniform- suction distributions on the variation of the N factor with streamwise distance for the same conditions in Figure 4.28. Non-similar boundary layer.

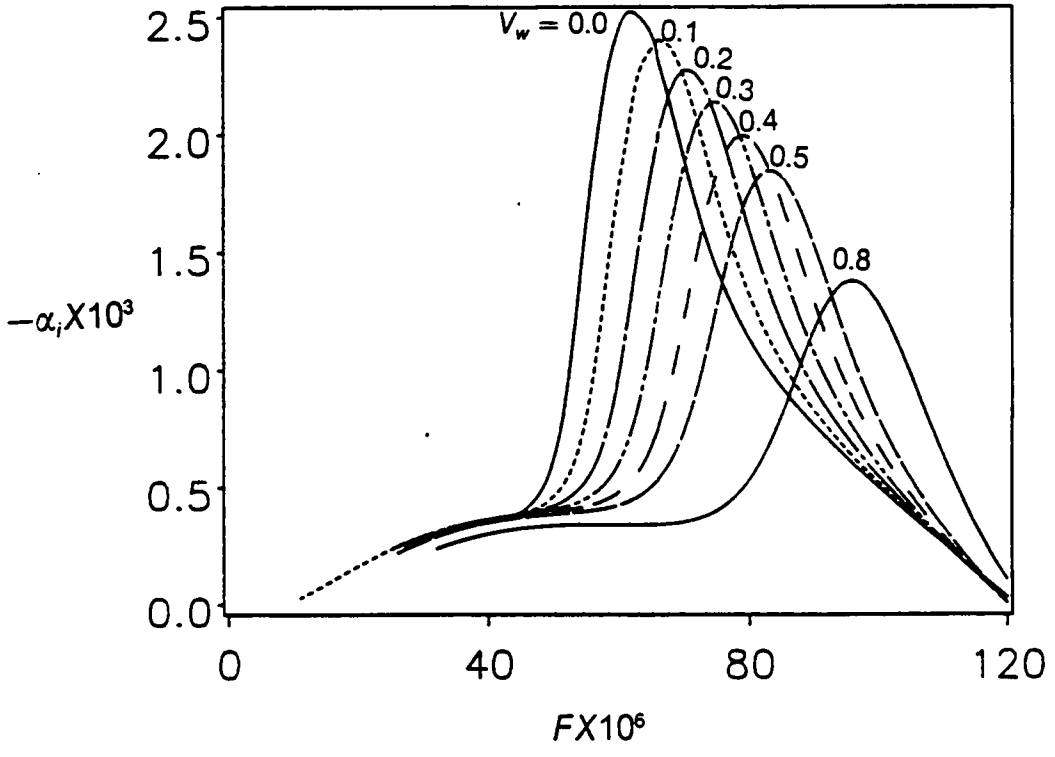

Figure 4. 30. Influence of self-similar suction distributions on the variation of the growth rate of second-mode waves with frequency for $M_\infty = 7.0$, Pr = 0.72, $T_\infty = 50K°$, $R = 1500$, and $\psi = 0$. Self-similar boundary layer.

The vita has been removed from the scanned document